



Universitat Autònoma de Barcelona

**ADVERTIMENT.** L'accés als continguts d'aquesta tesi queda condicionat a l'acceptació de les condicions d'ús establertes per la següent llicència Creative Commons:  [http://cat.creativecommons.org/?page\\_id=184](http://cat.creativecommons.org/?page_id=184)

**ADVERTENCIA.** El acceso a los contenidos de esta tesis queda condicionado a la aceptación de las condiciones de uso establecidas por la siguiente licencia Creative Commons:  <http://es.creativecommons.org/blog/licencias/>

**WARNING.** The access to the contents of this doctoral thesis it is limited to the acceptance of the use conditions set by the following Creative Commons license:  <https://creativecommons.org/licenses/?lang=en>

Doctoral thesis

# **Targeting MYC in B-cell haematologic malignancies**

**Sandra Martínez-Martín**

Director: Dr Laura Soucek

Mouse Models of Cancer Therapy Laboratory

Vall d'Hebron Institute of Oncology (VHIO)

Tutor: Dr Joaquín Arribas López

PhD programme in Biochemistry, Molecular Biology and Biomedicine

Department of Biochemistry and Molecular Biology

Universitat Autònoma de Barcelona

Barcelona, 2020





The director **Dr Laura Soucek** and the tutor **Dr Joaquín Arribas López**,

Certify:

That the experimental work and the writing of the memory of this doctoral thesis entitled "Targeting MYC in B-cell haematologic malignancies" have been performed by Sandra Martínez-Martín under their direction and consider that it is suitable to be presented for the degree of PhD in Biochemistry, Molecular Biology and Biomedicine at Universitat Autònoma de Barcelona.

Barcelona 31<sup>st</sup> of March of

**Director: Dr Laura Soucek**

**Tutor:**

**Dr Joaquín Arribas López**

**PhD student:**

**Sandra Martínez Martín**



## SUMMARY

The importance of MYC function in cancer (and the origin of the oncoprotein's name) was discovered in the late '70s when the sequence of the avian retrovirus that causes myelocytic leukaemia was identified.

Since then, over 40 years of unceasing research have highlighted the significance of this protein in regular cell division, and importantly, its involvement in malignant transformation. Indeed, some of the earliest connections between the higher expression of proto-oncogenes (such as MYC), genetic rearrangements and their relation to cancer development were made in Burkitt lymphoma, chronic myeloid leukaemia and mouse plasmacytomas.

Given the role of MYC in cancer, the need for the design of therapeutic strategies against it seems obvious. However, targeting MYC was - and somehow, still is - challenging due to its unique properties: lack of defined three-dimensional, structure nuclear localisation and absence of enzymatic pocket. Despite these difficulties, many studies have shown the potential therapeutic impact of direct or indirect MYC inhibition.

In this thesis, we outline the potential of direct MYC inhibition in Burkitt lymphoma (BL) and multiple myeloma (MM) making use of 2 different strategies: small molecule peptidomimetics and disruptors of the MYC/MAX/DNA complex (using either Omomyc mini-protein or its derivative variant 26 or V26):

- In the first case, the validation of the peptidomimetics therapeutic potential was done in collaboration with a start-up biotech company. Despite evidencing some promising efficacy *in vitro*, the compounds displayed severe local toxicity *in vivo*, accompanied by changes in animal behaviour that prompted us to discontinue the investigation.
- Secondly, regarding the validation of Omomyc mini-protein as a pharmacological approach in the treatment of BL and MM, we demonstrated *in vitro* efficacy and showed preliminary results in the prevention of bone marrow homing upon Omomyc pre-treatment in a zebrafish model, indicating, for the first time, the potential use of this drug candidate to treat liquid tumours.

Our *in vivo* data in mice show that, even if the administration of Omomyc as monotherapy has limited efficacy (probably due to insufficient delivery of peptide to BL and MM target cells), the combination with a proteasome inhibitor (the standard of care for myeloma) both *in vitro* and *in vivo* displays synergic effects in myeloma models.

In addition, we were able to show that intravenous administration of the Omomyc mini-protein encapsulated in liposomes was safe and the

liposomal formulation prolonged the serum half-life of the mini-protein, although it did not promote increased penetrance in MM target cells.

- In addition, we characterised V26, a rationally designed derivative of the Omomyc mini-protein, meant to display improved nuclear localisation and endosomal escape. Here we evidenced that, like Omomyc, V26 can homodimerise and heterodimerise with MAX, as well as bind DNA in both dimeric forms. As expected, V26 displayed better nuclear localisation and induced cell death *in vitro*. However, it also turned out to be less soluble than Omomyc, indicating that it would require further formulation efforts to be used *in vivo*.

Altogether, our results suggest that Omomyc mini-protein itself or other Omomyc-derivatives, like V26, can serve as the backbone for the design of new anti-MYC agents to treat BL and MM. In this context, combination therapy with the standard of care seems to be a promising strategy, while encapsulation in liposomes might help to address potential bioavailability issues that might arise from its use *in vivo*.







# TABLE OF CONTENTS

SUMMARY .....	i
ABBREVIATIONS.....	1
INTRODUCTION .....	11
1.1 Haematologic malignancies .....	11
1.1.1 Multiple myeloma.....	11
1.1.2 Burkitt Lymphoma.....	14
1.2 Personalised medicine and its limitations.....	15
1.3 MYC as a key regulator in cancer.....	19
1.4 MYC inhibition strategies .....	21
1.4.1 Indirect MYC inhibitors.....	22
1.4.2 Direct MYC inhibitors.....	24
HYPOTHESIS AND OBJECTIVES .....	29
Hypothesis.....	29
Objectives.....	29
MATERIALS AND METHODS .....	31
2.1 Cell lines.....	31
2.2 Omomyc mini-protein and derivatives production .....	31
2.3 Buffer recipes .....	32
2.4 Cell culture experiments .....	33
2.4.1 Proliferation .....	33
2.4.2 IC <sub>50</sub> calculations.....	33
2.4.3 Cell cycle .....	33
2.4.4 Migration assay .....	34
2.4.5 Synergy .....	34
2.5 Western blot analysis.....	35
2.6 ChIP-qPCR.....	36
2.7 ELISA .....	38
2.8 Immunofluorescence and immunohistochemistry .....	38
2.9 Flow cytometry analysis.....	40

2.9.1	Entrance and endocytosis inhibition.....	40
2.9.2	Tumour burden from bone marrow flush.....	40
2.10	Circular dichroism.....	41
2.11	Liposomes production.....	42
2.12	Animal studies .....	43
2.12.1	Zebrafish .....	43
2.12.1a	Migration to the CHT (pretreatment in culture) .....	44
2.12.1b	Biodistribution and toxicity studies.....	44
2.12.1c	Migration to the CHT (treatment by immersion).....	45
2.12.2	Mice.....	45
2.12.2a	Xenograft lymphoma model .....	45
2.12.2b	Xenograft myeloma model .....	46
2.12.2c	Syngeneic myeloma model .....	47
2.13	Scoring and paralysis follow-up .....	48
2.14	mCT imaging .....	48
2.15	Figures .....	49
2.16	Statistical analysis .....	49
RESULTS	.....	51
	Validation of novel strategies for MYC inhibition in B-cell malignancies .....	51
3.1	MYC inhibition with small molecules .....	51
3.1.1	<i>In vitro</i> characterisation of compounds X, Y and Z.....	51
3.1.2	<i>In vivo</i> therapeutic effect of X and Z.....	53
3.1.3	<i>In vitro</i> and <i>in vivo</i> characterisation of Z <sub>1</sub> and X <sub>1</sub> .....	61
3.2	MYC inhibition with the Omomyc mini-protein.....	69
3.2.1	Efficacy and mechanism of action of Omomyc on myeloma and lymphoma cell lines .....	69
3.2.2	Therapeutic effect of Omomyc in a zebrafish model .....	78
3.2.3	Therapeutic effect of Omomyc in xenograft mouse models of multiple myeloma and Burkitt lymphoma.....	87
3.2.4	Variant 26 (V26): a derivative of Omomyc mini-protein sequence..	103

DISCUSSION .....	109
4.1 Small molecule peptidomimetics.....	109
4.1.1 <i>In vitro</i> .....	109
4.1.1 <i>In vivo</i> .....	110
4.2 Omomyc derived peptides .....	112
4.2.1 Omomyc mini-protein <i>in vitro</i> .....	112
4.2.2 Omomyc mini-protein <i>in vivo</i> : zebrafish model.....	114
4.2.3 Omomyc mini-protein <i>in vivo</i> : mouse models.....	115
4.3.1 Variant 26 .....	118
CONCLUSIONS .....	121
REFERENCES .....	123



## ABBREVIATIONS

**ABL:** Abelson Murine Leukaemia Viral oncogene

**AF488:** Alexa Fluor 488

**AF647:** Alexa Fluor 647

**AML:** Acute Myeloid Leukaemia

**ATP:** Adenosine Triphosphate

**AV:** Annexin V

**BET:** Bromodomain and Extra-terminal Motif

**BETi(s):** BET inhibitor(s)

**BCA:** Bicinchoninic Acid Assay

**Bcl-2:** B-Cell Lymphoma 2

**BCR:** Breakpoint Cluster Region Protein

**BDP 650/665:** Borondipyrromethene Dye 650/665

**bHLHLZ:** Basic Helix-Loop-Helix Leucine Zipper

**Bis-Tris:** Bis(2-hydroxyethyl)amino-tris(hydroxymethyl)methane

**BL:** Burkitt Lymphoma

**Blebb:** Blebbistatin

**BM:** Bone Marrow

**BMC:** Bone Mineral Content

**BMSC:** Bone Marrow Stromal Cell

**BRD4:** Bromodomain-containing Protein 4

**BSA:** Bovine Serum Albumin

**BTK:** Bruton's Tyrosine Kinase

**BTZ:** Bortezomib

**CAR-T:** Chimeric Antigen Receptor T-cell

**Cav:** Caveolin-mediated

**CCL9:** Chemokine Ligand 9

**CCND3:** Cyclin D3  
**CD38:** Cluster of Differentiation 38  
**CD47:** Cluster of Differentiation 47  
**CD138:** Syndecan-1  
**CD:** Circular Dichroism  
**CDC25:** Cell Division Cycle 25  
**CDC:** Complement-dependent Cytotoxicity  
**CDK4:** Cyclin-dependent Kinase 4  
**CDK7:** Cyclin-dependent Kinase 7  
**CEEA:** Ethical Committee for the Use of Experimental Animals  
**CFZ:** Carfilzomib  
**CHEMS:** Cholesteryl Hemisuccinate  
**ChIP:** Chromatin Immunoprecipitation  
**Chlor:** Chlorpromazine  
**Chr8:** Chromosome 8  
**CHT:** Caudal Haematopoietic Tissue  
**Clat:** Clathrin-mediated  
**CML:** Chronic Myeloid Leukaemia  
**CRBN:** Cereblon  
**CRC:** Colorectal Cancer  
**CTRL:** Control  
**CXCL12:** C-X-C Motif Chemokine Ligand 12 or SDF1  
**CXCR4:** C-X-C Chemokine Receptor Type 4  
**CytD:** Cytochalasin D  
**DAB:** 3,3'-Diaminobenzidine  
**DAPI:** 4', 6-Diamino-2-phenylindole  
**del:** deletion

**DiO:** Benzoxazolium, 3-octadecyl-2-[3-(3-octadecyl-2(3H)-benzoxazolylidene)-1-propenyl]-Perchlorate

**Dil:** 1,1'-Dioctadecyl-3,3,3',3'-Tetramethylindocarbocyanine Perchlorate

**DMSO:** Dimethyl Sulfoxide

**DNA:** Deoxyribonucleic Acid

**DOPE:** 1,2-dioleoyl-sn-glycero-3-phosphoethanolamine

**dpf:** days post fertilisation

**dpi:** days post inoculation

**DPPC:** 1,2-dipalmitoyl-sn-glycero-3-phosphocholine

**DSG:** Disuccinimidyl Glutarate

**DTT:** Dithiothreitol

**EAE:** Experimental Autoimmune Encephalomyelitis

**E-box:** Enhancer Box Consensus DNA Sequence

**EBV:** Epstein-Barr Virus

***E.coli:*** *Escherichia coli*

**EDTA:** Ethylenediaminetetra Acetic Acid

**EE:** Encapsulation Efficiency

**eF660:** eFluor 660

**EGF:** Epidermal Growth Factor

**eIF:** Eukaryotic Translation Initiation Factor

**EIPA:** 5-Ethyl Isopropyl Amiloride

**EMA:** European Medicines Agency

**EPR:** Enhanced Permeability and Retention

**ERK:** Extracellular signal-regulated Kinases

**5-FU:** Fluorouracil

**FBS:** Foetal Bovine Serum

**FC:** Flow Cytometry

**FDA:** Food & Drug Administration (US)



**FITC:** Fluorescein Isothiocyanate

**FMO:** Fluorescence Minus One Control

**FPLC:** Fast Protein Liquid Chromatography

**FS:** Forward Scatter

**FVB/NJ:** Friend Leukaemia Virus B Strain

**FVS510:** Fixable Viability Stain 510

**GADD45:** Growth Arrest and DNA Damage-inducible 45

**GEEC:** Glycosylphosphatidylinositol (GPI)–Enriched Early Endosomal Compartment

**GEMMs:** Genetically Engineered Mouse Models

**GLUT1:** Glucose Transporter 1

**GWAS:** Genome-wide Association Study

**Gy:** gray

**H3K4me3:** Histone H3 Lysine 4 Trimethylation

**H3K9me3:** Histone H3 Lysine 9 Trimethylation

**H3K27ac:** Histone H3 Lysine 27 Acetylation

**HEPES:** 4-(2-hydroxyethyl)-1-piperazineethanesulfonic Acid

**HIV:** Human Immunodeficiency Virus

**hot:** hours of Omomyc treatment

**hpf:** hours post fertilisation

**hpi:** hours post inoculation

**HPLC-MS:** High-Performance Liquid Chromatography-Mass Spectrometry

**hpt:** hours post treatment

**HRD:** Hyperdiploid

**HRP:** Horseradish Peroxidase

**IC<sub>50</sub>:** Half Maximal Inhibitory Concentration

**ICAM1:** Intracellular Adhesion Molecule 1

**ID3:** Inhibitor Of DNA Binding 3

**IDP:** Intrinsically Disordered Protein

**IF:** Immunofluorescence

**IFN- $\gamma$ :** Interferon-gamma

**IFRD2:** Interferon-related Developmental Regulator 2

**IgE:** Immunoglobulin E

**IgG:** Immunoglobulin G

**IgH:** Immunoglobulin Heavy Chain

**IL-1 $\beta$ :** Interleukin-1 beta

**IL-6:** Interleukin-6

**IL-23:** Interleukin-23

**IMiDs:** Immunomodulatory Imide Drugs

**IP:** Immunoprecipitation

**i.p.:** intraperitoneal

**i.v.:** intravenous

**IVIS:** *In Vivo* Imaging System

**LDHA:** Lactate Dehydrogenase A

**lncRNA:** long non-coding RNA

**M:** Macropinocytosis

**mAb:** Monoclonal Antibody

**Mad2:** Mitotic Arrest Deficient 2

**MAX:** MYC-associated Factor X

**M $\beta$ CD:** Methyl- $\beta$ -cyclodextrin

**mCT:** micro Computed Tomography

**MEFs:** Mouse Embryonic Fibroblasts

**MEK:** Mitogen-activated Protein Kinase

**MGUS:** Monoclonal Gammopathy of Undetermined Significance

**MM:** Multiple Myeloma

**MoM:** Mouse on Mouse

**miR-34a:** microRNA 34a

**miRNA:** microRNA

**mRNA:** Messenger Ribonucleic Acid

**MTD:** Maximum Tolerated Dose

**mTOR:** Mammalian Target of Rapamycin

**MYBL2:** MYB Proto-oncogene-like 2

**NaAc:** Sodium Acetate

**NaCl:** Sodium Chloride

**NC:** Nitrocellulose

**Ncl:** Nucleolin

**NGS:** Next-Generation Sequencing

**NHL:** Non-Hodgkin lymphoma

**NLS:** Nuclear Localisation Signal

**NPs:** Nanoparticles

**Npm1:** Nucleophosmin 1

**NSCLC:** Non-small Cell Lung Cancer

**NSG:** Non-Obese Diabetic (NOD) Severe Combined Immunodeficiency Disease (SCID) gamma

**mAb:** Monoclonal Antibody

**OMO:** Omomyc

**Omolips:** Omomyc liposomes

**OPG:** Osteoprotegerin

**p21<sup>Cip1</sup>:** Cyclin-dependent Kinase Inhibitor 1

**p27<sup>Kip1</sup>:** Cyclin-dependent Kinase Inhibitor 1B

**PAGE:** Polyacrylamide Gel Electrophoresis

**PBMCs:** Peripheral Blood Mononuclear Cells

**PBS:** Phosphate Buffered Saline

**PBST:** PBS Tween20

**PCR:** Polymerase Chain Reaction

**PD-1:** Programmed Death-1

**PD-L1:** Programmed Death-ligand 1

**PE:** Phycoerythrin

**PEG:** Polyethylene Glycol

**PEGe:** Empty liposomes PEGylated

**PEGo:** Omomyc liposomes PEGylated

**PHH3:** Phospho-Histone H3

**PI:** Propidium Iodide

**PI3K:** Phosphoinositide 3-kinase

**PK:** Pharmacokinetics

**qPCR:** Quantitative Polymerase Chain Reaction

**RAF:** Rapidly Accelerated Fibrosarcoma

**RFP:** Red Fluorescent Protein

**RIPA:** Radioimmunoprecipitation Assay

**RNA:** Ribonucleic Acid

**rpm:** Revolutions Per Minute

**RPMI:** Roswell Park Memorial Institute Medium

**RTV:** Relative

**SCID-Bg:** Severe Combined Immunodeficiency Disease Beige

**SD:** Standard Deviation

**SDF1:** Stromal-derived Factor 1

**SDS:** Sodium Dodecyl Sulphate

**shRNA:** Short Hairpin RNA

**siRNA:** Small Interfering RNA

**SLAMF7:** Signalling Lymphocytic Activation Molecule family member 7

**SMM:** Smouldering Multiple Myeloma  
**SNPs:** Small-nucleotide Polymorphisms  
**SoC:** Standard of Care  
**SS:** Side Scatter  
**t:** translocation  
**TAD:** Transcriptional Activation Domain  
**TCEP:** Tris(2-carboxyethyl)phosphine  
**TCF-3:** Transcription Factor 3  
**TCT:** Targeted Combined Therapies  
**TERT:** Telomerase Reverse Transcriptase  
**TF:** Transcription Factor  
**TKI:** Tyrosine Kinase inhibitors  
**TLE:** Transducin-like Enhancer of split  
**TMC:** Tissue Mineral Content  
**TNF- $\alpha$ :** Tumour Necrosis Factor Alpha  
**TP53:** Tumour Protein p53  
**TSSs:** Transcriptional Start Sites  
**Ub:** Ubiquitin  
**USP:** Ubiquitin Specific Protease  
**UV:** Ultraviolet  
**V26:** Omomyc Variant 26  
**VCAM1:** Vascular Cell Adhesion Protein 1  
**VEGF:** Vascular Endothelial Growth Factor  
**VHIO:** Vall d'Hebron Institute of Oncology  
**VLA-4:** Very Late Antigen-4  
**WHO:** World Health Organization

- Nature never ceases to surprise us and so little about her I can claim to know, and from her it seems we never stop learning and my wonder of her only seems to grow -

**Francis Duggan**



## INTRODUCTION

### 1.1 Haematologic malignancies

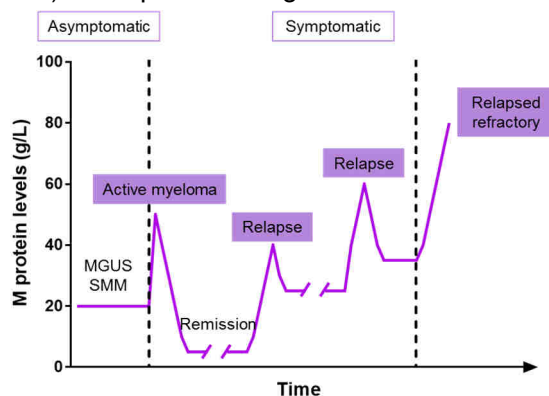
Haematologic malignancies are cancers affecting blood, bone marrow (BM) and lymph nodes. Depending on the type of cell affected, they are classified in myelomas, lymphomas and leukaemias. The three types of malignancies are connected through the immune system, from which they arise.

#### 1.1.1 Multiple myeloma

Multiple myeloma (MM), although a rare disease, is the second most common blood cancer (Kazandjian, 2016) with over 48,000 estimated new cases in Europe and 159,000 worldwide in 2018 (GLOBOCAN, 2018a). It is a neoplasm that originates from the clonal expansion of plasma cells in the BM (Kumar et al., 2017). A benign and asymptomatic condition, termed monoclonal gammopathy of undetermined significance or MGUS, precedes it and can evolve into another asymptomatic disorder, also classified among monoclonal gammopathies, termed smouldering multiple myeloma or SMM. All these diseases are characterised by the invasion of proliferating plasma cells in the BM, and the secretion of monoclonal protein referred to as M protein or M spike, present in large amounts in the blood and urine, and used for the disease diagnosis (Landgren et al., 2009, Kyle et al., 2002, Kyle et al., 2007). This protein is also known as paraprotein, which is essentially a single antibody excessively produced by abnormal plasma cells.

Even if recent advances in medicine have quadrupled MM patient survival in the last 40 years (from 6 to 33% for 10 or more years), it remains virtually incurable, as relapse rates are as high as 90% (de la Puente and Azab, 2017). The disease adopts a cyclical pattern of response to therapy and remission followed by disease progression or reappearance (Kurtin, 2013) as depicted in Figure 1.

**Figure 1: Response-relapse pattern in MM patients.** Monoclonal gammopathies that undergo malignant transformation are likely to respond initially to the therapy and enter in remission. However, the disease eventually relapses, and the response becomes less durable until resistance appears, resulting in relapsed refractory myeloma. Figure adapted from (Kurtin, 2013).



To make things worse, due to progressive ageing of the population and the fact that the peak rate of MM cases is at 85-89 years (Ravi et al., 2018, Cancer Research UK, 2016), MM's incidence



trend over time has increased 32% since the early '90s and keeps growing. In fact, estimates predict that the number of incident myeloma cases will almost double by 2040, as depicted in Figure 2 (GLOBOCAN, 2018b).

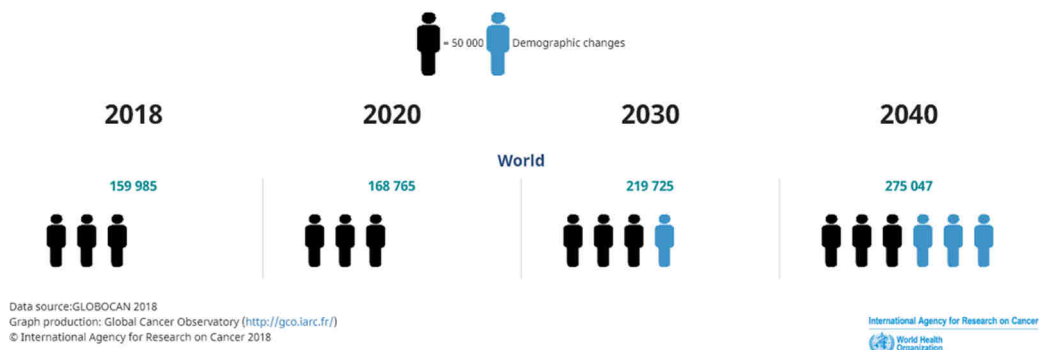


**Figure 2: Estimated number of incident cases of myeloma, including both sexes and all ages from 2018 to 2040. Figure obtained from (GLOBOCAN, 2018b).**

Myelomagenesis is a complex process that requires various driver genetic alterations to collude with each other, resulting in the development and progression of MM (Manier et al., 2017). MM is a highly heterogeneous cancer marked by clonal diversity (Kovalchuk et al., 2000). It starts with underlying germline events, followed by primary -frequently initiating- and secondary genomic aberrations that lead to tumour progression. Focusing on secondary events, we can observe how MYC is associated with disease progression (Figure 3). In fact, MYC is deregulated in a large percentage (67%) of MM cases (Jovanovic et al., 2018). In one of the largest GWA studies to date, researchers have found several single-nucleotide polymorphisms (SNPs) associated with MYC activation, considered a critical exacerbating event and related to poor outcomes, especially when it is found translocated along with an Ig partner (Kumar et al., 2017).

Heterogeneity of MM imposes a big challenge for its treatment with tailored therapies, which are typically directed against a unique target. Besides, as mentioned above, patients commonly relapse after receiving first-line therapy, often due to a selective pressure exerted by the treatment leading to resistant subclones outgrowth (Weinhold et al., 2016). This is the main reason why researchers are currently proposing alternating the use of therapies with different mechanisms of action, which could overcome future relapses.

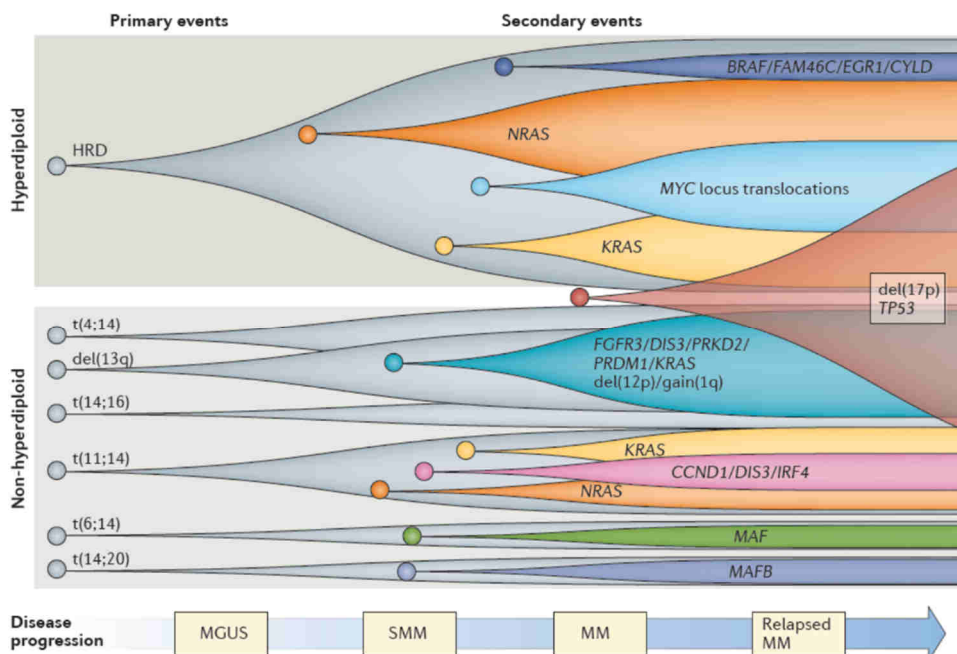


**Figure 3: Model of disease progression by clonal evolution in myeloma by (Manier et al., 2017).** The primary events driving the development of MM are typically classified into hyperdiploid (HRD) or non-hyperdiploid. In the cartoon, we can observe the different mutations that appear in the early stages of the monoclonal gammopathy and then co-exist with secondary mutations accounted responsible for the progression to late-stage MM. The grey circles represent the clones bearing the initiating aberrant genetic events. The coloured circles show the additional genetic mutations acquired throughout the evolution of the disease and are associated with specific primary mutations. Besides, *del(17p)* can appear in any clone, thus is represented in the intersection between HRD and non-hyperdiploid tumours; *del* stands for deletion and *t* for translocation.

Another critical aspect of MM pathophysiology is its dependence on the BM niche. Probably one of the most critical interactions in the creation of a favourable microenvironment for MM cells proliferation, survival and apoptosis resistance, is their relationship with BM stromal cells (BMSCs) (Kumar et al., 2017). The cell-cell crosstalk through adhesion molecules such as VCAM1 and VLA-4 expressed by BMSCs and MM cells, respectively, results in the secretion of cytokines responsible for the formation of an appropriate cancerous milieu. This interaction also accounts for bone destruction, a hallmark of late-stage myeloma that significantly deteriorates the quality of life of MM patients (Terpos et al., 2018). Indeed, the development of osteolytic lesions, present in more than 80% of myeloma patients (Garcia-Gomez et al., 2014), is one of the most devastating consequences of advanced MM, caused by an imbalance between bone formation

and resorption, partly due to a significant reduction in circulating osteoprotegerin (Higgs et al., 2017).

Taken together, all these pieces of evidence appeal for the research of new therapeutic options, either directed against novel targets or focused on bone disease management, to achieve fewer side effects. These new therapies could be combined or sequentially administered together with already approved drugs to render myeloma a preventable or, even better, curable disease.

### 1.1.2 Burkitt Lymphoma

Burkitt Lymphoma (BL) is a highly aggressive and rare form of B-cell non-Hodgkin lymphoma (NHL) caused by translocations of the *MYC* locus (Ferry, 2006). It is the most common childhood cancer in areas where malaria is endemic (Molyneux et al., 2012), afflicting 50% of African children diagnosed with NHL. The World Health Organization (WHO) recognises 3 clinical variants of the disease: endemic (affecting mostly kids in malaria-endemic regions and highly associated with Epstein-Barr virus or EBV infection), sporadic (also known as non-African, occurring where malaria is not holoendemic) and immunodeficiency-associated (usually occurring in HIV positive patients) (Hammerl et al., 2019). According to data from GLOBOCAN, there were over 500,000 new cases of NHL worldwide in 2018, of which over 100,000 were registered in Europe (GLOBOCAN, 2018a).

*MYC* is pathologically active in 100% of BL cases (Albiñ et al., 2010). As such, *MYC* translocation is a genetic hallmark of this disease. Hence, genetically engineered mouse models (GEMMs) were generated based on *MYC* deregulation, such as the *Eμ-Myc* lymphoma model, used to study *MYC*-driven tumourigenesis and predict therapy response (Cai et al., 2015, Rempel et al., 2014). The most common translocation involving *MYC* and IgH enhancer elements, *t(8;14)*, is present in 80% of BL patients (Figure 4). The remaining 20% harbour translocations involving chromosomes 2 and 8, *t(2;8)(p12;q24)*, or 8 and 22, *t(8;22)(q24;q11)*, placing *MYC* next to the  $\kappa$  or  $\lambda$  light chain loci and enhancer elements, respectively (Blum et al., 2004). *MYC* aberrations are necessary but not enough on their own to induce lymphomagenesis. Indeed, other mutations can also contribute to the appearance and progression of this cancer. Among them, we find inactivating mutations in *TP53*, mutations

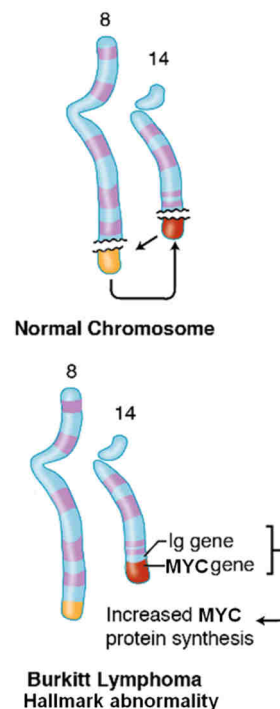


**Figure 4: Hallmark translocation *t(8;14)* involving *MYC* in BL.** Figure adapted from (Kaplan-Medical).

in transcription factors (TFs) like *TCF3*, *ID3*, or *MYC*, as well as in other genes such as *CCND3*, all of which have an impact on cell proliferation and survival. Some of these mutations often contribute to the overactivation of several oncogenic signalling pathways, ultimately promoting the development and maintenance of BL (Schmitz et al., 2014).

Both adults and children affected by BL luckily present a high cure rate (80-90% survival) compared to all subsets of aggressive lymphoma, but the significant toxicity caused by treatment with the multiagent chemotherapy regimens is still a major issue (Dozzo et al., 2017, Jacobson and LaCasce, 2014). Moreover, poor prognosis patients, such as those in an advanced-stage, with relapsed disease or in an HIV infection setting, receive suboptimal treatment (Maifrede et al., 2017). Besides, these intensive regimens are not as accessible for resource-poor areas where BL is endemic. As a consequence, children in Africa receive lower treatment doses than in developed countries, achieving only a 30-50% cure rate (Schmitz et al., 2014). Hence, the discovery of new treatment regimens, for instance, targeted against one of the essential oncogenic TFs that appear aberrantly expressed in BL such as *MYC*, constitutes an urgent medical need.

## 1.2 Personalised medicine and its limitations

Personalised medicine, also known as precision medicine, aims to design tailored treatments against major molecular drivers of different pathologies (Badalian-Very, 2014). Oncology is one of the most invested fields in the discovery of new drug options, in an insatiable search for alternative therapies able to overcome the limitations of the already existing ones (Chae et al., 2017). Precision oncology performs molecular profiling of tumours to identify alterations that can be translated into actionable targets (Schwartzberg et al., 2017).

The first step in the profiling is to stratify the patients using new technologies, such as NGS or multi-omics approaches, to choose the most appropriate treatment for each individual, based on their unique molecular aberrations. Very often, the most affected proteins in cancer are kinases, involved in many physiological processes of the cell (Badalian-Very, 2014). One very well-characterised example is the BCR-ABL gene fusion in chronic myeloid leukaemia (CML). This chromosomal defect, known as the Philadelphia chromosome, is the signature of CML, present in all patients suffering from this condition (Shin et al., 2017). Its discovery led to the development of imatinib, a selective inhibitor of the constitutively active tyrosine kinase resulting from the gene fusion (Hantschel et al., 2008). Thanks to imatinib, the survival rates for CML patients notably improved to 90% over 5 years and 88% over 8 years (Shin et al., 2017). Other tyrosine kinase inhibitors (TKI) became then very popular because of the broad involvement of the kinome in different malignancies. So, numerous small molecules against the enzymatic core or

binding pockets of these proteins have been developed ever since, changing the clinical management of cancer ([Bhullar et al., 2018](#)).

Currently, there are over 55 targeted therapies approved for the treatment of different haematologic malignancies ([NIH](#)). As such, they are directed against actionable molecules identified to play essential roles in the biology of immune cells or represent proteins that are highly expressed in these types of tumours. They can be categorised according to the type of target they inhibit: 1. B-cell surface markers (e.g. rituximab, an anti-CD20 monoclonal antibody (mAb) or daratumumab, an anti-CD38 mAb); 2. survival or proliferation factor receptors (e.g. siltuximab, an anti-IL-6 mAb); 3. cell signalling markers (e.g. ibrutinib, a BTK inhibitor, or idelalisib, a PI3K inhibitor); 4. cell cycle, apoptosis and proteasome machinery (e.g. bortezomib, a proteasome inhibitor, or venetoclax, a Bcl-2 inhibitor); 5. metabolism (e.g. lonidamine, a hexokinase inhibitor) and 6. microenvironment (including immune modulators, such as plerixafor, an anti-CXCR4; pembrolizumab, an anti-PD-1 antibody; CAR-T cells or bispecific antibodies) ([Rossi, 2015](#)).

Despite the success of all these different therapeutic strategies, most patients are likely to benefit from them initially, but they eventually relapse. Hence, the emergence of drug resistance is not only limited to conventional chemotherapy, but it extends to drugs with a targeted mode of action ([Fabbro et al., 2015](#)). There are, of course, several mechanisms of resistance that have been largely studied and described, including drug efflux, acquired mutations that impair drug binding, trapping in acidic vesicles, enhanced metabolism, activation of compensatory signalling pathways or remnant quiescent stem cells inherently resistant ([Balik et al., 2019](#)).

As mentioned in 1.1.1, MM is an excellent example of frequent disease recurrence due to resistance appearance through multiple compensatory mechanisms (Figure 5). For instance, the occurrence of mutations in the proteasome machinery and the RAS/RAF signalling pathway confer resistance to proteasome inhibitors (e.g. bortezomib) and immunomodulatory agents (e.g. lenalidomide), respectively. Similarly, sequestration of drugs in autophagosomes or active pumping to the outside are typical mechanisms of resistance as well. On the other hand, cells can get protection from the microenvironment by increasing the interaction with supporting cells through integrins and other adhesion molecules, or by increase in proliferation and survival signalling. Lastly, reduction in the expression levels of certain proteins like cereblon, CD38 and SLAMF7 impairs the activity of the agents targeted against them. In addition, CD38 and SLAMF7 can be secreted, acting as decoy receptors for the mAbs (daratumumab or elotuzumab), further weakened by increased expression of complement inhibitory proteins that hamper their ability to activate the complement-dependent cytotoxicity (CDC) ([Wallington-Beddoe et al., 2018](#)). Ideally, liquid and on-treatment standard biopsies could shed some light into

the identification of biomarkers of resistance or response, to intervene ahead of the point of no return, for instance by switching to a different drug and dosing regimen, or even decide to start combinations with other therapies (Sabnis and Bivona, 2019).

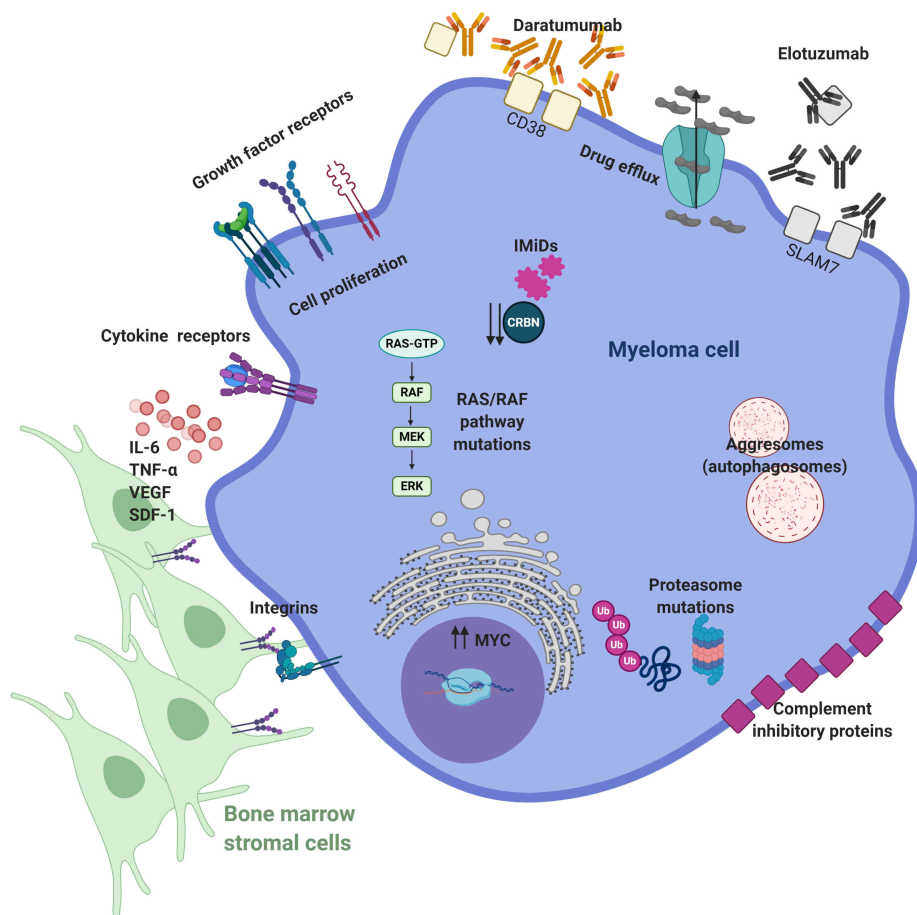


**Figure 5: Examples of the most common resistance mechanisms to MM therapies.** See text for details. CD38, Cluster of Differentiation 38; CRBN, Cereblon; ERK, Extracellular signal-regulated Kinases; IMiDs, Immunomodulatory agents; IL-6, Interleukin-6; MEK, Mitogen-activated Protein Kinase; RAF, Rapidly Accelerated Fibrosarcoma; SDF-1, Stromal cell-derived Factor; SLAMF7, Signalling Lymphocytic Activation Molecule family member 7; TNF $\alpha$ , Tumour Necrosis Factor alpha; Ub, Ubiquitin; VEGF, Vascular Endothelial Growth Factor. Figure adapted from (Wallington-Beddoe et al., 2018) and created with BioRender.

One of the strategies adopted to circumvent the resistance to first-line treatments is the use of rational combination therapies, which is becoming widely prevalent in oncology and is also known as targeted combination therapy (TCT). The objective

of TCT is to attack tumours from multiple angles, either targeting several signalling pathways at a time or the same one at different levels. (Danko et al., 2019). There are increasing numbers of Phase II and III clinical trials enquiring their potential. Many of the examples of TCTs already approved for marketing by the EMA in 2019 are treatments for metastatic melanoma and MM, such as carfilzomib with dexamethasone or lenalidomide, binimetinib with encorafenib, daratumumab with bortezomib and dexamethasone, or dexamethasone with lenalidomide (Danko et al., 2019).

On the other hand, combination therapies do not come without caveats. Other than obtaining synergistic effects in the best-case scenario, they are also likely to induce combined toxicity (Keefe and Bateman, 2019). One reason for that is to be found in the different pharmacokinetics (PK) of the drugs that are biodistributed, metabolised and eliminated at varying rates. To compensate for these differences in PK, patients are continuously exposed to high doses of all the agents, attempting to achieve a durable inhibition of the targets, but also negatively impacting on healthy tissues as well, ultimately resulting in undesired toxicities (Tolcher and Mayer, 2018). Importantly, the growing number of TCTs with potential for offering prolonged survival to cancer patients supposes a substantial economic challenge to health systems, which could consequently limit their access (Danko et al., 2019, Balik et al., 2019).

Notwithstanding the above, the goal of new combination therapies remains to increase the efficacy of 2 or more drugs against tumour cells, but also reducing any harmful side effects to surrounding healthy tissues (Tolcher and Mayer, 2018). Nanomedicines, in this case, can come to the aid and limit these adverse reactions related to off-target toxicity or even accumulation of high drug doses in the organism. In addition, they can also increase the stability, solubility, bioavailability, PK and selective targeting of their delivered cargo (Matos et al., 2019).

There are several types of nanocarriers, including polymeric, lipid and metal or inorganic nanoparticles (Conniot et al., 2014). Within the lipid nanoparticles, liposomes have shown great promise in the delivery of peptides and proteins like insulin, EGF or IFN- $\gamma$  (Kim et al., 1999, Li et al., 2003, van Slooten et al., 2000).

These nano-sized technologies take advantage of the enhanced permeability and retention (EPR) effect described to happen in tumours. EPR relies on the necessity of cancer cells to uptake nutrients through the formation of new immature blood vessels, characterised by their leakiness, thus helping the accumulation of nanomedicines in the interstitial space (Fathi and Oyelere, 2016). Hence, frequently the drug delivery with liposomes rests upon passive diffusion into cancerous tissues through what is known as “passive targeting” (Olusanya et al., 2018). Another point chalked up for nanocarriers is their potential to coordinately distribute 2 drugs concomitantly, while maintaining the synergistic drug ratio of the

combination. An example of that would be CPX-351, a dual-drug liposomal mixture of cytarabine and daunorubicin approved in 2017 by the FDA for the treatment of acute myeloid leukaemia (AML) patients (Tolcher and Mayer, 2018). Interestingly, the researchers involved in the study in a mouse preclinical model reported an accumulation of the drugs for days in the BM, and more specifically, in the leukaemic cells (Alfayez et al., 2020). These results highlight the importance of delivering the right amount of the correct drug(s), at the right time, to cancerous tissues, to improve the therapeutic effect while reducing the adverse effects at once.

### 1.3 MYC as a key regulator in cancer

*MYC* is one of the most powerful oncogenes found to be deregulated in over half of human cancers (Hann, 2014). The *MYC* gene encodes for a family of basic helix-loop-helix leucine zipper (bHLHZ) TFs, comprised by c-MYC, L-MYC and N-MYC, which conduct partially redundant functions depending on the tissue where they are expressed (Barrett et al., 1992, Nesbit et al., 1998). In order to mediate the many biological processes in which it is involved, MYC forms transcriptionally active dimers with its obligate partner MAX, and together they bind DNA, more precisely sequences known as canonical E-boxes (CACGTG motifs) (Dang, 2012). The physiological functions of MYC include, but are not restricted to, cell proliferation and growth, apoptosis, differentiation, migration, stem cell biology, metabolism and transcriptional control over the non-coding transcriptome (miRNAs and lncRNAs) (Nasi et al., 2001, Soucek and Evan, 2010, Conacci-Sorrell et al., 2014, Stine et al., 2015). Of note, unlike other TFs and signalling molecules, MYC functionality is non-redundant, as demonstrated by the lethality observed in MYC deficient mouse embryos (Davis et al., 1993).

MYC, which is a mostly unstructured protein, displays characteristics of an intrinsically disordered protein (IDP) in its monomeric form in solution. It comprises an unstructured N-terminal transcriptional activation domain (TAD), followed by a canonical nuclear localisation signal and the C-terminal bHLHZ domain, which is mainly unfolded until it dimerises with MAX (Dang, 2012, Stefan and Bister, 2017). Given the extremely central role MYC plays in cell proliferation, its transcription is tightly regulated at the transcription, mRNA and protein levels (Dang, 2012).

Nonetheless, many of the genetic alterations that occur in cancer uncouple *MYC* expression from these usual regulatory constraints: either constitutive activation of signal transduction pathways (e.g. Notch, Wnt, receptor tyrosine kinases) or direct alterations of *MYC*, like point mutations leading to protein stabilisation, amplifications or translocations (Dang, 2012, Schaub et al., 2018) can lead to its deregulated expression. Interestingly, though, deregulation of MYC alone is not always enough to induce tumourigenesis, so that some other genetic alterations are required. The reason is that continuous expression of MYC usually has a dual



effect on healthy tissues, inducing proliferation at first, followed by proliferative arrest, senescence or apoptosis (Gabay et al., 2014, Dhillon and Evan, 2019).

So, how does MYC contribute to tumour initiation and maintenance, then? In order for MYC to drive relentless proliferation, a permissive epigenetic or genetic context that prevents arrest, senescence and apoptosis, is required. Only then, amplified expression of its target genes promotes deregulated entry and exit of the cell cycle, increased cell mass through protein biogenesis, restraint of the host immune response, relentless DNA replication, remodelling of the microenvironment, activation of the angiogenic switch, suppression of the response to autocrine and paracrine regulatory programmes and metabolic rewiring (Figure 6). Hence, MYC activation seems to constitute a molecular hallmark of cancer (Dominguez-Sola and Gautier, 2014, Gabay et al., 2014, Sabo and Amati, 2014, Stine et al., 2015).

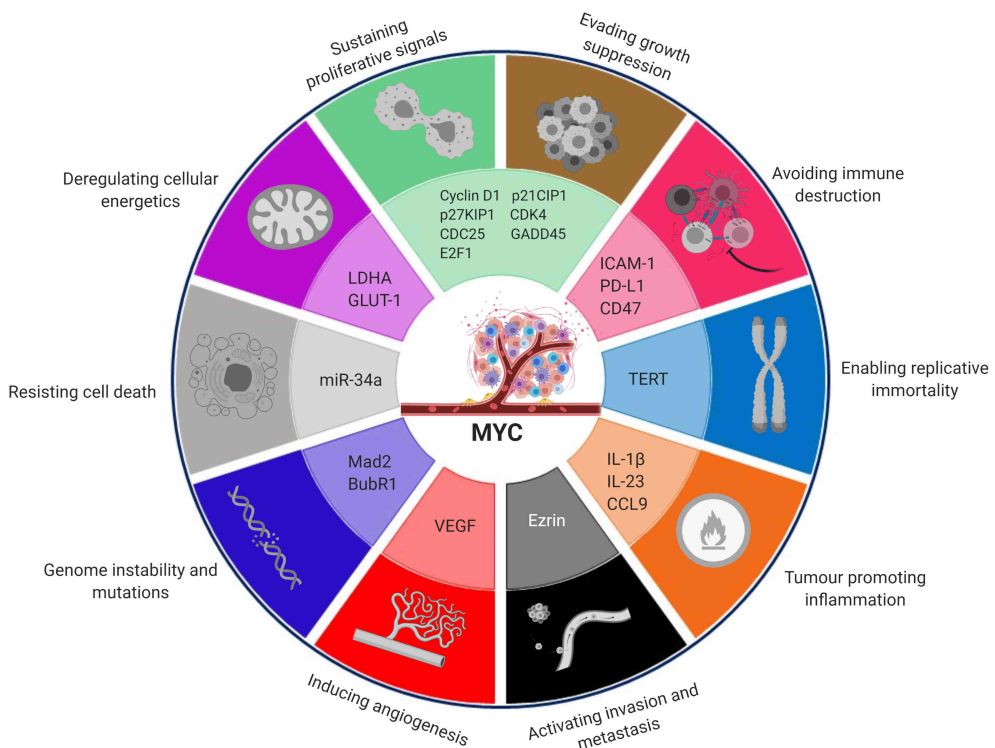


**Figure 6: MYC as a central node in the hallmarks of cancer.** MYC is a TF and master regulator of the expression of around 30% of all human genes. As such, it instructs the differential expression of many genes, contributing to the acquisition of cancer-like properties, as defined by Hanahan and Weinberg (Hanahan and Weinberg, 2011). In the image, there are some examples of these MYC target genes, involved in the tumourigenesis process. However, it is likely for many others to be responsible for the carcinogenesis in each particular tissue. Figure adapted from (Tannock et al., 2013) and created with BioRender.

Many researchers around the world have experimentally confirmed MYC's role in carcinogenesis, in many cases using conditional expression of MYC in different tissues using *in vivo* models, including studies on the reversibility of the process upon MYC withdrawal (Felsher and Bishop, 1999, Pelengaris et al., 1999, Giuriato et al., 2004, Arvanitis and Felsher, 2005). In these studies, suppression of MYC has proven to induce tumour regression not only in those tumours considered MYC-addicted (Felsher and Bishop, 1999, Jain et al., 2002, Pelengaris et al., 2002, Marinkovic et al., 2004) but also in those in which MYC is not the initiating oncogenic lesion (Soucek et al., 2008, Soucek et al., 2013), suggesting that restoration of normal MYC activity through its inhibition would represent an effective treatment for many cancer types.

## 1.4 MYC inhibition strategies

Certainly, there is extensive literature in support of the potential impact that MYC inhibitors would have in the treatment of cancer, and still, there is no such drug available in the clinic yet.

As it happens, MYC is still considered “undruggable”, a term coined for proteins believed not pharmacologically targetable (Dang et al., 2017).

The reasons are multiple:

1. The MYC family comprises 3 potentially-redundant members, as mentioned in 1.3, so that full MYC inhibition would require simultaneous blockade of all 3 at a time.
2. MYC is a mainly unstructured TF, lacking a binding pocket to tamper with, and functions mainly through protein-protein interactions (PPIs), so that targeting it with the classical small molecule therapeutic design is hardly achievable, in part due to their small interacting surface.
3. Its localisation in the nucleus supposes another challenge since the inhibitory compound would need to reach this subcellular compartment to exert its function.
4. Last but not least, given the pivotal role of MYC, not only in tumour biology but also in physiological conditions, inhibition of MYC could potentially cause catastrophic adverse effects in healthy tissues (Whitfield et al., 2017).

However, challenging the dogma, Dr Soucek designed Omomyc, a dominant negative mutant of the bHLHZ of MYC that bears 4 aminoacid substitutions able to change its dimerisation specificity, allowing it to homodimerise and heterodimerise with both MYC and MAX. Given that neither Omomyc nor MAX have a TAD, Omomyc/Omomyc and Omomyc/MAX heterodimers are transcriptionally inactive and able to compete with MYC/MAX dimers to bind DNA, while Omomyc/MYC

dimers are not able to bind DNA, so that MYC is sequestered away from its target sites (Soucek et al., 2002, Savino et al., 2011).

The real shift in paradigm for MYC targeting was made few years later when the authors showed that systemic inhibition of MYC by Omomyc was possible *in vivo*. To do so, Soucek et al. used a construct of Omomyc under the control of a tetracycline response element (TRE) in a lung adenocarcinoma mouse model, to conditionally express it upon addition of doxycycline to the drinking water of mice. In this model, the animals expressed Omomyc in virtually every tissue. Strikingly, upon Omomyc treatment, lung tumours regressed (Soucek et al., 2008) and were eradicated, even in a context in which TP53 was mutated (Soucek et al., 2013).

Importantly, mice only showed mild, well-tolerated and completely reversible side effects in their healthy, physiologically proliferative tissues. Among those mild effects, for example, the authors observed that while the small intestine showed shortened villi, there was no interference in nutrient absorption nor weight loss. In addition, there was no hair regrowth upon shaving, spermatogenesis was temporarily inhibited, and there was a slight thinning of the skin epidermis but without compromising the integrity of the organ. Upon withdrawal of Omomyc treatment, all tissues regained their normal function (Soucek et al., 2008).

Follow-up studies also demonstrated that there was no emergence of resistance to MYC inhibition upon metronomic expression of Omomyc (4 weeks on and 4 off), which extended mouse survival indefinitely and resulted in fewer emergent tumours after each cycle of Omomyc induction (Soucek et al., 2013).

Furthermore, transgenically expressed Omomyc proved to be effective in cancers from different tissue-origin, causing shrinkage of insulinomas (Sodir et al., 2011) and extending the survival of transgenic mice that spontaneously develop gliomas (Annibali et al., 2014) or mice inoculated with patient-derived glioblastoma cells (Galardi et al., 2016).

Up until this point, the Omomyc construct could only be delivered through gene therapy (Fukazawa et al., 2010).

However, thrilled by the potential of MYC inhibition as a feasible therapeutic option, several investigations were or are being conducted to develop drug candidates against this TF. The strategies used can be classified as 1. indirect or 2. direct MYC inhibitors, and are summarised in Figure 7.

### 1.4.1 Indirect MYC inhibitors

Because MYC was “slippery as an eel” target, researchers mostly opted for indirect pharmacological approaches to inhibit it, targeting its transcription, translation or degradation.

## Blockade of *MYC* transcription

### Bromodomain and extra-terminal motif (BET) inhibitors

BET inhibitors (BETis) were unexpectedly found to alter the transcription of the *MYC* gene, which is regulated by BET proteins like BRD4. JQ1, a BETi widely studied for *in vitro* purposes, significantly downregulated *MYC* expression in some specific cellular contexts, causing a reduction in tumour burden and extending the overall survival in an MM mouse model (Delmore et al., 2011). However, the success of BETis in the clinical setting has been limited (take OTX015 as an example), due in part to dose-limiting toxic effects. Besides, BETis also target key transcriptional networks controlled by tissue- and disease-specific enhancer regions. That is the main reason why the transcriptional effects of BET inhibition are highly context-dependent (Cochran et al., 2019). Still, many of these class molecules are being evaluated in Phase I/II clinical trials (e.g. CPI-0610, CC-90010), but not considered as *MYC* inhibitors only (Siu et al., 2017, Moreno et al., 2019).

### Cyclin-dependent kinase 7 (CDK7) inhibitors

The blockade of CDK7 can also downregulate *MYC* expression and reduce mRNA levels, through inhibition of RNA Polymerase II-dependent transcription, by affecting the stability of preinitiation complexes (Kelso et al., 2014). Some studies, for example, demonstrated that THZ1, a covalent CDK7 inhibitor, can indeed suppress master transcription-regulating oncogenes, like *MYC*, in neuroblastoma models (Chipumuro et al., 2014, Kwiatkowski et al., 2014). Thanks to the anti-tumour effect displayed by these molecules, the first covalent CDK7 inhibitor (SY-1365) entered clinical trials in 2017 for the treatment of solid tumours (Hu et al., 2019), while others are being preclinically validated for haematological malignancies (Choi et al., 2019).

## Blockade of *MYC* mRNA translation

### Mammalian target of rapamycin (mTOR) and PI3K inhibitors

mTOR seems to play an essential role in the translation of *MYC* mRNA (Chesler et al., 2006), laying the foundations for inhibition of the PI3K/mTOR pathway as another possible strategy to inhibit *MYC* indirectly. Indeed, several drugs have already been approved (e.g. everolimus, temsirolimus, torkinib) and some others are in earlier clinical developmental stages (e.g. INK128) (Roohi and Hojjat-Farsangi, 2017). Also interesting, the dual PI3K/HDAC inhibitor CUDC-907 showed potent suppressive activity against *MYC*-dependent tumours (Pei et al., 2016, Sun et al., 2017).

## **Blocking eukaryotic translation initiation factors (eIFs)**

In a mouse model of colorectal cancer (CRC) in which mTOR inhibition was unable to impair MYC translation, a different approach was used: targeting of eIF4A with silvestrol, a small molecule inhibitor (Wiegering et al., 2015). Similarly, in a preclinical study of premalignant breast cancer, the authors used a small molecule against the Src kinase, saracatinib, inhibiting the MNK-eIF4E-mediated translation of MYC as well (Jain et al., 2015).

## **Promoting MYC degradation**

MYC is ubiquitinated by ubiquitin ligases, like FBW7, which induce its degradation through the proteasome machinery. Inhibition of deubiquitinases that stabilise MYC (e.g. USP28, USP36) (Sun et al., 2015) or triggering the FBW7-mediated proteasomal degradation of MYC with oridonin (Huang et al., 2012) could both be used as indirect MYC inhibition strategies.

### **1.4.2 Direct MYC inhibitors**

As mentioned before, the MYC protein is hard to target with traditional small molecule drugs due to its large, disordered protein interface and lack of deep pockets. In addition, it is inaccessible to large biologicals, which are often incapable of crossing cell membranes.

## **Direct inhibition of MYC expression**

### **G-quadruplex stabilisation**

G-quadruplexes are 4-stranded DNA structures formed in guanine-rich regions. The MYC promoter happens to have such a structure, which acts as a silencer element, repressing its transcription (Yang and Hurley, 2006). Several studies have shown that some small molecule ligands (e.g. cationic porphyrins, quindolines) can stabilise such G-quadruplexes in the MYC promoter, like CX-33543, resulting in MYC downregulation (Brooks and Hurley, 2010, Brown et al., 2011).

### **Antisense oligonucleotides and small interfering RNA (siRNA)**

A different strategy to inhibit MYC's expression is to promote the degradation of the mRNA, thus preventing it from translation. For this purpose, investigators had used antisense oligonucleotides (INX-3280) (Webb et al., 2001) or antisense oligomers (AVI-4126) (Arora et al., 2000).

Slightly differently, yet with a similar mode of inhibition, the lentiviral delivery of shRNA (Wang et al., 2008) or RNAi encapsulated in a lipid nanoparticle (DCR-MYC) (Tolcher et al., 2015) can also result in the elimination of MYC mRNA. Even

though DCR-MYC reached clinical trials, the efficacy results obtained did not fulfil the expectations of the company that ultimately discontinued its development.

## Direct inhibition of PPIs or binding to DNA

### Peptidomimetics and other small molecule inhibitors against PPIs

Peptidomimetics are small molecules designed to mimic the binding of a peptide sequence to a target (Sorolla et al., 2020). The first inhibitor of the MYC/MAX interaction, ILA6B17, was identified after screening a 7000 molecule peptidomimetic library and demonstrated to suppress the growth of MYC-transformed chicken embryo fibroblasts (although it was suggested to be slightly unspecific since it could inhibit Jun-induced transformation as well) (Berg et al., 2002).

In 2003, Yan et al. screened 10000 compounds from the ChemBridge DIVERSet library and identified 7 inhibitors able to interfere with the dimerisation of MYC and MAX, among those, 10058-F4 and 10074-G5 significantly reduced the cell growth of MYC-transformed rat fibroblasts (Yin et al., 2003). However, both molecules were rapidly metabolised, preventing their use *in vivo* (Fletcher and Prochownik, 2015).

Further screens identified more PPI inhibitors such as Mycro3 and KJ-Pyr-9 with improved pharmacokinetics, bioavailability and overall *in vivo* activity, demonstrating efficacy in mouse models of pancreatic and breast cancers respectively (Kiessling et al., 2007, Hart et al., 2014).

### DNA binding inhibitors

Some research groups have instead targeted the binding of MYC, MAX or their dimers, to DNA, using small molecules like MYRA-A or KSI-3716 (Mo and Henriksson, 2006, Jeong et al., 2014), or with peptides and mini-proteins, known to have increased selectivity and affinity, as well as lower toxicity. An example of a peptide is H1, a 14 amino acid peptide derived from the helix 1 C-terminal region of MYC itself (Giorello et al., 1998). In subsequent studies, the H1 peptide was administered using a targeted delivery or given in combination, sequentially after docetaxel, to improve its efficacy (Bidwell et al., 2013, Li et al., 2016).

Montagne et al. made use of the bHLHZ domain of MAX as a different therapeutic agent to inhibit MYC. This peptide proved to transduce into cells and, as a MAX homodimer, compete with the binding of MYC/MAX to DNA (Montagne et al., 2012). Similarly, Beaulieu and colleagues recently demonstrated that the purified Omomyc mini-protein could also behave as a cell-penetrating peptide, translating the transgenic Omomyc construct from a MYC inhibition proof-of-principle into a pharmacological approach (Beaulieu et al., 2019).

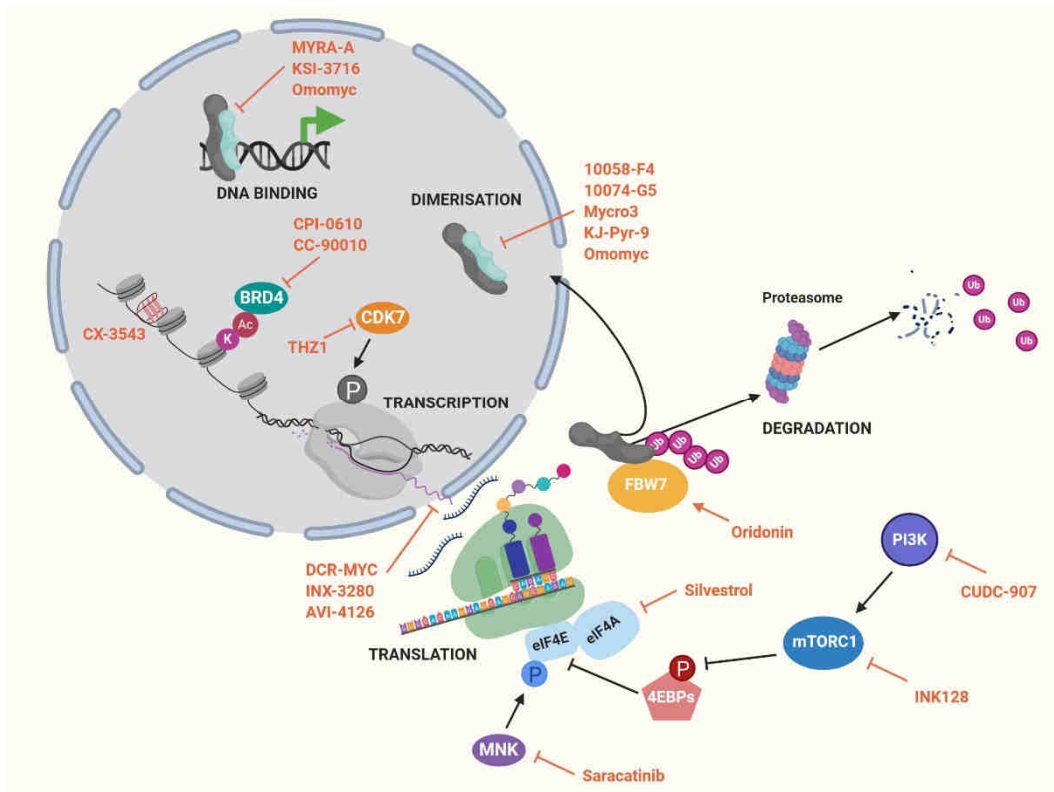


**Figure 7: MYC inhibition strategies at different levels of its life cycle.** Some examples of the various drugs used to interfere with MYC are listed. For more details, see text. Figure adapted from (Koh et al., 2016) and created with BioRender.

In their publication, the authors showed that the recombinantly-produced Omomyc mini-protein is shown to conserve, at least in part, the mechanism of action described for the transgenically-expressed Omomyc, in that it can form homodimers and heterodimers with MYC and MAX and thus act as an inactive competitor (Omomyc/Omomyc or Omomyc/MAX) for DNA binding or promote the removal of MYC from E-boxes (Omomyc/MYC). The Omomyc mini-protein exerted potent interference with MYC which, upon Omomyc treatment, appears displaced from its target promoters on DNA. This results in the downregulation of several cancer-relevant transcriptional programmes.

Consistently, the mini-protein blocked the growth of lung tumours upon intranasal and intravenous administration and displayed therapeutic superiority when compared to a standard chemotherapeutic drug (paclitaxel). In fact, when administered in combination (Omomyc + paclitaxel), the two drugs confer to mice a significant survival advantage compared to the other treatment groups (Beaulieu et al., 2019).







## HYPOTHESIS AND OBJECTIVES

### Hypothesis

MYC is often deregulated in MM and BL. Thus, we hypothesise that treatment with novel anti-MYC therapeutic strategies will be efficacious for both diseases.

In this thesis, we tested 2 different anti-MYC approaches:

1. New compounds based on small molecule strategies developed by our collaborators. These compounds target intrinsically disordered proteins (IDPs).
2. Anti-MYC cell-penetrating mini-proteins: a) Omomyc: a dominant negative mutant form of the MYC bHLHLZ domain, which acts as a direct inhibitor of MYC activity, and b) a designed variant form of it, termed V26.

We aimed to ultimately validate these strategies against MYC *in vivo*, predicting their efficacy in MM and BL and reinforcing the notion that MYC is a key therapeutic target in cancer.

### Objectives

#### Strategy 1: Peptidomimetics (causing MYC degradation)

- Confirmation of the *in vitro* activity of the molecules
- Evaluation of the compounds' safety and efficacy in murine myeloma models

#### Strategy 2: Anti-MYC cell-penetrating mini-proteins (direct disruptors of the MYC-MAX dimer)

- Characterisation of the *in vitro* applicability of Omomyc mini-protein for the treatment of myeloma and lymphoma
- Evaluation of the therapeutic potential of Omomyc mini-protein in animal models of myeloma and lymphoma
- Engineering of improved formulations or use of combination approaches to overcome biodistribution limitations
- Characterisation of a derivative of Omomyc's mini-protein sequence, V26, as a potential example of second-generation MYC inhibitors.



## MATERIALS AND METHODS

### 2.1 Cell lines

The human MM cell lines (U266, RPMI-8226, KMS-12-BM, and NCI-H929) were a kind gift from Dr Valentina Caputo and Prof Anastasios Karadimitris. Dr Babatunde Oyajobi kindly gifted the mouse cell line (5TGM1-eGFP). CA46, Raji, and H1299 cells were purchased from the ATCC. All cells were grown in RPMI culture medium (Life Technologies) supplemented with 10% of FBS and 1% of glutamine for the experiments (complete medium).

All cells were maintained in a humidified incubator at 37°C and 5% CO<sub>2</sub>. To freeze cells, 5% DMSO was added to the supplemented medium, cell vials were placed in a Mr Frosty™ freezing container (Thermo Fisher) with isopropanol, and maintained at -80°C for at least 48 hours. Then, cells were transferred to liquid nitrogen.

To thaw cells, vials were placed into a water bath at 37°C until their contents were completely melted, then transferred to 40 mL of unsupplemented medium and centrifuged at 1200 rpm for 5 minutes to remove the DMSO. Finally, cells were plated in 10 mL of the complete medium into a T25 flask (EasYFlasks™ Nunc™; Thermo Fisher) and kept upside down. The complete medium was RPMI 10% FBS/1% glutamine for all cell lines except for CA46 and NCI-H929 (20%FBS) and 5TGM1-eGFP (IMDM 10% FBS).

All cell lines were tested mycoplasma free (MycoAlert™; Lonza) or cleaned using ciprofloxacin.

### 2.2 Omomyc mini-protein and derivatives production

The protein production platform from Peptomyc S.L. took care of the Omomyc and Omomyc-derived mini-proteins production according to their in-house protocols. Maleimide conjugation with AF488 (Invitrogen) or BDP 650/665 (Lumiprobe) moieties to the unique C-terminal cysteine residue of Omomyc or variant 26 was performed according to the manufacturers' indications. The fluorescently labelled mini-proteins were purified from any free labelling agent.

## 2.3 Buffer recipes

In the following table, it is detailed the composition and name of the buffers used for the different techniques (Table 1).

Buffer	Technique/Assay	Composition
<b>RIPA</b>	Western blot (WB)	1% Triton X-100, 0.5% sodium deoxycholate, 0.1% SDS, 50 mM HEPES pH 7.4, 150 mM NaCl and 5 mM EDTA
<b>Laemli (6x)</b>	Western blot (WB)	375 mM Tris-Cl pH 6.8, 12% SDS, 60% glycerol, 0.06% bromophenol blue and 0.6 M DTT
<b>Red solution</b>	Western blot (WB)	5% BSA, 0.02% NaN <sub>3</sub> , PBS 1x and phenol red (pH 7.5)
<b>SDS lysis</b>	ChiP	100 mM NaCl, 50 mM Tris-Cl pH 8.1, 5 mM EDTA pH 8, 10% SDS and 0.02% NaN <sub>3</sub>
<b>Triton dilution</b>	ChiP	100 mM NaCl, 100 mM Tris-Cl pH 8.6, 2.5 mM EDTA pH 8, 5% Triton X-100 and 0.02% NaN <sub>3</sub>
<b>Mixed micelle</b>	ChiP	150 mM NaCl, 20 mM Tris-Cl pH 8.1, 5 mM EDTA pH 8, 65% sucrose, 20% Triton X-100 and 10% SDS and 0.02% NaN <sub>3</sub>
<b>500</b>	ChiP	0,1% sodium deoxycholate, 1 mM EDTA pH 8, 50 mM HEPES pH 7.5, 500 mM NaCl, 1% Triton X-100 and 0.02% NaN <sub>3</sub>
<b>LiCl detergent</b>	ChiP	0.5% sodium deoxycholate, 1 mM EDTA pH 8, 250 mM LiCl, 0.5% NP-40, 10 mM Tris-Cl pH 8 and 0.02% NaN <sub>3</sub>
<b>TE</b>	ChiP	10 mM Tris-Cl pH 8 and 1 mM EDTA pH 8
<b>Carbonate/bicarbonate</b>	ELISA	0.05 M sodium carbonate/bicarbonate pH 9.6
<b>Blocking</b>	ELISA	50 mM Tris-Cl, 0.14 M NaCl and 1% BSA, pH 8
<b>Wash</b>	ELISA	50 mM Tris-Cl, 0.14 M NaCl and 0.05% Tween 20, pH 8
<b>Sample/conjugate diluent</b>	ELISA	50 mM Tris-Cl, 0.14 M NaCl, 1% BSA and 0.05% Tween 20
<b>Stop solution</b>	ELISA	0.18 M H <sub>2</sub> SO <sub>4</sub>
<b>Citrate</b>	Immunofluorescence (IF)	10 mM sodium citrate and 0.05% Tween 20, pH 6
<b>Tris/EDTA pH 9</b>	Immunohistochemistry (IHC)	10 mM Tris-Cl, 1 mM EDTA and 0.05% Tween 20, pH 9
<b>PBST</b>	WB, IF, IHC	PBS 1x with different concentrations of Tween 20 (0.1% WB, 2% IF or 0.05% IHC)
<b>Encapsulation</b>	Liposome production	10 mM HEPES and 9% sucrose, pH 7.4

**Table 1: Buffers used for different techniques.**

## 2.4 Cell culture experiments

### 2.4.1 Proliferation

Cells were seeded at different densities (depending on their growth rate) in a 24 well plate. The day after Omomyc mini-protein or V26 were added at 20 or 10  $\mu\text{M}$  or kept untreated as a control. The total number of live and dead (trypan blue positive) cells was determined after 5 days with the Vi-CELL™ Cell Counter (Beckman Coulter).

### 2.4.2 IC<sub>50</sub> calculations

For the experiments with peptidomimetic compounds, first, we reconstituted the lyophilised powder with the appropriate amount of PBS to obtain a 1 mM solution. 10000 cells were plated per well in 96 well plates. Next, we treated the cells with increasing concentrations (1, 5, 10, 15, 20, and 100  $\mu\text{M}$ ) for 3 days. For the experiments with Omomyc derived mini-proteins, cells were treated for 5 days with the following concentrations (40, 20, 10, 5, 2.5, 1.25, 0.63, 0.31, and 0.16  $\mu\text{M}$ ).

Cell viability was assessed at the end of the experiment using alamarBlue™ (Thermo Fisher). The reagent was directly added to the well using a 1:10 dilution, according to the manufacturer's instructions. The plate was then incubated at 37°C for ~4h to allow cells to metabolise the resazurin. Finally, the fluorescence signal was measured at excitation/emission of 530/590 nm with a Spark® microplate reader (Tecan) and made relative to the untreated control. IC<sub>50</sub> was calculated using GraphPad Prism 6.

### 2.4.3 Cell cycle

Cells were plated in 24 well plates and treated with Omomyc derived peptides at 20  $\mu\text{M}$  or untreated for 3 days. Cells were then collected, washed with PBS, and centrifuged (1200rpm at 4°C).  $1 \times 10^6$  PBS-washed cells were pelleted in a 1.5 mL tube. The pellet was resuspended in 0.875 mL of cold PBS. Next, 0.125 mL of cold 2% paraformaldehyde solution was added, and the mixture was vortexed immediately. The samples were incubated at 4°C for 1 hour, centrifuged for 5 min at 250 g, and the supernatant was decanted. The fixed cell pellet was gently resuspended in 1 mL of 0.2% Tween 20 in PBS at room temperature (RT). The mixture was incubated for 15 min at 37°C (Schmid et al., 1991). Cells were washed and incubated for 30 minutes with propidium iodide (PI) solution: 25mg/L of PI + Triton X-100 1:1000 in PBS. PI intensity was measured by cell cytometry (Navios, Beckman Coulter). Analysis and representation of the cytometry results were done either using FCS Express v4 software (De Novo Software, Los Angeles, CA, USA).

### 2.4.4 Migration assay

U266 and CA46 cells were plated in complete medium in the presence or absence of 20  $\mu\text{M}$  of Omomyc mini-protein. After 5 days, cells were washed with PBS and counted with the Vi-CELL™ Cell Counter (Beckman Coulter). 1 million cells/well were seeded on top of 6.5 mm Transwell® (5.0  $\mu\text{m}$  pore polycarbonate membrane) inserts in 300  $\mu\text{L}$  in a 24 well plate. Cells were seeded in 5 replicates, in complete medium in the upper chamber, while the lower chamber was filled with 600  $\mu\text{L}$  of complete medium +/- CXCL12 (100 ng/mL). After 4 hours, cells at the bottom chamber were collected, washed with PBS, centrifuged, and counted using Tali™ Image-based Cytometer (Life Technologies).

### 2.4.5 Synergy

Similarly to the assay performed to calculate the  $\text{IC}_{50}$  values (2.4.2), 10000 U266 and 1000 5TGM1 cells were plated per well in 96 well plates. The day after, cells were treated as exemplified in Figure 8. After 5 days of treatment, the cell viability was measured using alamarBlue™ as previously described and the therapeutic effect exerted by each combination of drug concentrations (B2-F10), Omomyc alone (B11-F11) or by CFZ alone (G2-G10) was made relative to the untreated control (G12). The effect was considered synergistic when the experimental inhibitory value obtained was smaller than that of the arithmetic sum of either individual compound (additive effect) plus the standard deviation of the 2 independent biological experiments performed for each combination of concentrations.

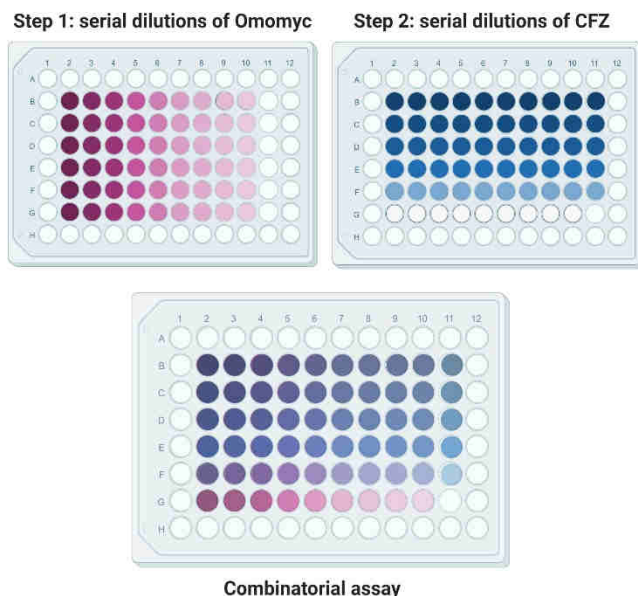


**Figure 8: Scheme of the assay used to assess the synergy between 2 drugs.** Omomyc highest starting concentration was 40  $\mu\text{M}$  (column 2), following serial dilutions to the right. CFZ highest concentration was 20 nm (row B) following serial dilutions to the bottom. The final plate shows the mixture at different concentrations in which each well has a unique combination, while the G row is only CFZ treated and the 11<sup>th</sup> column is only Omomyc-treated. Figure created with BioRender.

## 2.5 Western blot analysis

Cells were either treated with Omomyc mini-protein or untreated for 3 or 5 days. Cells were washed with PBS, centrifuged, and resuspended in 1 mL of trypsin-EDTA at 0.25% (Gibco) and incubated at 37°C for 30 minutes to remove any extracellularly bound Omomyc. Then, trypsin was inactivated with supplemented medium. The pellet was resuspended in 1mL of cold PBS, transferred into a 1.5 mL tube and centrifuged at 1200 rpm, the supernatant removed, and the pellet was quickly frozen using dry ice and stored at -80°C.

The frozen pellet was resuspended in the appropriate volume of cold RIPA buffer complemented with a Halt Protease Inhibitor Cocktail (Thermo Fisher) to obtain 20k cells/ $\mu$ L. Samples were incubated on ice for 15 minutes, to disrupt the cell membrane, then centrifuged at 4°C at maximum speed (13000 rpm) to separate insoluble cell debris from soluble components. The pellet was discarded, and supernatant kept on ice. Laemmli buffer 6x was added to the samples to obtain a 1x solution.

Equivalent cell numbers of each sample or 7  $\mu$ L of molecular marker (Precision Plus Protein™ Dual Color Standards, Bio-Rad) were loaded in 12%, 15-well NuPAGE Bis-Tris precast gels (Thermo Fisher). For electrophoresis, XCell SureLock Electrophoresis Cell (Thermo Fisher) was used, and gels were run at 170 volts for 50 minutes in NuPAGE MES SDS running buffer (Thermo Fisher). Gel cassettes were disassembled, and gels incubated in 20% ethanol for 5 minutes. For the transfer, we used an iBlot 2 Gel Transfer Device (Thermo Fisher) and the nitrocellulose iBlot 2 transfer stacks (consumable stacks, already containing all the adequate components for the transferring). The gels (pre-incubated in ethanol) and blotting paper were soaked in ddH<sub>2</sub>O before being placed within the sandwich in the stack. Next, we run the P0 default programme.

Afterwards, the membranes were stained with Ponceau S (Bio-Rad). The stained membranes were scanned and used as a protein loading control. Membranes were then washed with PBS-Tween (PBST) until complete removal of the staining, then blocked for 1 hour in PBST + 5% milk (Panreac Applichem). Membranes were washed 3 times before overnight incubation with the primary antibody.

Primary antibodies were diluted in red solution and used at the concentrations described in Table 2. The next day membranes were washed 3 times and incubated for 1 hour with secondary antibodies (according to the host species of the primary) conjugated to horseradish peroxidase (HRP) diluted in PBST + 5% milk (concentrations in Table 2). Membranes were washed again thrice before detection using Pierce™ ECL Western Blot Substrate (Thermo Fisher). Chemiluminescent signal was detected using an Amersham™ Imager 600 (GE Healthcare Life Sciences) and images quantified using ImageJ ([Schindelin et al., 2012](#)).



Primary antibodies			
Target	Dilution WB	Antibody (clone)	Supplier
c-MYC	1:5000	Y69	Abcam
c-, L- and N-MYC	1:1000	EPR18863	Abcam
MAX	1:500	C-17	Santa Cruz Biotechnology
Omomyc	1:6000	M2 (21-1-3)	Proprietary Ab from Biogenes
Actin	1:25000	A5441	Sigma
VLA-4	1:1000	EPR1355Y	Abcam
Secondary antibodies			
Target	Dilution WB	Antibody (clone)	Supplier
Mouse IgG	3,513888889	NA931	GE Healthcare
Rabbit IgG	3,513888889	NA934V	GE Healthcare

**Table 2: Primary and secondary antibodies used for immunoblotting.**

## 2.6 ChIP-qPCR

U266 and Raji cells were seeded at 1 million/mL in T25 flasks and treated with Omomyc mini-protein 20  $\mu$ M for 3 or 5 days. Next, the medium was removed, and cells were cross-linked with 1% formaldehyde solution in PBS for 10 minutes (2 million cells/mL). Glycine (0.125 M) was added to the formaldehyde and incubated for 5 minutes to quench. Then cells were washed twice with PBS, centrifuged, and the pellet resuspended in 5 mL of SDS lysis buffer and frozen at  $-80^{\circ}\text{C}$ .

For the double cross-link protocol, we added an extra step before fixation with formol. First, cells were fixed at 4 million/mL with DSG (2 mM, Thermo Fisher) and incubated for 45 minutes in a rotating wheel at RT. Then, we continued with the ChIP protocol for fixation as usual (see paragraph above).

Cells were centrifuged 10 minutes at 2000 rpm and the pellet resuspended in 3 mL of IP buffer (1 volume of SDS lysis buffer + 0.5 volumes of Triton dilution buffer supplemented with a protease inhibitor cocktail (Halt<sup>TM</sup>, Thermo Fisher)) before sonication (fragmentation of DNA in 100-400 base pairs pieces) using a Bioruptor (Diagenode). Next, we quantified protein concentration using DC<sup>TM</sup> Protein Assay (Bio-Rad), and the absorbance was measured at 750 nm using a Spark<sup>@</sup> microplate reader (Tecan). Then, we pipetted 500  $\mu$ g of protein per MYC or Omomyc IP and 100  $\mu$ g for histones and histone marks, keeping 10% as the INPUT.

We incubated our sample lysates with the primary antibody of choice and their corresponding isotypes as a control as described in Table 3. The protein/chromatin-antibody complex was allowed to form overnight (O/N) at  $4^{\circ}\text{C}$  in a rotating wheel, and at the same time, the Protein A dynabeads (Thermo Fisher) were blocked with 0.5% BSA (VWR).

Primary antibodies (ChIP)				
Target	Antibody ID or clone	Source/Isotype	$\mu\text{g}/500 \mu\text{g}$ of protein	Supplier
c-MYC	D3N8F	Rabbit IgG	3	Cell Signaling
c-, L- and N-MYC	EPR18863	Rabbit	3	Abcam
Omomyc	M2 (21-1-3)	Mouse IgG2a,k	3	Proprietary Ab from Biogenes
Rabbit IgG	ab171870	-	3	Abcam
Mouse IgG	MOPC-31C	-	3	BD Biosciences
Target	Antibody ID or clone	Source/Isotype	$\mu\text{g}/100 \mu\text{g}$ of protein	Supplier
Histone H3	ab1791	Rabbit	1	Abcam
H3K27ac	CMA309	Mouse IgG1	1	Millipore
H3K4me3	07-473	Rabbit	1	Millipore
H3K9me3	07-442	Rabbit	1	Millipore
Rabbit IgG	ab171870	-	1	Abcam

**Table 3: Primary antibodies and isotypes used for ChIP experiments.**

The day after, the protein lysates were centrifuged at 13000 rpm for 20 minutes to remove any aggregates formed during the O/N incubation. Then, the lysates were incubated with the blocked dynabeads for 3 hours at 4°C in a rotating wheel, after which the beads were washed twice with mixed micelle buffer, buffer 500, LiCl detergent buffer and TE buffer. Lastly, the protein-chromatin complexes were eluted and reverse crosslinked from the dynabeads and antibodies by incubation with 2% SDS in TE at 65°C O/N.

To purify the chromatin eluted, the samples were purified using a PCR purification kit (Qiagen) according to the manufacturer's protocol, and the columns were eluted with 60  $\mu\text{L}$  of nuclease free water (Ambion).

Primer	Sequence
Chr8 F	GGCAAGGAAGAGCAAGTCAC
Chr8 R	TTCCCACATGTCGTGAAAGA
IFRD2 F	CGTGCCCCAGCAGTCATT
IFRD R	GCAGTGGGCAGCGAGC
MYBL2 F	GGTCTTCGCTATGTGGGATAC
MYBL2 R	GCTACTTCGGAGTTGTGGAG
Ncl F	CTACCACCCTCATCTGAATCC
Ncl R	TTGTCTCGCTGGGAAAGG
Npm1 F	CACGCGAGGTAAGTCTACG
Npm1 R	TTCACCGGGAAGCATGG
PVT1 F	CACCTTCCAGTGGATTTCT
PVT1 R	GGAAGTACTGGAGGGCAGA

Samples were next analysed by qPCR. To do so, the DNA was mixed with PerfeCTa SYBR® Green SuperMix (Quantabio) and the primers corresponding to each promoter region of our MYC target genes of interest (Table 4). Samples were loaded in triplicates in 384 well plates, and the qPCR run in a 7900HT Fast Real-Time PCR System (Thermo Fisher). The analysed results were represented using GraphPad Prism 6.

**Table 4: Primers used for qPCR after ChIP.**

## 2.7 ELISA

To analyse the levels of IgE or IgG2b (used as surrogate markers of tumour burden) present in the serum of mice bearing myeloma we used human (IgE) and mouse (IgG2b) ELISA quantitation sets (Bethyl Laboratories) and followed the manufacturer's instructions. Briefly, the blood was centrifuged at 10000 g for 5 minutes and the sera collected and aliquoted.

ELISA 96 well plate wells were coated with 100  $\mu$ L of the primary capture antibodies diluted in carbonate/bicarbonate buffer and incubated 1 hour at RT. They were then blocked for 30 minutes with 200  $\mu$ L of blocking buffer per well. The serum was added at variable dilutions (in sample diluent) depending on the experimental time-point of analysis (ranging from 1:50 to 1:200000). Each ELISA was run including a standard curve. Samples were incubated in duplicates at RT for 1 hour, then washed with wash buffer. Next, the secondary detection antibody (conjugated to HRP and diluted in conjugate diluent) was incubated for another hour, washed, and finally, the plate was revealed with TMB substrate, and the reaction stopped with the stop solution. Finally, the absorbance was measured at 450 nm using a Spark® microplate reader (Tecan). The analysis was done graphing the standard curve as a 4-parameter curve fit using GraphPad Prism 6 and interpolating the unknown mouse sera samples.

## 2.8 Immunofluorescence and immunohistochemistry

To check the entrance of V26, H1299 cells were seeded on a Millicell EZ SLIDE 8 well glass slide (Millipore), treated with vehicle or 20  $\mu$ M V26-AF488 for 4 hours, and washed with sodium acetate (NaAc, 25 mM) to remove membrane- and glass-bound mini-protein. Immediately after, cells were washed twice with PBS, stained with 10  $\mu$ g/mL Hoechst 33342 trihydrochloride, trihydrate (Thermo Fisher) for 5 minutes, washed twice with PBS, mounted using Vectashield mounting medium (Vector Laboratories), and analysed. Confocal microscopy images of the live cells were captured using a Nikon C2+ confocal microscope and NIS-elements software.

To perform immunofluorescence on tissue sections, femurs were introduced in tissue cassettes and fixed in a beaker containing 4% formaldehyde for 24 hours and transferred into 70% ethanol for 1 week (to allow acquisition of *ex vivo* images with the mCT). Next, the bones were decalcified in 8% EDTA pH 8 for approximately 2 weeks at 37°C. Once the tissue was soft, the samples were paraffin-embedded, cut, and placed on microscope slides. Slides were heated at 65°C overnight and let cool down before proceeding with the deparaffinisation. To dewax, samples went through the subsequent washes, during 5 minutes each: xylene (x2), ethanol 100% (x2), ethanol 95% (x2), ethanol 70%, and H<sub>2</sub>O.

For the antigen retrieval, slides were introduced in citrate buffer and boiled in a microwave (20 minutes at 400 watts). Buffer and samples were left to recover at RT for around 30 minutes. Slides were washed with PBS twice, permeabilised using PBST 2% for 30 minutes, and washed again. Then, samples were blocked using protein block (Agilent) for 1 hour. Where applies, the mouse tissues were blocked with Goat F(ab) (ab6668, Abcam) diluted in Dako REAL Antibody Diluent (Agilent) at 1:1000 for 1 hour at RT. After washing, the primary antibody anti-Omomyc M2 (in-house/Biogenes) was added to Dako REAL Antibody Diluent at 1:100. Next, the slides were placed in a wet chamber. Each tissue section was covered with 120  $\mu$ L of antibody, and parafilm used to help spread it. Samples were incubated overnight at 4°C, then washed with PBS. The secondary antibody (anti-mouse AF488, Invitrogen) was mixed 1:500 in Dako REAL Antibody Diluent, and the incubation process of the primary antibody was repeated with the secondary. Samples were incubated for 1 hour at RT and protected from light. Slides were then washed and tissue sections covered by coverslips using mounting medium with DAPI (Abcam). Slides were left to dry at RT for at least 5 hours, and the fluorescent signal was analysed in the confocal microscope. Confocal microscopy images were captured using a Nikon C2+ confocal microscope and NIS-elements software.

To perform immunohistochemistry on tissue sections, as for IF, the soft organs were fixed in 4% formol in individual cassettes and transferred to 70% ethanol after 24 hours, while bones had to be decalcified prior to paraffin embedding. Adhesion of tissues to the slide and dewaxing were done the same way as for IF.

The antigen retrieval for IHC was done with Tris/EDTA pH 9. Next, the endogenous peroxidase was blocked with hydrogen peroxide 3% diluted in methanol and incubated 10 min at RT. Tissue sections were then washed with PBST 0.05% and blocked with commercial protein block (Agilent) for 30 minutes and an extra blocking step with Goat F(ab) anti-mouse H&L (Abcam) 1:1000 for 1 hour at RT was included to reduce the background of mouse on mouse detection. After washing, samples were incubated with primary antibody (ready to use CD79 $\alpha$ , Dako Omnis) for 1 hour at RT. Samples were washed and incubated with secondary Envision rabbit/mouse HRP kit (Agilent) for 40 min. Lastly, the slides were washed and developed with DAB chromogen and substrate buffer (Agilent). The reaction was stopped with distilled water after 6 min of incubation. Samples were then counterstained for 10 seconds with hematoxylin, followed by dehydration (5 minutes of incubation in the graded alcohols until reaching xylene). The slides were mounted with mounting medium (Agilent) and evaluated under an optical microscope. The stained tissues were scanned using a NanoZoomer 2.0-HT (Hamamatsu Photonics, Japan) and analysed using the QuPath software v0.1.2.

## 2.9 Flow cytometry analysis

### 2.9.1 Entrance and endocytosis inhibition

For the entrance experiments, U266, Raji and CA46 cells were treated with buffer (25 mM NaAc 2 M urea), 0.64  $\mu$ M, 3.2  $\mu$ M, 6.4  $\mu$ M or 12.8  $\mu$ M of Omomyc-AF488 for 15 minutes. In order to ensure that the fluorescent signal detected was exclusively intracellular, cells were trypsinised for 30 minutes with 0.25% trypsin-EDTA (Gibco) at 37°C before their acquisition in the flow cytometer (Navios, Beckman Coulter).

For the endocytosis inhibition experiments, U266 and CA46 cells were plated in 12-well plates at 500000 cells per well. The following day, cells were pretreated for 1 hour with endocytosis inhibitors: 2 mM of blebbistatin (Sigma), 70  $\mu$ M of 5-ethylisopropylamiloride (EIPA, Sigma) and 5  $\mu$ M of cytochalasin D (Sigma) macropinocytosis inhibitors; 150  $\mu$ M of chlorpromazine (Sigma) and 67  $\mu$ M of dynasore (Abcam), clathrin inhibitors; 150  $\mu$ M of genistein (Sigma), a caveolae inhibitor and 23.4 mM of methyl- $\beta$ -cyclodextrin (Sigma), a lipid-raft disruptor; or at 4°C as a control for inhibition of ATP-dependent endocytosis. Then, cells were incubated with 0.64  $\mu$ M of Omomyc-AF488 for 15 minutes, followed by trypsinisation (for extracellular removal of Omomyc) and acquired with the flow cytometer (Navios, Beckman Coulter). The percentage of inhibition was calculated relative to the untreated control.

### 2.9.2 Tumour burden from bone marrow flush

At the end of the mouse *in vivo* myeloma experiments, we flushed the contents of the BM for flow cytometric analysis of tumour burden and proliferative status of the myeloma cells colonising it, using the antibodies described in Table 5.

To do so, we inserted a 30xG needle plunged into a 1 mL syringe and washed both the femur and tibia from both ends with 1.5 mL of PBS several times (until the appearance of the bone was completely white). Then, the contents were centrifuged at 1200 rpm and counted using a Tali™ Image-based Cytometer (Life Technologies). To study the proliferative status of CD138 positive myeloma cells, we used intracellular markers (Ki67 and PHH3) that require the permeabilisation of membranes. For that, we used the commercial kit Foxp3/Transcription Factor Staining Buffer Set (eBioscience).

1. 1 million cells were transferred to a cytometer tube and stained with fixable viability stain (FVS510, BD Biosciences) for 15 minutes at RT protected from light (from the rest of the protocol on).
2. Cells were washed with PBS-azide, centrifuged at 1500 rpm for 5 minutes, and the supernatant decanted leaving 50  $\mu$ L of volume.
3. The pellet was resuspended and the Fc receptors blocked with anti-CD16/32 (BioLegend) for 10 minutes at RT.

4. The samples were washed again and incubated for 20 minutes at 4°C with anti-CD138 or the isotype control for surface staining.
5. Cells were washed with PBS-azide, centrifuged at 1500 rpm for 5 minutes and the supernatant discarded.
6. The cell pellets were fixed and permeabilised using the Fix/Perm solution according to the manufacturer's protocol for 30 minutes at 4°C, followed by washing with 2 mL of the permeabilisation solution.
7. Anti-Ki67 and anti-PHH3 were added and left to incubate for 30 minutes at 4°C.
8. Finally, samples were washed with the wash/perm buffer and resuspended in PBS-azide before acquisition in the flow cytometer (Navios, Beckman Coulter).

Data were analysed using FCS Express v4 software.

Antibody	Isotype	Clone	Supplier
AF647 anti-human CD138	Mouse IgG1, k	MI15	BioLegend
AF488 anti-human Ki67	Mouse IgG1, k	Ki-67	BioLegend
PE anti-human phospho histone H3 (Ser 10)	Mouse IgG2b, k	11D8	BioLegend

**Table 5: Antibodies used to determine tumour burden and proliferative status of myeloma cells in the BM.**

## 2.10 Circular dichroism

Circular dichroism measurements were performed on a Jasco J-810 spectropolarimeter equipped with a Jasco Peltier-type thermostat. The instrument was calibrated with an aqueous solution of d-10(+)-camphor-sulfonic acid at 290.5 nm. Protein samples were prepared in 50 mM KH<sub>2</sub>PO<sub>4</sub>, 50 mM KCl, 1 mM tris(2-carboxyethyl)phosphine (TCEP) pH 6.8, and incubated 24 hours at RT to ensure reduction and equilibrium, and then loaded into quartz cuvettes of 0.1 cm pathlength. Far-UV spectra were recorded at 25°C by averaging 3 scans at 0.1 nm intervals. Thermal denaturations were recorded at 222 nm from 25°C to 95°C with a heating rate of 2°C/min and a bandwidth of 1.0 nm

## 2.11 Liposomes production

1,2-dipalmitoyl-sn-glycero-3-phosphocholine (DPPC, Avanti), 1,2-dioleoyl-sn-glycero-3-phosphoethanolamine (DOPE, Avanti), and cholesteryl hemisuccinate (CHEMS, Avanti) dissolved in chloroform were mixed in a round-bottom flask to obtain the desired formulation. Such formulation was chosen based on the data previously generated by our lab in which several formulations with different combinations of lipids were used and is described in detail in (Jauset González, 2018).

Chloroform was evaporated in a rotary evaporator creating lipid films at the bottom of the flasks, which were left overnight in a freeze dryer to eliminate residual chloroform. 100  $\mu$ M (or 1 mg/mL) of Omomyc mini-protein (or 90  $\mu$ M of Omomyc mini-protein + 10  $\mu$ M of Omomyc-AF488 when specified) were dissolved in encapsulation buffer and the mixture used to hydrate the lipid films. The flasks were gently agitated and ultrasonicated to dissolve the lipids completely, allowing the formation of multilamellar vesicles. Resulting liposomes went through 5 cycles of freeze-thaw. At this point, an aliquot of liposomes was collected, named before extrusion (BE) and the size distribution of the nanoparticles measured.

Then, liposomes were extruded through 200- followed by 100- nm membranes to obtain a homogeneous population of liposomes, after which another aliquot of liposomes was collected (after extrusion or AE) for size measurement.

Next, we added 1,2-Distearoyl-sn-glycero-3-phosphoethanolamine-N-(methoxy (polyethylene glycol)-2000) (PEG2000-PE, Avanti) to a round-bottom glass tube (2% of the total amount of lipids) and chloroform was evaporated using nitrogen gas. The tube was next placed in a vacuum chamber for 2 hours. Extruded liposomes were added into the tubes containing PEG2000-PE and incubated overnight at 4°C in agitation. The day after, another aliquot of liposomes was collected for size determination (after PEGylation or AP).

To determine the encapsulation efficiency (EE), non-encapsulated Omomyc mini-protein was separated from the Omomyc-encapsulating PEGylated liposomes (PEGo) by injecting the mixture in HiTrap SP HP columns (GE Healthcare Life Sciences) according to manufacturer's instructions. After this final step, a last aliquot of liposomes was taken (after column or AC) and used to determine the EE and the final concentration of Omomyc mini-protein using the DC Protein Assay (Bio-Rad) while the concentration of Omomyc-AF488 was measured by SDS PAGE followed by coomassie staining.

The size of the liposomes after each step in the process (BE, AE, AP and AC) was determined using a Zetasizer (Malvern). The concentration of Omomyc mini-protein was also assessed at the different steps as described above. A schematic diagram of the complete process is represented in Figure 9.

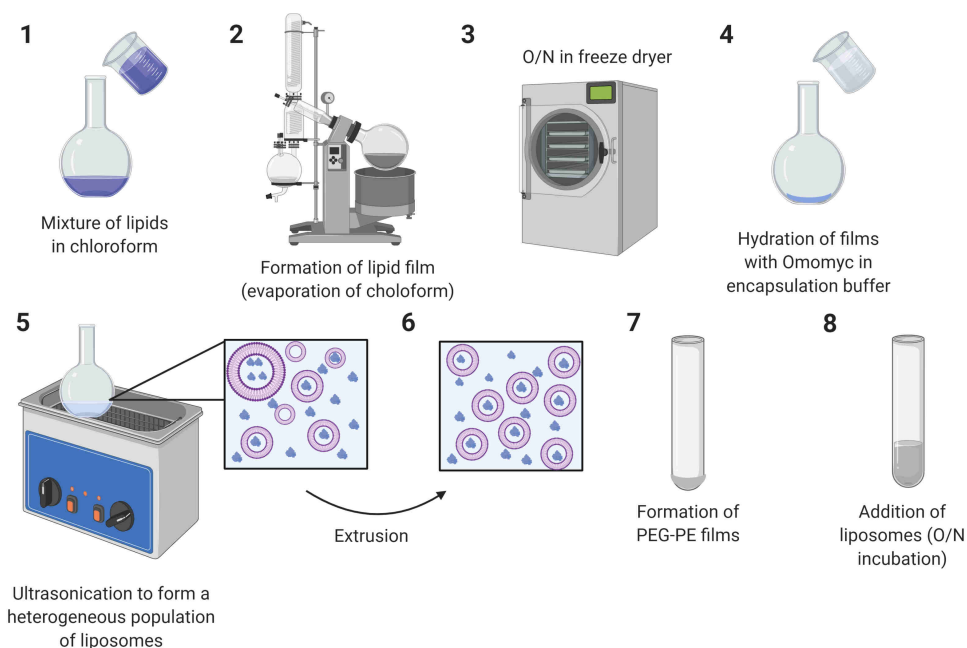


**Figure 9: Scheme of the liposomal production and encapsulation of Omomyc mini-protein.** For details, see text. Figure adapted from (Caldeira de Araújo Lopes et al., 2013) and created with BioRender.

## 2.12 Animal studies

### 2.12.1 Zebrafish

All experiments with live animals were performed using protocols prepared according to the European Union Council Guidelines (86/609/EU) and approved by the Bioethical Committee of the University of Murcia (approval no. #537/2011, #75/2014 and #216/2014). Zebrafish fertilised eggs were obtained from natural spawning of the transgenic fish held at Dr Mulero lab's facilities following standard husbandry practices. Animals were maintained in a 12 hours light/dark cycle at 28°C. The transgenic zebrafish line used was the transparent *roy<sup>a9/a9</sup>*; *nacre<sup>w2/w2</sup>* (Casper) (White et al., 2008) in which pigment cell production is inhibited.

Zebrafish larvae were anaesthetised with a solution of 0.16 mg/mL buffered tricaine (Sigma-Aldrich) in embryo medium, both before xenotransplantation of human cells, and prior to image acquisition with an epifluorescence LEICA MZ16FA stereomicroscope equipped with green and red fluorescent filters.



### 2.12.1a Migration to the CHT (pretreatment in culture)

U266 and CA46 cells were plated in the same conditions as for the proliferation assays (2.4.1). After 3 or 5 days of treatment (for CA46 and U266, respectively), cells were washed with PBS, and while control ones (vehicle-treated) were labelled with Dil Stain (1,1'-Dioctadecyl-3,3,3',3'-Tetramethylindocarbocyanine perchlorate ('Dil'; DiIC18(3))) (Thermo Fisher) according to the manufacturer's instructions, Omomyc-treated cells were stained with a green dye, DiO'; DiOC18(3) (3,3'-Dioctadecyloxacarbocyanine perchlorate) (Thermo Fisher) to allow their distinction. Stained cells were then counted and their viability assessed by trypan blue exclusion. Next, an equal number of live control and Omomyc-treated cells were resuspended in PBS supplemented with 5% of FBS, 0.02% of EDTA (to avoid cell aggregation) and 20% phenol red.

Around 400 cells in 2 nL ( $\varnothing = 0,15$  mm droplet) were then microinjected in the duct of Cuvier of 70–100 Casper mutant zebrafish larvae of 48 hours post fertilisation (hpf), and 1 hour postinoculation (hpi), larvae were imaged in an epifluorescence microscope (Figure 10). The number of cells that reached the CHT were counted manually, or the relative fluorescence intensity was measured using Image J.

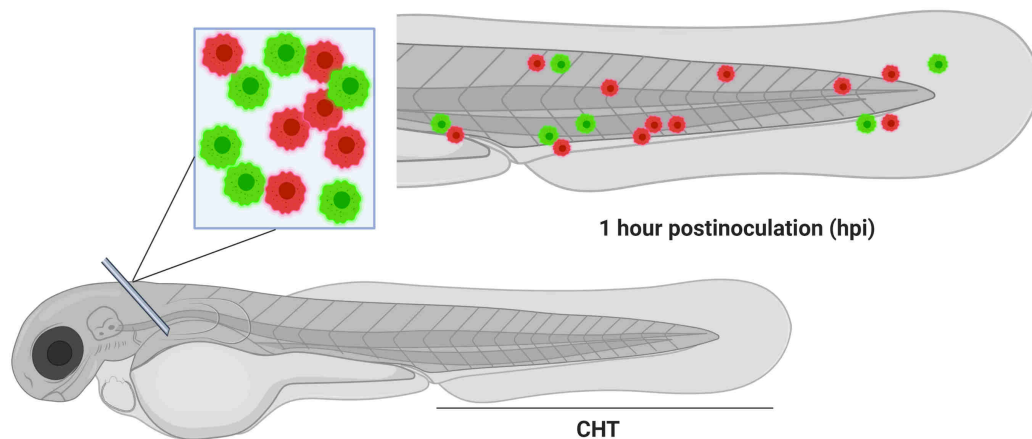


**Figure 10: Schematic diagram of microinjection in zebrafish larvae.** Figure created with BioRender.

### 2.12.1b Biodistribution and toxicity studies

For biodistribution experiments, between 10-15 Casper zebrafish larvae were treated with Omomyc mini-protein or Omolips diluted in their embryo medium (Table 6) and incubated for 1 hour at 35°C.

Larvae age	Treatment	Concentration (treatment)	DMSO	Dose (times of treatment)
48 hpf	Omomyc mini-protein	20 $\mu$ M	1%	Once
72 hpf	Omolips	5 $\mu$ M	No	Twice

**Table 6: Details of the biodistribution studies in zebrafish larvae.**

In order to establish a safe dose that would allow us to perform several treatments, 20 Casper zebrafish larvae (48 hpf) were treated with increasing concentrations of Omomyc mini-protein (1, 5, 10, 15 and 20  $\mu$ M) for 1 hour at 35°C diluted in their embryo medium supplemented with 1% DMSO to help permeabilise the membranes, and the signs of toxicity reported (slowed blood flow, haemorrhages or death).

### 2.12.1c Migration to the CHT (treatment by immersion)

To evaluate the efficacy of Omomyc mini-protein administered dissolved into the embryo medium, between 40-50 Casper zebrafish larvae (48 hpf) were inoculated with 400 U266 cells stained with DiO, randomised into control (vehicle-treated) and Omomyc-treated groups and received either 5 or 10  $\mu$ M of Omomyc mini-protein (+ 1% DMSO) for 1 hour at 35°C following the treatment regimen specified in each case (3.2.2). The day after each treatment, larvae were anaesthetised, and images were taken so that the number of cells migrated to the CHT could be counted manually with ImageJ.

### 2.12.2 Mice

All the animal studies were performed under the ARRIVE guidelines and the 3 Rs rule of Replacement, Reduction and Refinement principles. Mice were maintained and treated following the protocols approved by the CEEA (Ethical Committee for the Use of Experimental Animals) at the Vall d'Hebron Institute of Oncology, Barcelona, Spain.

#### 2.12.2a Xenograft lymphoma model

In order to recapitulate the reduction of engraftment of lymphoma cells in a BM structure as we had seen with the zebrafish model, we used a xenograft mouse model with Raji cells as previously described (Lee et al., 2011). For that, immunocompromised Fox Chase SCID Beige (CB17.Cg-Prkdc<sup>scid</sup>Lystbg-J/CrI) mice purchased from Janvier were inoculated with 1 million Raji cells intravenously (i.v.). The day after, mice were randomised into control (vehicle-treated) and Omomyc-treated (32 mg/kg) groups, comprised of 10 animals each and received the corresponding treatment i.v., as well. 7 days later, the animals were treated again and at day 10 euthanised to collect their organs for immunohistochemistry analysis.

### 2.12.2b Xenograft myeloma model

Immunocompromised NOD/SCID gamma (NSG, NOD.Cg-Prkdc<sup>scid</sup>Il2rg<sup>tm1Wjl</sup>/SzJ) mice purchased from Charles River Laboratories were irradiated with 2 Gy to deplete the BM and immediately after received an intravenous injection (i.v.) of 2 million of U266 cells to induce myeloma, as previously described (Miyakawa et al., 2004).

Because myeloma is a plasmacytoma in which antibody-secreting plasma cells are clonally expanded, we can make use of the immunoglobulins increase in the plasma of mice to monitor the establishment and progression of the disease. In the case of U266 cells, that secrete IgE, we performed biweekly blood extractions to follow up its levels. General health was monitored by physical appearance, weight and score as described in the next section (2.13).

Mice were randomised into the treatment groups (Table 7) the moment the IgE levels in sera were detectable by ELISA, which varied between 3-5 weeks postinoculation of U266 cells.

Experiment	Treatment groups and doses	n per group
1: <i>in vivo</i> Z	a. Control (vehicle-treated)	8
	b. Z (5 mg/kg; every 12 hours i.p.)	
2: <i>in vivo</i> X	a. Control (vehicle-treated)	8
	b. X (5 mg/kg; 1010100 i.p.)	
3: <i>in vivo</i> X&Z	a. Control (vehicle-treated)	6 control 7 treatment groups
	b. Z (5 mg/kg; 1010100 i.p.)	
	c. X (5 mg/kg; 1010100 i.p.)	
4: <i>in vivo</i> X <sub>1</sub> &Z <sub>1</sub>	a. Control (vehicle-treated)	3 control 4 treatment groups
	b. Z <sub>1</sub> (5 mg/kg; 1010100 i.v.)	
	c. Z <sub>1</sub> (10 mg/kg; 1010100 i.v.)	
	d. X <sub>1</sub> (5 mg/kg; 1010100 i.v.)	
	e. X <sub>1</sub> (10 mg/kg; 1010100 i.v.)	
5: <i>in vivo</i> Z <sub>1</sub> &BTZ	a. Control (vehicle-treated)	6
	b. Z <sub>1</sub> (5 mg/kg; 1010100 i.v.)	
	c. Z <sub>1</sub> (10 mg/kg; 1010100 i.v.)	
	d. BTZ (0.5 mg/kg; 1000100 i.p.)	
6: <i>in vivo</i> Omomyc	a. Control (vehicle-treated)	8
	b. Omomyc (50 mg/kg; 1000000 i.v.)	
7: <i>in vivo</i> Omolips	a. Control (empty liposomes)	8
	b. Omomyc (12 mg/kg; 0101000 i.v.)	
	c. Omolips (12 mg/kg; 0101000 i.v.)	

**Table 7: Treatment groups' details per experiment (xenograft myeloma model).**  
i.p. intraperitoneal; i.v. intravenous

Also, in Table 7 is detailed the dosing regimen administered for each drug, the administration route, as well as the number of animals comprising each group. The vehicle administered was sterile PBS unless otherwise specified.

Every 2 weeks, we extracted blood from the saphenous vein, collected the serum and followed up the progression of the disease by the increase in IgE levels until the end of the experiment (~50 days postinoculation). The animals' weight was recorded as a measure of their general health: once a week before treatment onset, and before every treatment administration or at least twice a week. We also video recorded any abnormal sign or behaviour detected after treatment and noted every lesion observed in the site of injection if any.

At the end of the experiment, 16 hours after the last administration (for the Omomyc experiments), animals were euthanised, and 1 hind limb was used for flushing the BM for flow cytometric analysis, while the other was fixed with formol for histological analysis.







### **2.12.2c Syngeneic myeloma model**

To study the therapeutic impact of Omomyc in immunocompetent mice, we used one of the 5T series myeloma models widely used to investigate the pathobiology of the disease and validate new potential drug candidates, given its simplicity and reproducibility ([Asosingh et al., 2000](#)).

32 C57BL/KaLwRijHsd mice were purchased from Envigo (The Netherlands) and inoculated i.v. with 1 million of 5TGM1-eGFP cells as previously described ([Oyajobi et al., 2007](#)). We extracted blood from the saphenous vein before the inoculation of cells and every week after to follow up the increase in IgG2b levels in sera. The first week after cell implantation, mice were randomised into 4 groups: control (vehicle-treated), Omomyc (50 mg/kg), BTZ (0.25 mg/kg) and OMO/BTZ (receiving both therapies at the dosing mentioned). The weight of the animals was recorded before every treatment, and twice a week when we started noticing weight loss associated with treatment toxicity. Animals were euthanised after 4 weeks of treatment

## 2.13 Scoring and paralysis follow-up

Mice from the myeloma models (both syngeneic and xenograft) were weighed and examined once a week until the treatment onset, and twice (syngeneic) or thrice (xenograft) from then until the end of the experiment to assess the appearance and severity of paralysis signs as described in Table 8, as a surrogate marker of the osteolytic lesions (secondary bone disease, characteristic of advanced disease). The scoring system was based on the Experimental Autoimmune Encephalomyelitis (EAE) guidelines (Baker and Amor, 2012). Animals that scored 3 were euthanised, as we established it as our humane endpoint.

	Clinical score	Paralysis signs
	0	No clinical signs
	0.5	Partial tail paresis
	1	Tail paralysis
	1.5	Mild paraparesis of one hind limb
	2	Mild paraparesis of both limbs
	3	Severe paraparesis or paraplegia of hind limbs

**Table 8: Evaluation of clinical signs of paralysis due to osteolytic lesions.**

## 2.14 mCT imaging

Micro-computed tomography ( $\mu$ CT or mCT) studies were performed with a Quantum GX microCT Imaging System (Perkin Elmer). Acquisition and analysis were carried out by the Preclinical Imaging Platform staff at VHIR. Mice were anaesthetised with isoflurane (5% for induction and 2% during acquisition). Airflow was set at 0.8 L/min. The images were analysed using MicroView (Parallax Innovations) or AMIDE software.

## 2.15 Figures

Where indicated so, figures were created with BioRender.com.

## 2.16 Statistical analysis

Statistical analysis and representation of the data were performed using GraphPad Prism 6. For histograms, mean + standard deviation (SD) is shown. For scattered dot plots, mean + SD is shown. For XY graphs, in which superimposed symbols with a connecting line are shown, we plotted the median and interquartile ranges. When the number of biological replicates ( $n$ ) < 8, parametric tests were used. When  $n \geq 8$ , a d'Agostino-Pearson omnibus normality test was used. If the test confirmed a Gaussian distribution of the data, a parametric test was used. Otherwise, non-parametric tests were used.

To determine statistical significance among two groups, a two-tailed unpaired t test (parametric) or a two-tailed Mann-Whitney test (non-parametric) was used. When comparing 3 or more groups, one-way or 2-way ANOVA were used for the analysis of variance, and the statistical difference between groups was determined via Dunnett's multiple comparisons test.

For all tests, an alpha level of 0.05 was established. In all graphs, \*, \*\*, \*\*\* and \*\*\*\* are used to describe p values below 0.05, 0.01, 0.001 and 0.0001 respectively, and ns stands for non-significant, as stated in figure legends. For all histograms, asterisks above one bar indicate statistical significance between that bar and the control group (filled with black). For other graphs, a line between the statistically significant groups is drawn.



## RESULTS

### Validation of novel strategies for MYC inhibition in B-cell malignancies

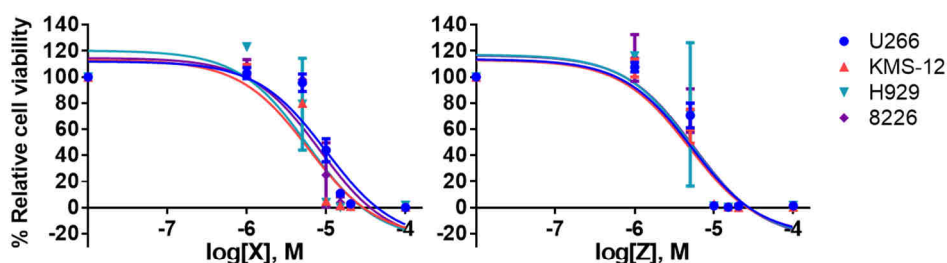
#### 3.1 MYC inhibition with small molecules

We performed these experiments in collaboration with a biotech start-up company. Due to our confidentiality agreement, the name of the company and the exact formula of the compounds will not be further described. Starting from a library designed to target intrinsically disordered proteins or IDPs, of which MYC is a great example, 3 molecules were chosen to be tested in myeloma models based on their ability to reduce MYC levels.

##### 3.1.1 *In vitro* characterisation of compounds X, Y and Z

First, we screened the therapeutic effect of 2 leading compounds (X and Z) in a panel of 4 human multiple myeloma (hMM) cell lines with different levels of MYC expression (2 high versus 2 low) as well as various other driver mutations, to choose the best responder before proceeding with *in vivo* experiments. We treated the cells and calculated the median inhibitory concentration ( $IC_{50}$ ) that ranged from ~5-10  $\mu$ M for both compounds in all the cell lines (Figure 11A and B).

A



B

Cell line	$IC_{50}$ X	$IC_{50}$ Z
U266	9.98 $\mu$ M	5.24 $\mu$ M
KMS-12-BM	6 $\mu$ M	4.88 $\mu$ M
NCI-H929	5.90 $\mu$ M	5.34 $\mu$ M
RPMI-8226	8.34 $\mu$ M	5.58 $\mu$ M

**Figure 11: Compounds X and Z reduce the proliferation of MM cell lines in a dose-dependent manner.** (A) Dose-response of the MM panel of cells to increasing concentrations of X and Z as measured by resazurin dye fluorimetric assay. (B) Summary of the  $IC_{50}$  values calculated for each cell line and compound. The experiment was done twice and the average values are shown.



## Results

Since the different cell lines responded similarly to the compounds regardless of their MYC levels and mutational profile, we picked U266 cells for *in vivo* studies because of the feasibility and practicality of the corresponding animal model, which had been widely used and described in the literature. In the meantime, we received a third molecule (Y) from our collaborators that asked us to test it *in vitro* to compare its performance compared to X and Z (Figure 12A). Again, U266 cells responded to all compounds within the micromolar range (Figure 12B).

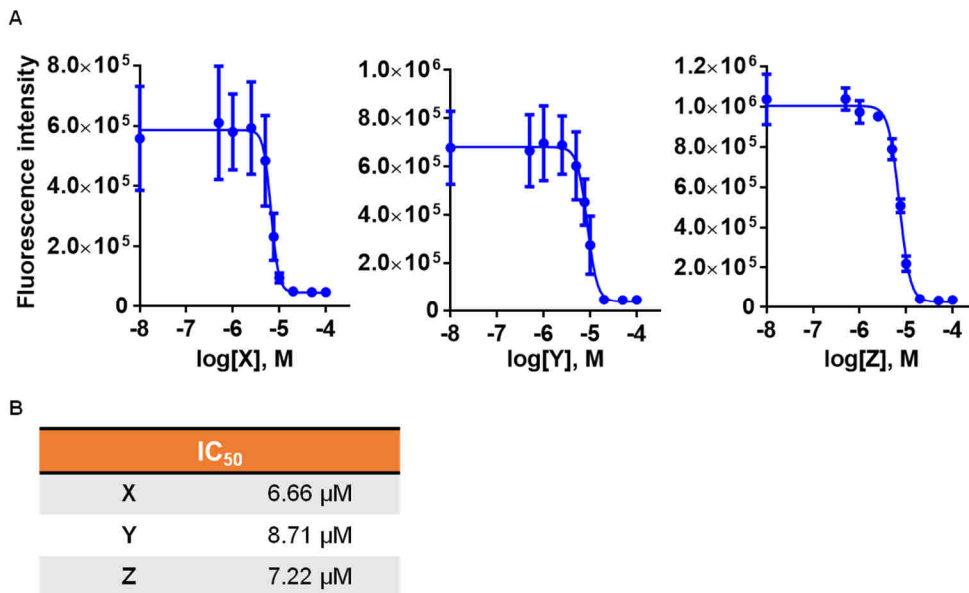


**Figure 12: Comparison of the IC<sub>50</sub> values for X, Y and Z in U266 cells.** (A) Dose-response of U266 cells to increasing concentrations of X, Y and Z as measured by resazurin dye fluorimetric assay. (B) Summary of the IC<sub>50</sub> values calculated for each compound. The experiment was done once.

To determine whether the effect seen on cell proliferation was due to an on-target effect or just mere toxicity, we also calculated the IC<sub>50</sub> of all 3 compounds in non-cancerous immortalised human (MRC5-T) and mouse (MEF) fibroblasts. The IC<sub>50</sub> values were significantly higher for X and Y (40 and 50 μM, respectively) in MRC5-T. However, Z gave values around 9 μM, quite comparable to those seen in U266 cancer cells, which could suggest a more toxic effect independent of the on-target effect (Figure 13A and C). In MEFs (mouse embryonic fibroblasts) instead, the IC<sub>50</sub> values were higher for all 3 compounds (Figure 13B and C).

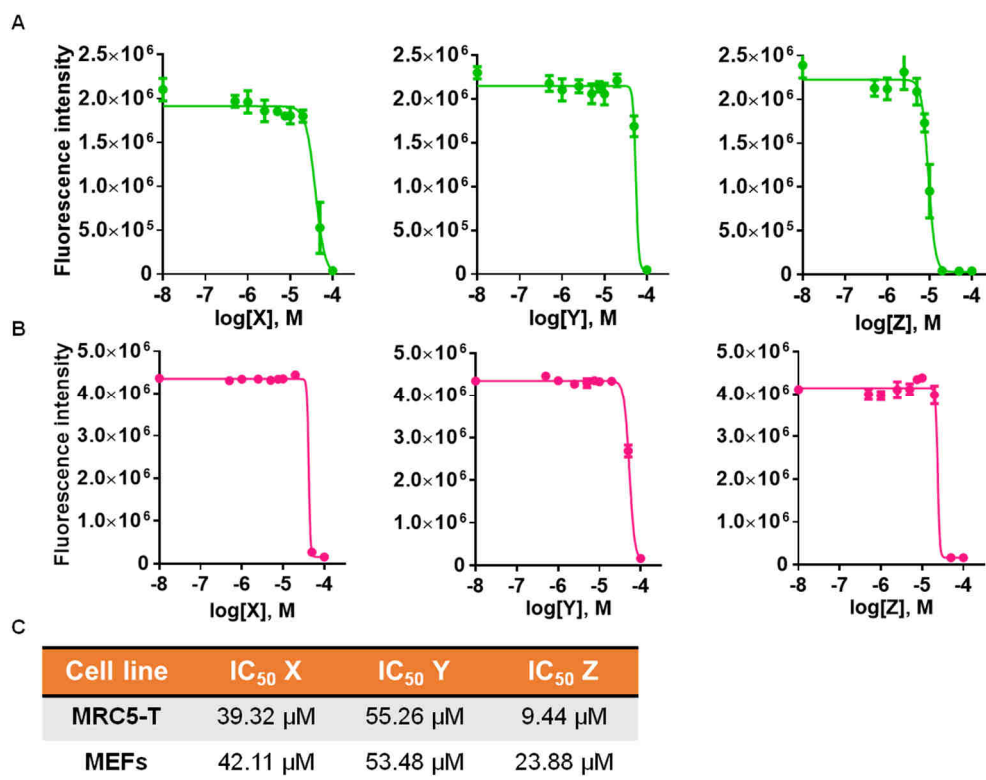


**Figure 13: X, Y and Z compounds were specific against cancer cells.** MRC5-T (A) and MEFs (B) dose-response to increasing concentrations of X, Y and Z as measured by resazurin dye fluorimetric assay. (C) Calculated IC<sub>50</sub> values for each compound and cell line. The experiment was done once.

### 3.1.2 *In vivo* therapeutic effect of X and Z

Once we confirmed that the compounds displayed an anti-proliferative effect on cancer cells *in vitro*, we set up a xenograft mouse model for the *in vivo* efficacy study. According to our collaborators' results, which suggested that compounds Z and Y were the most promising, we first tested the effect of compound Z, then of compound X, and finally, we compared their efficacy side by side in a third study. Compound Y was instead deprioritised. In every experiment, mice received an intravenous injection - via tail vein - of 2 million U266 cells, which were left to engraft for 3-5 weeks. Animals were then randomised into treatment groups (vehicle control and compound-treated) according to the IgE levels detected in serum. These levels were used as a surrogate marker of tumour burden, as it is the case in clinical practice for myeloma patients. From the treatment onset until the end of the experiment (8-9 weeks later), mice received their treatment through intraperitoneal (i.p.) injections.

We closely monitored the animals' wellbeing by checking their weight (Figure 14A-C) and video-recording abnormal behaviours.

At first, the dose regimen for Z was 5 mg/kg twice a day, to sustain its bloodstream drug concentration. However, after the 8<sup>th</sup> inoculation, mice started to show side effects affecting their behaviour that seemed consistent with severe irritation (according to the veterinary in charge), such as hunched posture, piloerection, abnormal gait, altered respiration as well as alternate bouts of excitation and apathy. Hence, the frequency of administration was reduced to twice a week, to try to avoid accumulated toxicity of more frequent dosing. Consistent with the hypothesis of toxicity, as depicted in (Figure 14A-C), there was a drastic reduction in weight in treated mice since the treatment onset, which was partially stabilised once the dosing was reduced. Upon reduction, also the behavioural alterations improved, although they did not disappear completely.

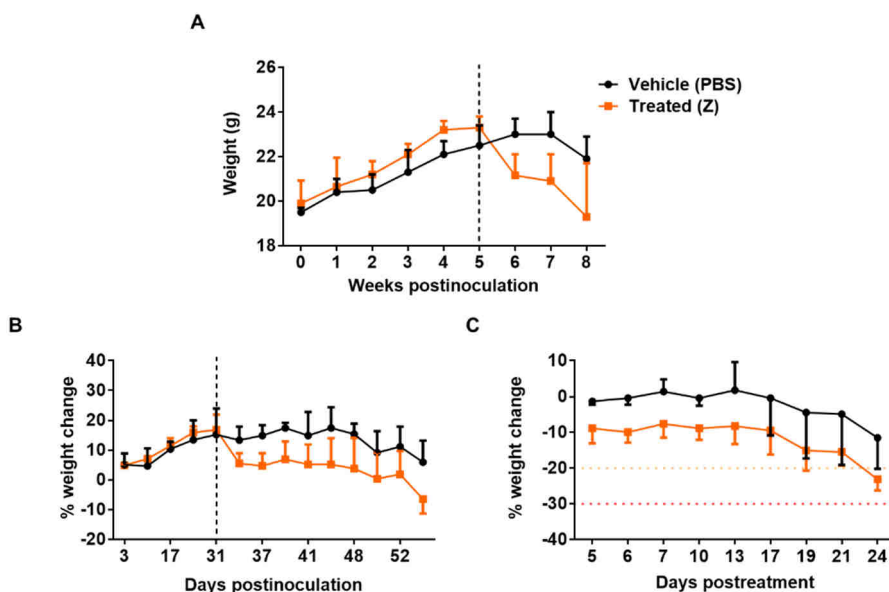


**Figure 14: Weight changes throughout the experiment with compound Z.** (A) Mice weight mean and standard deviation (SD) per group. The dashed vertical black line indicates the treatment onset. (B) Median percentage and interquartile range of weight change since the inoculation of U266 cells of each group. (C) Median percentage and interquartile range of weight change since the treatment onset. The dotted amber and red horizontal lines indicate the 20 and 30% weight loss.  $n=8$  mice per group.

To evaluate the therapeutic efficacy of molecule Z, we recorded the pathological “score” of the animals 3 times a week until the endpoint. This measurement reflects the symptoms caused by the appearance of osteolytic lesions as a consequence of the progressing disease. The scoring system was based on the guidelines for EAE normally ranging from 0 to 6, being 3 a humane endpoint criterion for

euthanasia in our model. Treatment with compound Z significantly improved the score of the treated group compared to the control one (Figure 15A-C).

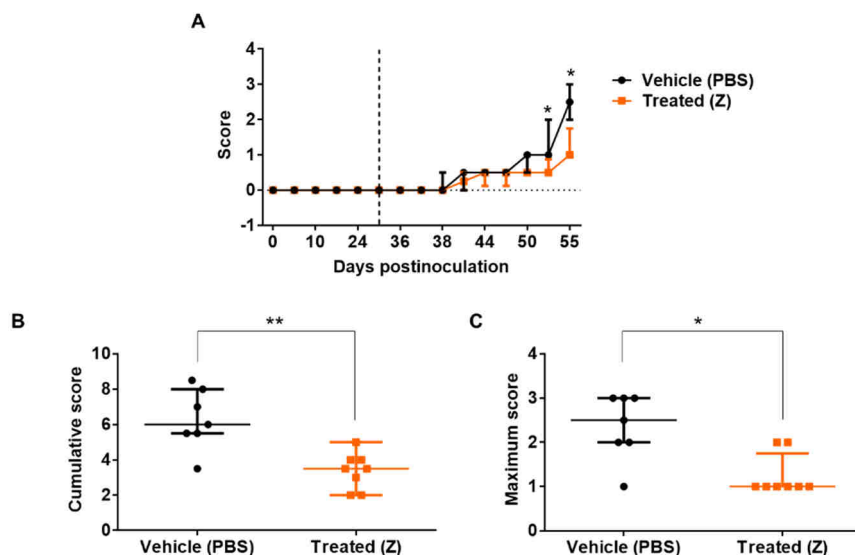
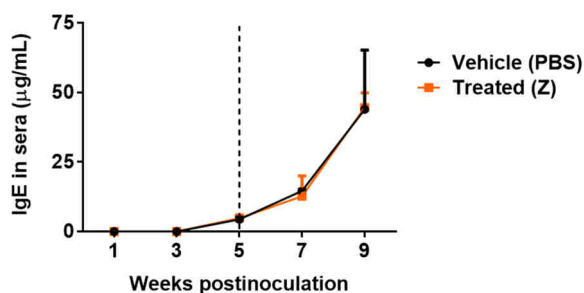


**Figure 15: Compound Z reduced the score after 3 weeks of treatment.** (A) Longitudinal record of the mean score and SD of each group. Statistical significance was calculated using multiple nonparametric *t*-tests. \* indicates a *p*-value ≤ 0.0001. (B) Cumulative score calculated as the sum of all the values recorded for each mouse throughout the experiment. (C) Maximum score refers to the highest value reached per mouse during the experiment. Mann-Whitney was the statistical analysis used to determine significance. \* indicates a *p*-value ≤ 0.05; \*\* indicates a *p*-value ≤ 0.01.

In contrast, the levels of IgE in serum remained unchanged between the treated and control groups (Figure 16).

**Figure 16: Z did not reduce the amount of IgE detected in mice sera.** Longitudinal analysis of the IgE levels every other week. There were no differences between the treated and control groups after 4 weeks of treatment. The dashed vertical black line indicates the treatment onset.



To complement these studies, at the end of the experiment, we flushed the BM from the hind leg of each mouse to analyse the tumour burden. To do so, we stained the cells with CD138, a B-cell surface marker that MM cells highly express. We also tested whether the treatment could have caused tumour cell death staining for Annexin V and Propidium Iodide (AVPI). Unfortunately, the quantifications

## Results

showed no differences between the 2 groups in the CD138/AVPI double staining (Figure 17A and B).

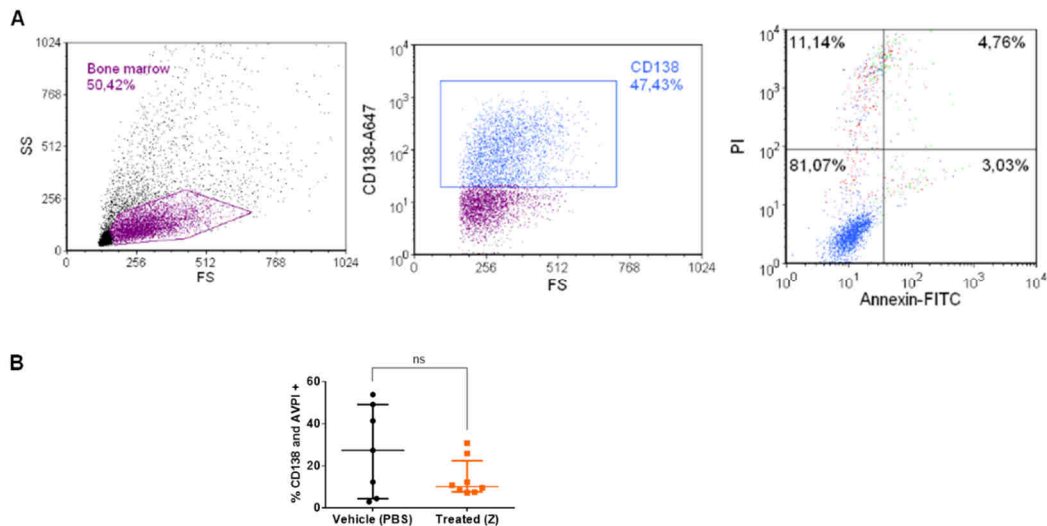


**Figure 17: Z did not reduce the number of myeloma cells in the BM, nor did it increase their death.** (A) Representative dot plot images showing the CD138/AVPI populations studied. (B) Quantification of the flow cytometer results of A. Mann-Whitney test was used to analyse statistical significance, where ns stands for non-significant results.

Next, we repeated the experiment, testing compound X. Based on our previous experience with compound Z and the behavioural reactions displayed by the animals, in agreement with our external collaborators, we decided to treat the animals 3 times a week with 5 mg/kg of X. The results obtained were quite comparable to those seen with Z. However, the treatment with X did not cause much loss of weight, although some behavioural abnormalities could still be observed. The reduction in weight that was especially obvious between the 6<sup>th</sup> and 7<sup>th</sup> weeks of the experiment was mainly due to the progression of the disease, as it also happens in the vehicle group ( Figure 18A-C).

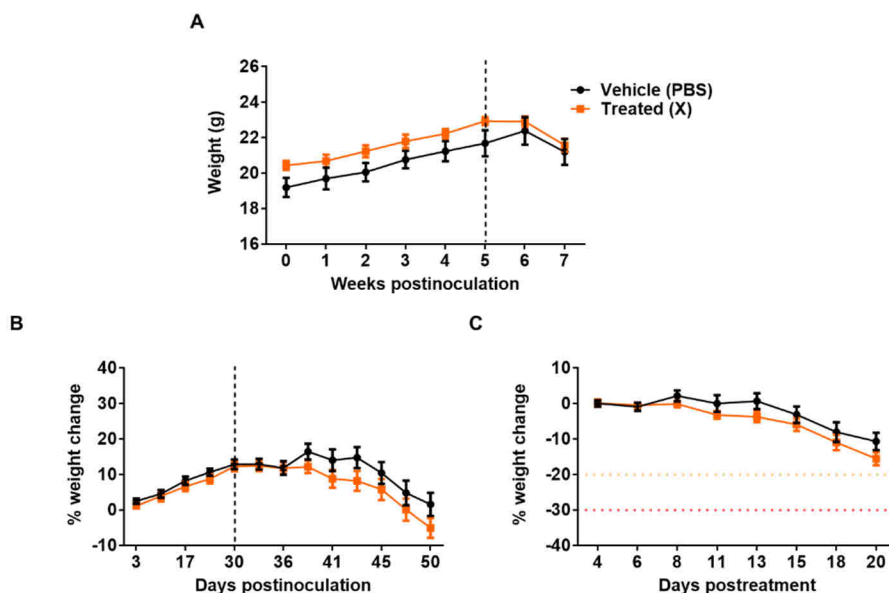


**Figure 18: Weight changes throughout the experiment with compound X.** (A) Mice weight median and interquartile range per group. The dashed vertical black line indicates the treatment onset. (B) Median percentage and interquartile range of weight change since the inoculation of U266 cells of each group. (C) Median percentage and interquartile range of weight change since the treatment onset. The dotted amber and red horizontal lines indicate the 20 and 30% weight loss.  $n=8$  mice per group.

In this case, the score did not reveal any statistically significant difference between the control and treated groups, although there was a tendency of a slight decrease by the end of the experiment in the group of animals treated with X (Figure 19A-C).

Once again, we could not detect any differences in the levels of IgE in the serum (Figure 20).

Finally, we analysed the proliferative status of CD138 positive cells through Ki67 staining. Surprisingly, we observed a significant decrease in the percentage of CD138 positive cells in the flushed BM, as well as in the population of double-positive CD138/Ki67 of treated animals (Figure 21A and B). In addition, we also saw an increase in the percentage of CD138/AVPI cells indicative of cell death (Figure 21C and D). Altogether, these results showed a decrease in proliferation and increase in cell death of myeloma cells colonising the BM, despite no improvement in pathological score or IgE levels in serum.

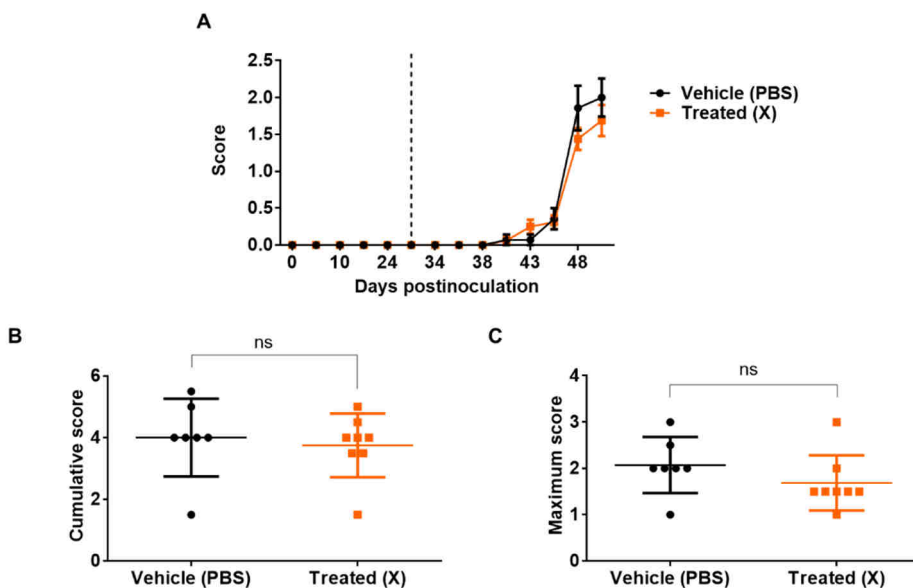


**Figure 19: Compound X showed no differences in the score after 3 weeks of treatment.** (A) Longitudinal record of the mean score and SD of each group. Statistical significance was calculated using multiple nonparametric t-tests. (B) Cumulative score calculated as the sum of all the values recorded for each mouse throughout the experiment. (C) Maximum score refers to the highest value reached per mouse during the experiment. Mann-Whitney was the statistical analysis used to determine significance, where ns stands for non-significant results.

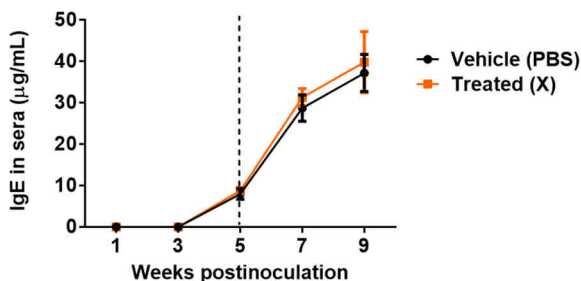


**Figure 20: X did not reduce the amount of IgE detected in mice sera.** Longitudinal analysis of the IgE levels every other week. There were no differences between the treated and control groups after 3 weeks of treatment.

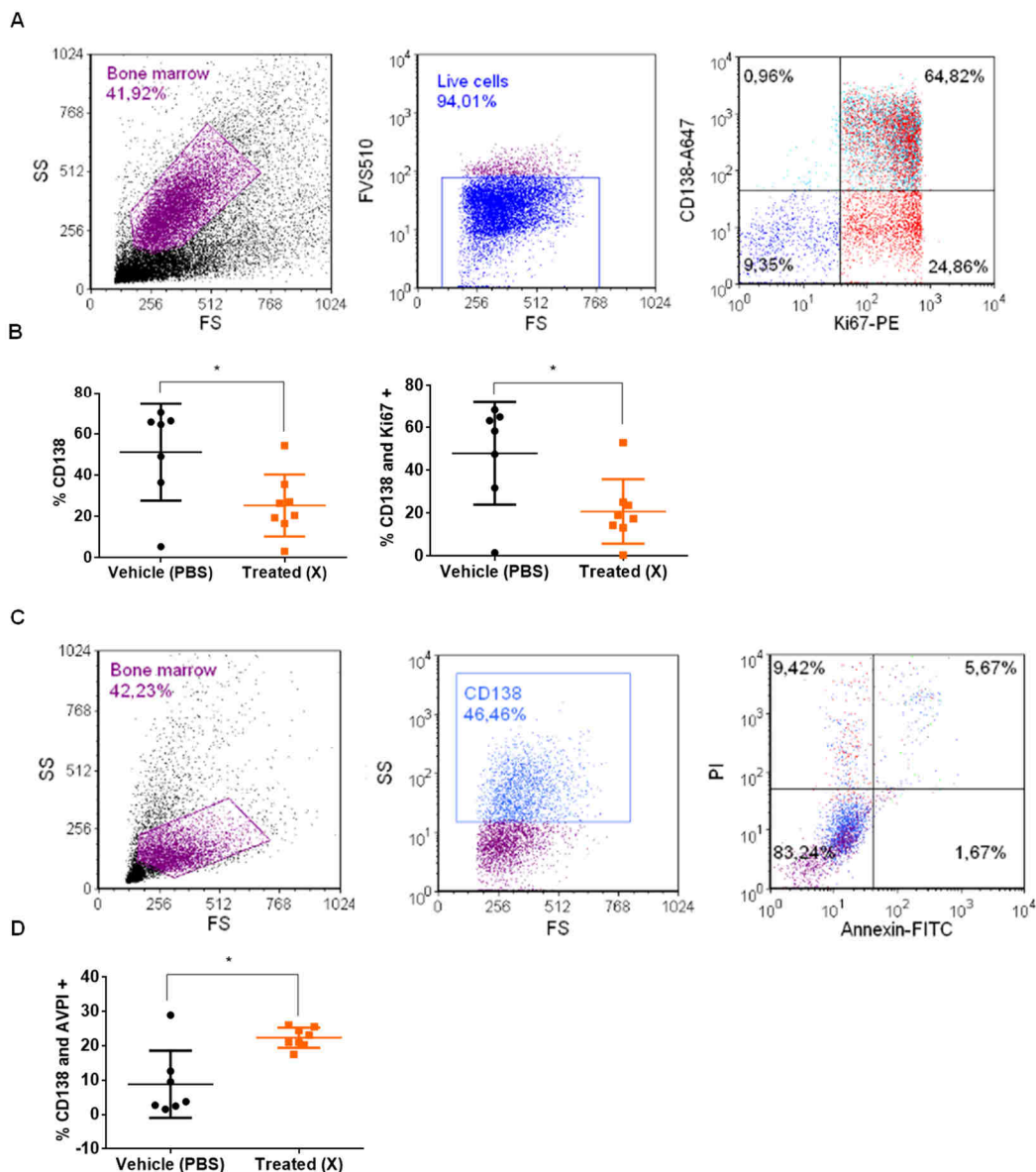


**Figure 21: X reduced the proliferation of BM colonising myeloma cells, and it increased their death.** (A) Representative dot plot images showing the CD138/Ki67 populations studied. (B) Quantification of the flow cytometer results of A. (C) Representative dot plot images showing the CD138/AVPI populations studied. (D) Quantification of the flow cytometer results of C. Statistical significance was analysed using a Mann-Whitney test. \* indicates a  $p$ -value  $\leq 0.05$ .

In light of these promising - yet not so striking - results, we directly compared X and Z impact on mice survival in a third study. We repeated the dosing schedule used for X (3 times a week). This time, thanks to the experience accumulated in



the previous studies, we took extra measures to reduce mouse stress. In order to avoid articulation swelling and bone pain due to the osteolytic lesions, for example, we used buprenorphine as analgesia to palliate it and prevented weight loss using an 18% protein diet (Figure 22A-C).

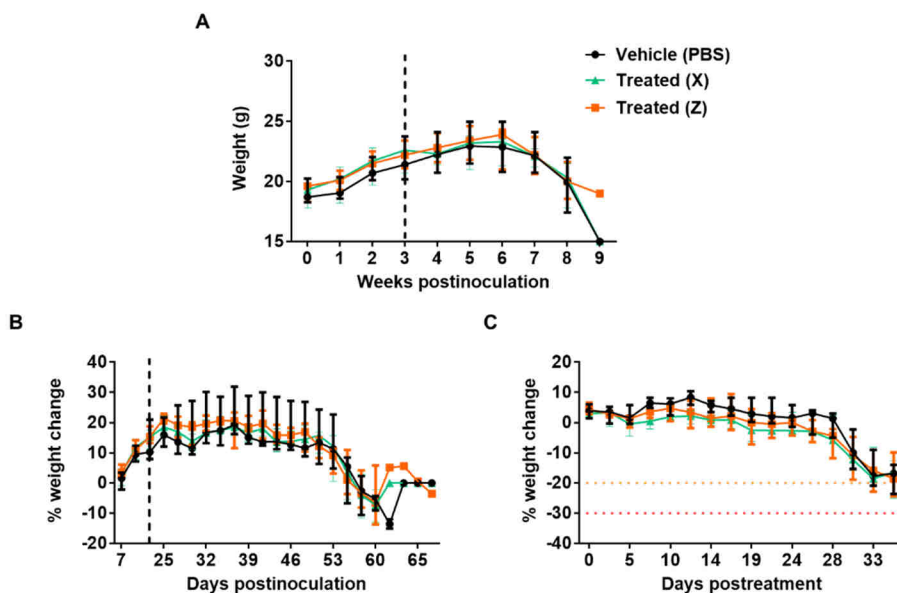


**Figure 22: Mice wellbeing improvement. Mice gained more weight and maintained it for longer thanks to the higher protein diet and the treatment with analgesics.** (A) Mice weight median and interquartile range per group. The dashed vertical black line indicates the treatment onset. (B) Median percentage and interquartile range of weight change since the inoculation of U266 cells of each group. (C) Median percentage and interquartile range of weight change since the treatment onset. The dotted amber and red horizontal lines indicate the 20 and 30% weight loss.  $n=8$  mice per group.

Despite these measures, though, we did not see any differences in the median survival of 60 days, which was the same for all 3 groups (Figure 23A) nor did we observe differences in IgE levels in serum (Figure 23B) and score (Figure 23C).

It is important to notice that, according to the original dosing schedule, we should have treated the animals twice a day to maintain higher blood levels of the compounds. However, this was not possible due to evident behavioural abnormalities displayed by the animals during and after treatment administration, suggestive of local toxicity. Bearing in mind this caveat, then, we deduced that the observed therapeutic effect was actually quite encouraging. Thus, we decided to proceed with a new formulation of the compounds that would allow i.v. administration, while reducing the local toxic reactions. For that purpose, our collaborators produced the improved compounds  $X_1$  and  $Z_1$  for further characterisation in our lab.

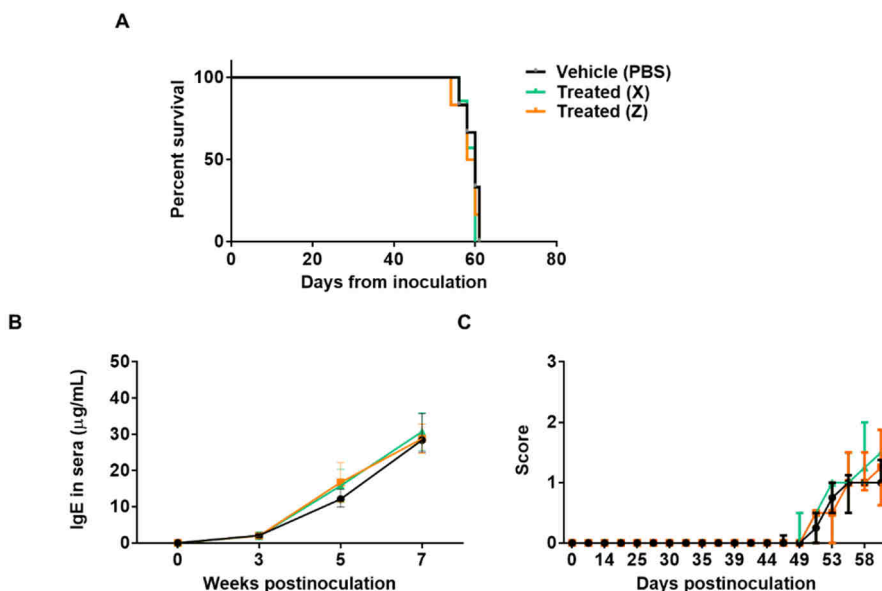


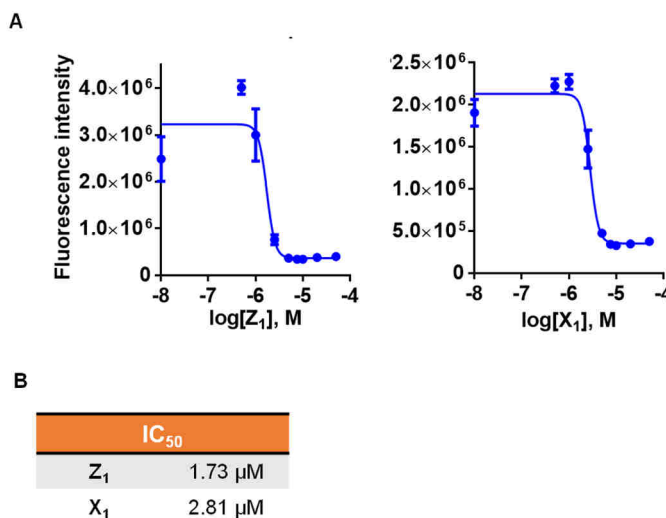
**Figure 23: Treatment with X or Z did not prolong the median survival of mice.** (A) Kaplan-Meier curve showing no differences between groups. (B) Longitudinal analysis of the immunoglobulin E levels in serum (C) Longitudinal record of the mean score of each group.

### 3.1.3 *In vitro* and *in vivo* characterisation of Z<sub>1</sub> and X<sub>1</sub>

The first step was to test the efficacy of these new formulated compounds *in vitro*. As in section 3.1.1, we used U266 cells and treated them for 3 days with increasing concentrations of X<sub>1</sub> or Z<sub>1</sub> in order to calculate their IC<sub>50</sub> value (Figure 24A and B).

#### Figure 24: Comparison of the IC<sub>50</sub> values for Z<sub>1</sub> and X<sub>1</sub> in U266 cells.

(A) Mean fluorescence intensity and SD of 5 technical replicates per concentration. Non-linear fit curves for each compound are also shown. (B) Calculated IC<sub>50</sub> values for each compound. The experiment was done once.



The efficacy *in vitro* was still in the micromolar range (~2-3 µM) but slightly improved compared to that of the original compounds (6.66 and 7.22 µM for X and

Z respectively). We then proceeded to perform *in vivo* studies using the same xenograft model as in 3.1.2.

First, we compared the therapeutic effect of 2 different doses (5 and 10 mg/kg) of Z<sub>1</sub> and X<sub>1</sub>. As for the original compounds, we treated the animals 3 times a week, but this time we switched to i.v. to avoid local reactions like those observed upon i.p. treatment. We found no toxicity, as demonstrated by the gradual increase in mouse weight throughout the first weeks of treatment (Figure 25A-C) (as mentioned before, the loss of weight observed during the last 2 weeks was due to disease progression).

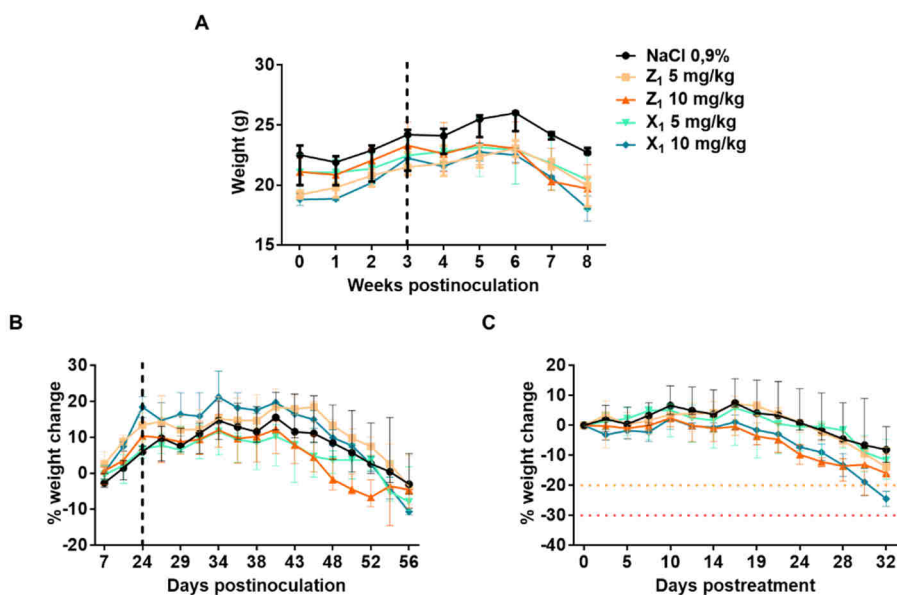


**Figure 25: Z<sub>1</sub> and X<sub>1</sub> i.v. formulations were not toxic.** (A) Mice weight median and interquartile range per group. The dashed vertical black line indicates the treatment onset. (B) Median percentage and interquartile range of weight change since the inoculation of U266 cells of each group. (C) Median percentage and interquartile range of weight change since the treatment onset. The dotted amber and red horizontal lines indicate the 20 and 30% weight loss. *n*=4 mice per group.

To assess bone disease, we obtained *ex vivo* micro CT images from the knee joint and tibia. We observed no differences between the groups, as depicted in Figure 26A. In line with these results, the score, indicative of osteolytic lesions, did not show any difference between the control and either treated group (Figure 26B and C).

Interestingly, though, after 6 weeks of treatment, we detected a reduction of IgE in sera from animals of the Z<sub>1</sub> 10mg/kg treated group (Figure 27A-C), although the difference was not statistically significant (2-way ANOVA analysis performed).

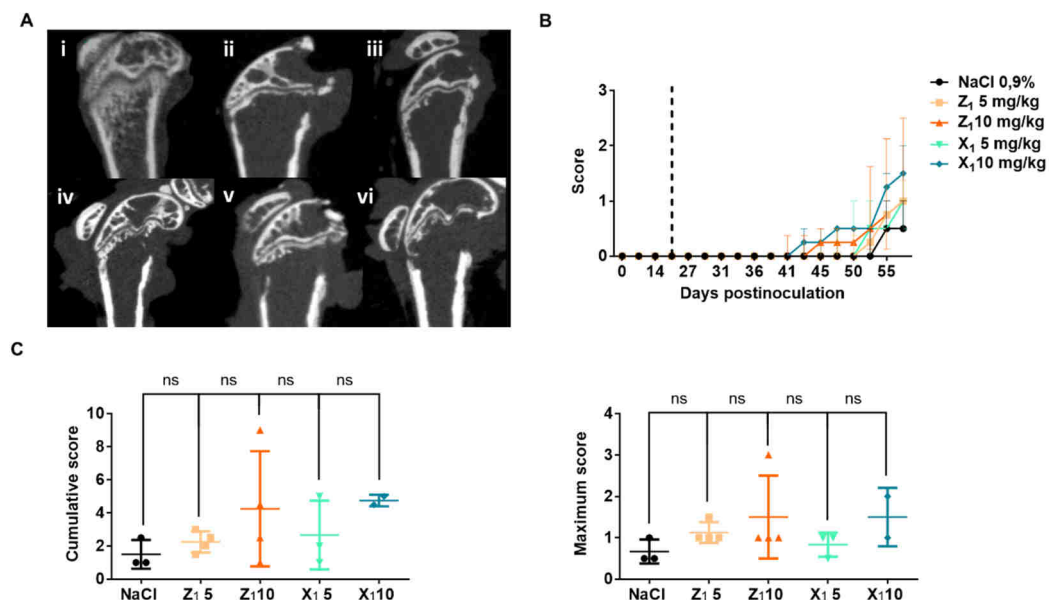


**Figure 26: Z<sub>1</sub> and X<sub>1</sub> did not improve the bone disease.** (A) Representative ex vivo mCT images are shown for each treatment group. i: basal scan; ii: vehicle; iii: Z<sub>1</sub> 5mg/kg; iv: Z<sub>1</sub> 10mg/kg; v: X<sub>1</sub> 5mg/kg; vi: X<sub>1</sub> 10mg/kg. (B) Longitudinal record of the mean score and SD of each group. Statistical significance was calculated using multiple nonparametric t-tests. (C) Neither cumulative nor maximum score showed differences between groups. Mann-Whitney was the statistical analysis used to determine significance, where ns stands for non-significant.

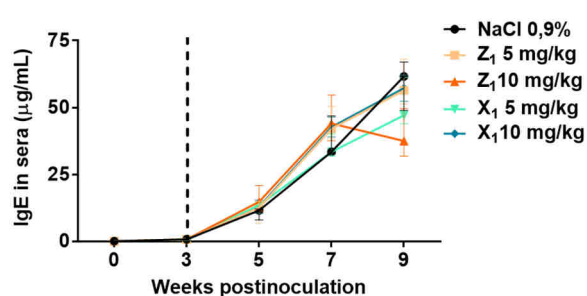


**Figure 27: Z<sub>1</sub> at the highest dose slightly reduced the IgE levels, while the others did not.** Longitudinal analysis of the immunoglobulin E levels in serum. There were no differences between the treated and control groups after 6 weeks of treatment.

To complement these data, we analysed the flushed BM of the mice using an anti-human CD138 and the proliferation marker Ki67. Unfortunately, also, in this case, there were no differences in the treated populations when compared to the control group. Of note, animals from the Z<sub>1</sub> 10 mg/kg group kept the smallest mean of double-positive CD138 and Ki67 cells (Figure 28A and B), showing a tendency

## Results

consistent with the reduced levels of IgE in sera. It is also important to emphasise that the  $n$  used for this experiment was quite small (4 mice per group), which could account for, at least in part, the little statistical power of the results.

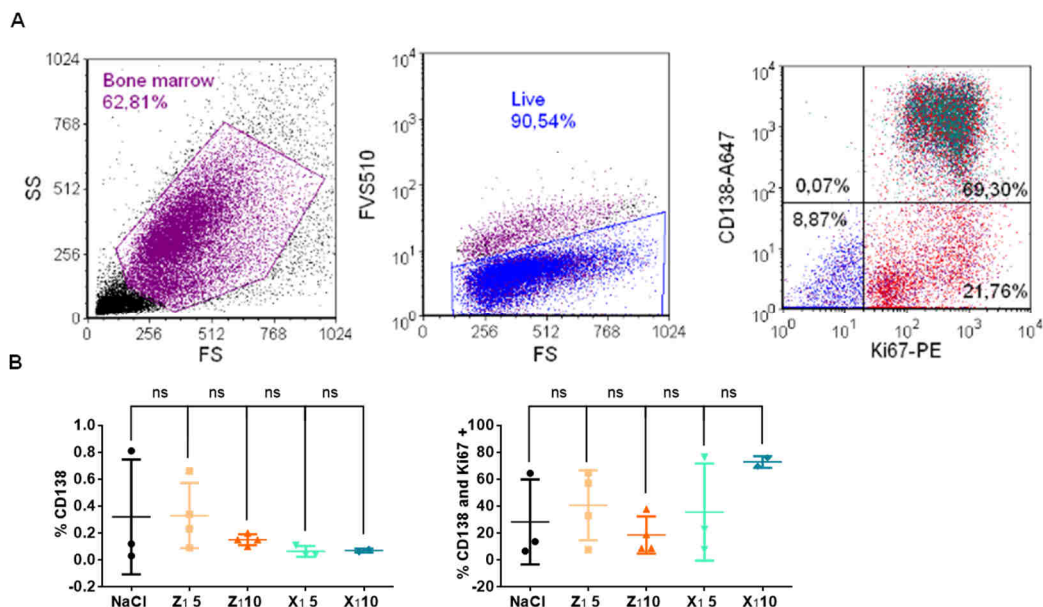


**Figure 28: Z<sub>1</sub> 10 mg/kg shows a promising reduction in the proliferation of BM colonising myeloma cells.** (A) Representative dot plot images showing the CD138/Ki67 populations studied. (B) Quantification of the flow cytometer results of A. One-way ANOVA and Dunnett's multiple comparisons test were used to determine the statistical significance, where ns stands for non-significant.

One more concern complicated the interpretation of the data: our collaborators informed us that the drugs could suffer from poor stability upon storage at 4°C. For that reason, we checked the integrity of the injectable solutions by HPLC-MS at the end of the experiment. Unfortunately, consistent with our concerns, we found that both compounds were degraded up to 80% compared to their initial concentration (data not shown), which translated in a reduced amount of active drug present in the injectable solutions.

To confirm if the lack of efficacy observed *in vivo* could be due to degradation issues, we tested again *in vitro* the stored and degraded compounds. To our surprise, the IC<sub>50</sub> values were quite similar to the ones obtained with 100% active drug ( Figure 29A and B). Then, we quantified the precipitated compound and found a significant positive correlation between the efficacy observed *in vitro* and the measured precipitation ( Figure 29C), suggesting that, at least in culture, the cytotoxic effect of the drugs could be mainly due to the precipitation itself and a toxic/off-target effect.

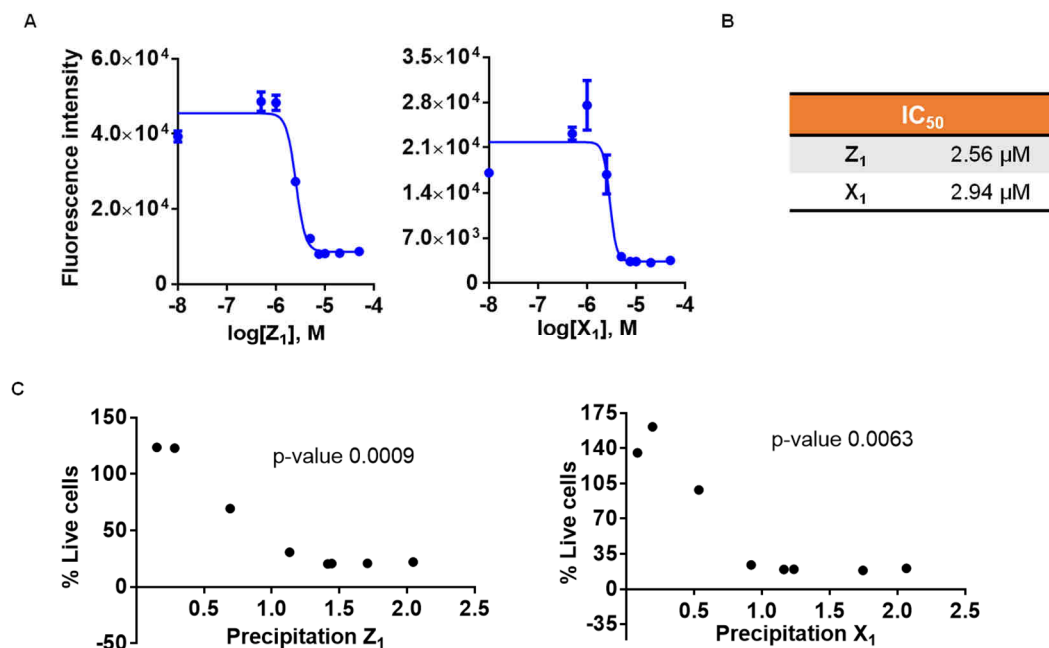
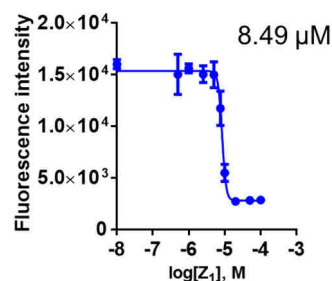


**Figure 29: Degraded Z<sub>1</sub> and X<sub>1</sub> compounds show *in vitro* effect.** (A) Mean fluorescence intensity and SD of 5 technical replicates per concentration. Non-linear fit curves for each compound are also shown. (B) Calculated IC<sub>50</sub> values for each compound. The experiment was done once. (C) Correlation between the precipitation measured by crystal violet and the efficacy was computed using Pearson correlation coefficients.

Nevertheless, our collaborators decided to proceed and prioritise compound Z<sub>1</sub> for further experiments. Given the previous results, we tested a new batch of non-degraded Z<sub>1</sub> injectable formulation. To prevent degradation, we stored it as frozen aliquots that were thawed only before their use. Then, we tested their efficacy *in vitro* again (Figure 30).

**Figure 30: The new batch of Z<sub>1</sub> injectable formulation shows efficacy *in vitro* in the micromolar range.** Mean fluorescence intensity and SD of 5 technical replicates per concentration. Non-linear fit curve and calculated IC<sub>50</sub> value are also shown.



Next, we repeated the *in vivo* study, comparing 2 doses of Z<sub>1</sub> (5 and 10 mg/kg) administered i.v. 3 times a week. We also compared them with the proteasome inhibitor bortezomib (BTZ), which is the standard of care (SoC) therapy for myeloma. The latter was administered i.p. twice a week at 0.5 mg/kg and was used as a positive control, to confirm that we could test the efficacy of experimental compounds in this xenograft mouse model.

Sadly, after the first inoculation with the high dose of Z<sub>1</sub> (10 mg/kg) all the animals died or needed euthanasia, leaving us with the remaining 3 groups (control, 5 mg/kg Z<sub>1</sub> and 0.5 mg/kg BTZ). We also noticed some weight loss associated with the treatment with Z<sub>1</sub> as the experiment advanced (Figure 31A-C). In contrast, mice from the BTZ group gained more weight throughout the experiment than any of the others.

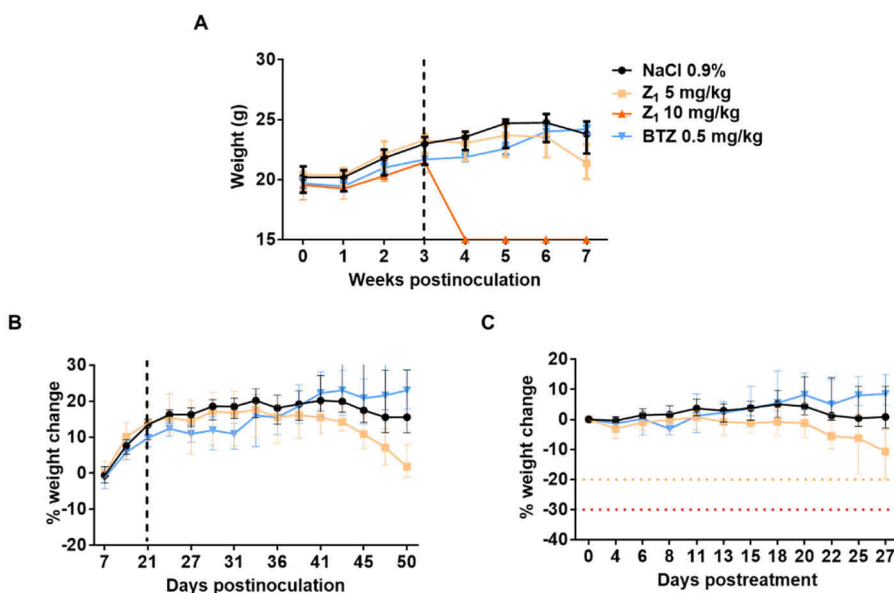


**Figure 31: Treatment with 10 mg/kg of Z<sub>1</sub> caused immediate death, but 5 mg/kg was a safe dose.** (A) Mice weight median and interquartile range per group. The dashed vertical black line indicates the treatment onset. (B) Median percentage and interquartile range of weight change since the inoculation of U266 cells of each group. Z<sub>1</sub> was not represented because all the mice died upon the first administration of the treatment. (C) Median percentage and interquartile range of weight change since the treatment onset. The dotted amber and red horizontal lines indicate the 20 and 30% weight loss. n=6 mice per group.

In addition, after several i.v. inoculations with Z<sub>1</sub>, we started to observe some tissue damage in the tail of the animals, where the injections were being performed. The longer we treated the mice, the more damage we observed. The damage was reported as necrotic tissue in all mice from the 5 mg/kg Z<sub>1</sub> group, where some animals even lost their tails by the end of the experiment. This severe phenotype made the scoring system very challenging since tail motility and strength could not be adequately assessed. In any case, the 5 mg/kg Z<sub>1</sub> group seemed to show a higher score compared to both the control and BTZ groups (Figure 32A and B). However, the mCT images showed no differences in the number (Figure 32D) or volume (Figure 32E) of the osteolytic lesions between the control and the 5 mg/kg Z<sub>1</sub> group, while BTZ clearly stabilised or even caused regression of the lesions (Figure 32C-E).

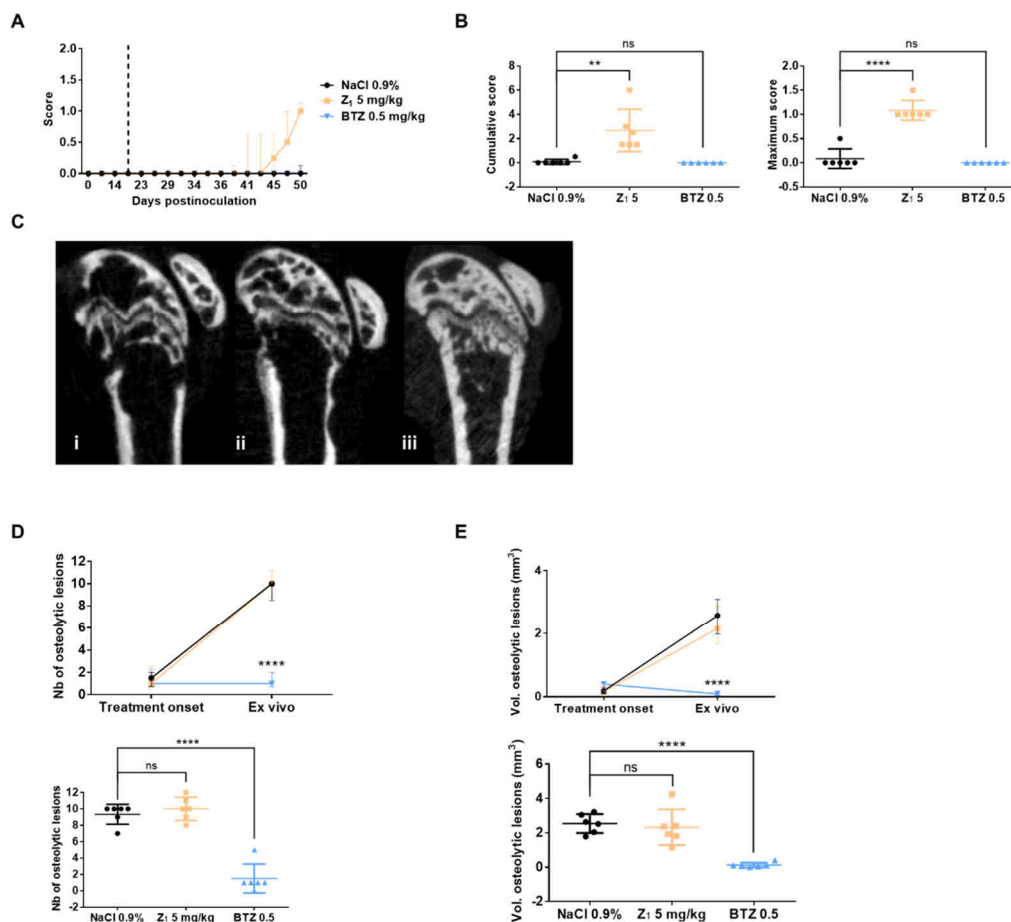


**Figure 32: BTZ stabilised or caused regression of the osteolytic lesions while Z<sub>1</sub> showed no effect.** (A) Longitudinal record of the mean score and SD of each group. Statistical significance was calculated using multiple nonparametric t-tests. (B) Neither cumulative nor maximum score showed differences between groups. (C) Representative ex vivo mCT images are shown for each treatment group. i: control; ii: Z<sub>1</sub> 5mg/kg; iii: BTZ. (D) Quantification of the number of osteolytic lesions comparing the treatment onset with the ex vivo (upper panel) and at the endpoint (lower panel). (E) Quantification of the volume of the osteolytic lesions comparing treatment onset with the ex vivo (upper panel) and at the endpoint (lower panel). Mann-Whitney was the statistical analysis used to determine significance; ns stands for non-significant, \*\* indicates a p-value  $\leq 0.01$  and \*\*\*\* indicates a p-value  $\leq 0.0001$ .

In terms of IgE levels, we found that only BTZ abolished U266 cells growth, while both the control and 5 mg/kg Z<sub>1</sub> groups kept progressing (Figure 33A and B).



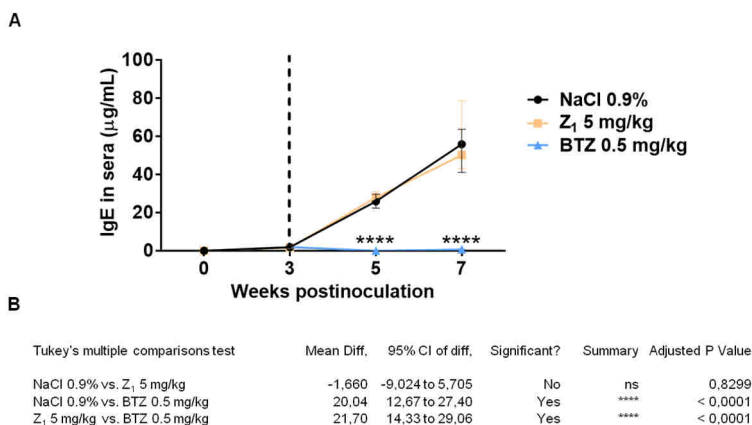


**Figure 33: BTZ blocked the proliferation of myeloma cells, whereas Z<sub>1</sub> did not.** (A) There were no differences in terms of IgE levels in serum between the Z<sub>1</sub> 5mg/kg treated and control groups after 4 weeks of treatment; nonetheless, BTZ completely stopped the proliferation of U266 cells. (B) 2way ANOVA statistical analysis showed significant differences between BTZ and the other 2 groups. Adjusted p-values are detailed in the table.

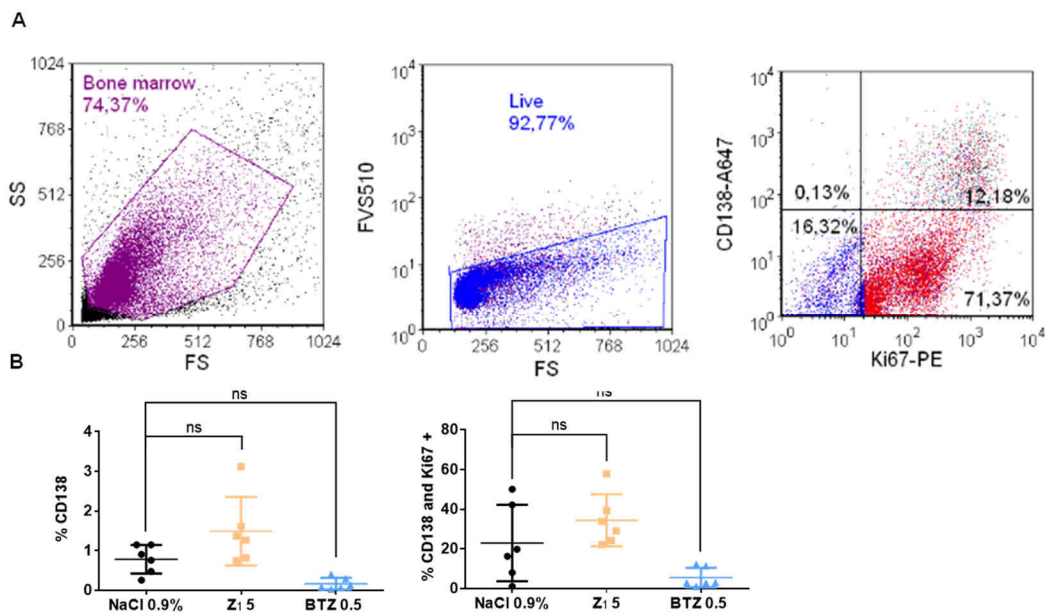


**Figure 34: BTZ showed a promising reduction in the proliferation of BM colonising myeloma cells, while Z<sub>1</sub> caused an increase.** (A) Representative dot plot images showing the CD138/Ki67 populations studied. (B) Quantification of the flow cytometer results of A. One-way ANOVA and Dunnett's multiple comparisons test were used to determine the statistical significance, where ns stands for non-significant.

To complete the study, we also analysed the tumour burden and proliferative status of myeloma cells in the BM. In line with the results obtained for IgE, mice treated

with BTZ showed a tendency, although not statistically significant, of decreased CD138 and CD138/Ki67 positive populations compared to the other 2 groups. In contrast, mice treated with 5 mg/kg of Z<sub>1</sub> showed increased populations of both CD138 and CD138/Ki67 positive cells (Figure 34A and B).

In light of the negative results obtained with the injectable formulation in terms of therapeutic efficacy, and especially due to the severe toxicity we observed during treatment (necrotic tissue in the tail), we agreed with our collaborators to call off the project. Because of this, no further tests were performed.

## 3.2 MYC inhibition with the Omomyc mini-protein

### 3.2.1 Efficacy and mechanism of action of Omomyc on myeloma and lymphoma cell lines

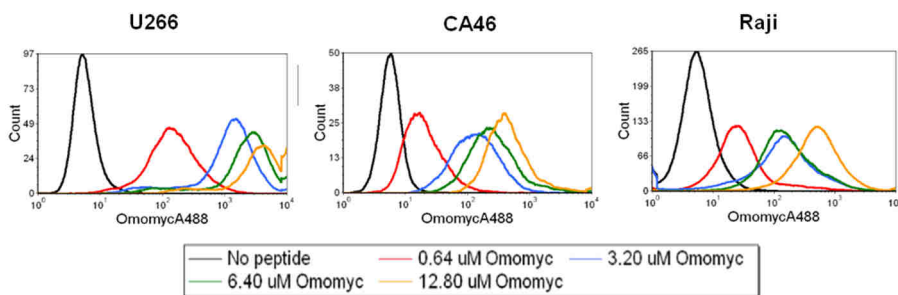
Another strategy to target MYC focused on the utilisation of the recombinantly-produced Omomyc mini-protein as a pharmacological approach against it, both *in vitro* and *in vivo*, to evaluate its efficacy in B-cell haematological malignancies and determine MYC's potential as a therapeutic target in cancer. The mini-protein was recombinantly produced in *E.coli* cultures and purified by cationic exchange using FPLC chromatography thanks to optimised in-house protocols.

As our lab has recently demonstrated ([Beaulieu et al., 2019](#)), the Omomyc mini-protein can penetrate different cancer cell types. For this thesis, we demonstrated that Omomyc also entered MM and BL cell lines, expanding the study for the first time to haematological malignancies. Indeed, after only 15 minutes of incubation with increasing amounts of a fluorescently labelled (AlexaFluor 488 or AF488) mini-protein, we could detect its internalisation even at the lowest concentration (Figure 35A). Apparently, U266 MM cells were slightly more permeable to Omomyc than the 2 BL cell lines (CA46 and Raji).

In addition, we determined the preferred mechanism of entry of the mini-protein in 2 representative cell lines, 1 MM (U266) and 1 BL (CA46). To do so, we used a selection of endocytosis inhibitors.

The results showed that, while the primary mechanism of entrance for U266 was clathrin- with some contribution of caveolin-mediated endocytosis and macropinocytosis, the endocytic pathway for CA46 was quite unclear. In fact, not even the incubation at 4°C (that prevents lipid raft- and Adenosine triphosphate (ATP)-dependent entry) could impede the entrance of Omomyc, suggesting a mixture of contributing mechanisms, including passive transport, independent of ATP hydrolysis (Figure 35B).

A



B

% ENTRANCE INHIBITION			
INHIBITOR	MECHANISM	U266	CA46
4°C	M, Clat, Cav, GEEC	96,51	3,87
MBCD	M, Clat, Cav, GEEC	85,64	37,38
Blebbistatin	M	1,91	4,14
EIPA	M	53,31	6,76
Cytochalasin D	M	15,17	12,87
Dynasore	Clat	97,34	10,82
Chlorpromazine	Clat, Direct	95,47	15,58
Genistein	Cav	61,36	2,68

**Figure 35: Omomyc mini-protein enters MM and BL cells through cell line-dependent endocytic mechanisms.** (A) Cell lines were preincubated at 4° or 37°C and treated with increasing concentrations of Omomyc-AF488 for 15 minutes at the same temperature, trypsinised and analysed by flow cytometry or (B) pretreated for 1 hour with inhibitors (Blebb, blebbistatin; Chlor, chlorpromazine; Cyt D, cytochalasin D; EIPA, 5-ethyl isopropyl amiloride; MβCD, methyl-β-cyclodextrin) of endocytosis or lipid-raft mediated macropinocytosis (M, macropinocytosis; Cav, caveolin-mediated; Clat, clathrin-mediated; GEEC, glycosylphosphatidylinositol (GPI)-enriched early endosomal compartment) and then treated with 0.64 μM Omomyc-AF488 for 15 minutes in the presence of the inhibitor followed by trypsinisation and flow cytometric acquisition. Inhibition of entrance (%) compared to untreated cells at 37°C is shown.

Next, we tested the therapeutic potential of Omomyc mini-protein in MM and BL, making use of a panel of cell lines bearing different genetic alterations. We treated the cells for 5 days with 20 μM of Omomyc, based on our previous results that indicated this concentration was above the IC<sub>50</sub> for other cancer types and therefore showed efficacy *in vitro*. In most of the cell lines, we observed a reduction in cell proliferation of around 50% compared to their control counterparts (Figure 36A). The best responder was a mouse MM cell line, 5TGM1, whose proliferation went down to 15%. Omomyc was also able to induce changes in the cell cycle profile after 3 days of treatment in all cell lines (Figure 36B and C). We could not find a common mechanism of growth arrest for the different types of MM cells, which seemed to arrest in different cell cycle phases. For BL cells, instead, we mostly observed a reduction in the G0/G1 phase and slight increases in S and G2/M populations in both cell lines. However, what was conserved between all MM

and BL cells was the increase in the subG1 population, suggestive of induction of cell death (even though the increases were not significant) (Figure 36B and C).

Since Omomyc is a direct MYC inhibitor, we investigated if it could affect the protein levels of MYC itself and its obligate partner, MAX. We treated our panel of MM and BL cell lines for 3 and 5 days and looked at the MYC and MAX protein levels in the presence or absence of Omomyc. To confirm the entrance of the mini-protein, we also probed for Omomyc using a specific monoclonal antibody developed at the lab in collaboration with Biogenes. As for the entrance experiments, to ensure that the Omomyc detected was only intracellular, we trypsinised cells before lysing them. Then, we loaded equivalent numbers of cells in each well, and we normalised MYC and MAX protein levels to those of actin. After 3 days of treatment, we observed a reduction in MYC levels in all of the cell lines except for 1 MM (KMS-12-BM) and 1 BL (Raji) (Figure 37A and C). Said reduction was more apparent after 5 days, where all the cell lines, except for KMS-12-BM, displayed a clear decrease (Figure 37B and D).

Similarly, MAX levels were reduced after 3 days of treatment in all the cell lines except for KMS-12-BM and Raji (Figure 37A and C). In contrast, all the cell lines, with no distinction, showed reduced levels of MAX after 5 days of treatment with Omomyc (Figure 37B and D). Finally, we confirmed that Omomyc was still present at 3 and 5 days post-treatment in all the samples that had been treated with the mini-protein on day 0. Interestingly, our Omomyc antibody detected 2 bands in every blot, the upper one corresponding to full-length Omomyc and the lower to a slightly smaller, cleaved version of it.

## Results

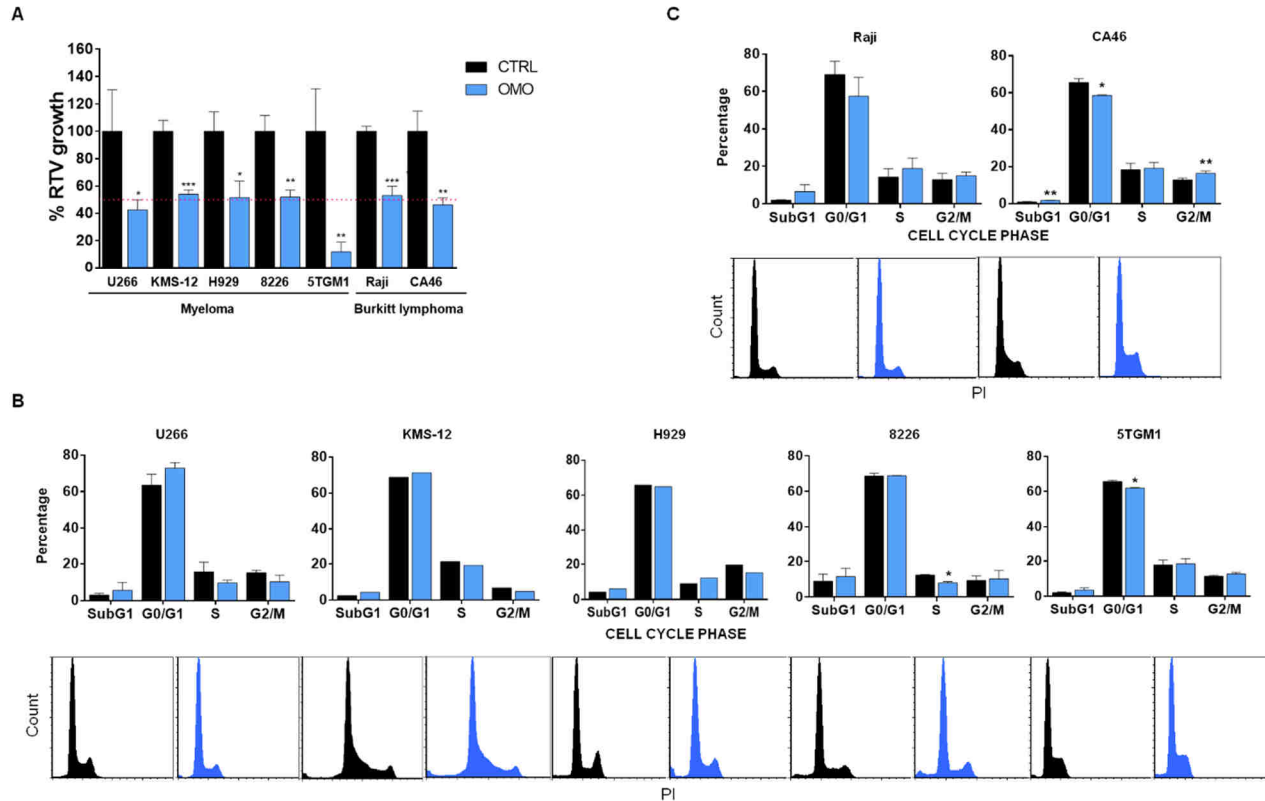


**Figure 36: Omomyc blocks MM and BL cell proliferation, inducing changes in the cell cycle profile.** (A) Quantification of viable cell number after 5 days of treatment with 20  $\mu$ M Omomyc (OMO) using a trypan blue exclusion assay made relative (RTV) to the untreated control (CTRL). (Upper panels) Quantification of cell cycle phase populations from flow cytometric analysis of PI incorporation after 3 days of treatment with 20  $\mu$ M Omomyc compared to the untreated control from (B) MM or (C) BL cells. (Lower panels) Cell cycle profiles. All experiments were performed at least twice. Mean and SD are shown, and a two-tailed unpaired Student's *t*-test was used to calculate the statistical significance. \* indicates a *p*-value  $\leq 0.05$ ; \*\* indicates a *p*-value  $\leq 0.01$ ; \*\*\* indicates a *p*-value  $\leq 0.001$ .

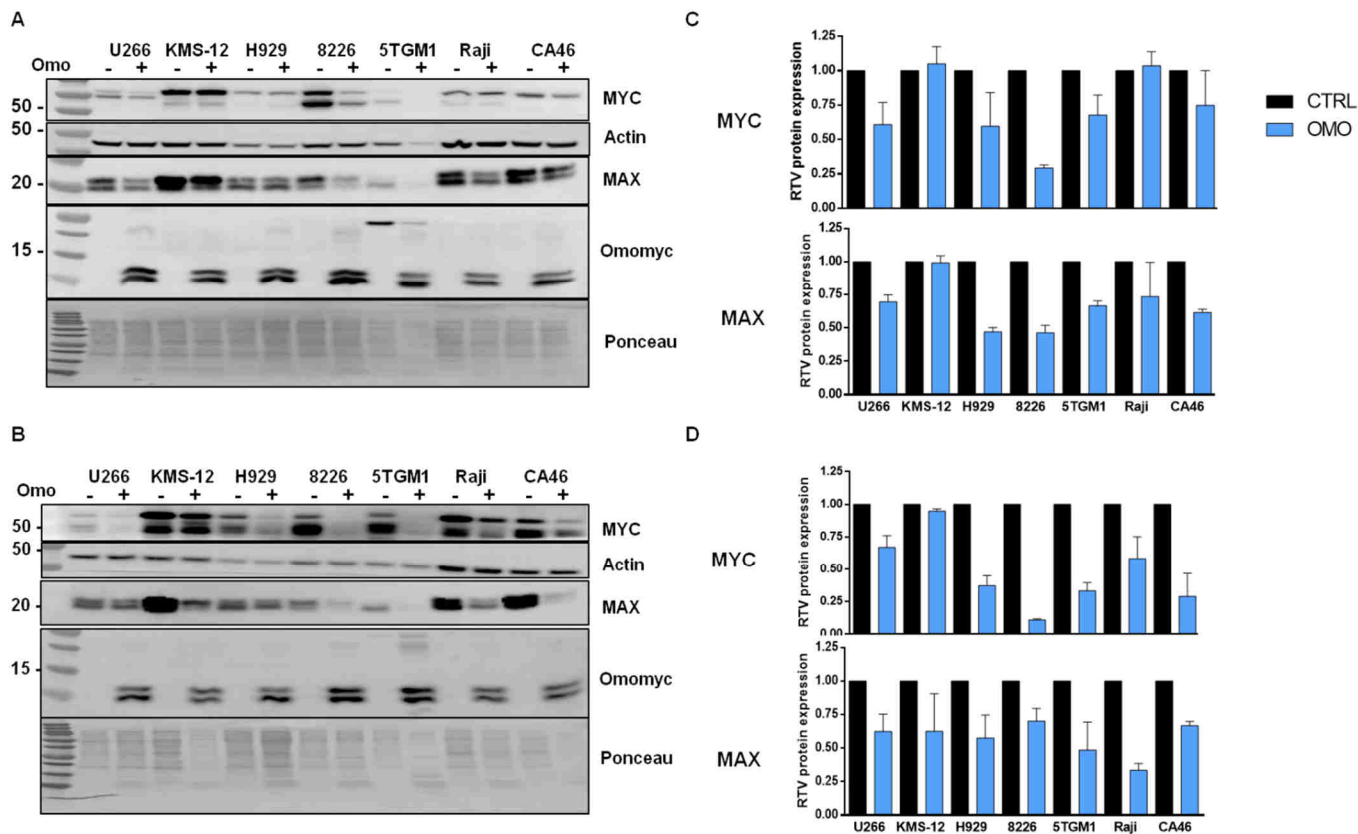


**Figure 37: Omomyc reduced MYC and MAX levels after 3 or 5 days of treatment.** Immunoblots against MYC, MAX, Omomyc and actin using extracts from samples untreated (-) and treated with 20  $\mu$ M Omomyc (+) for 3 (A) and 5 (B) days. Ponceau is shown as a secondary protein loading control. A representative Western blot out of 3 independent experiments is shown. (C) Quantification of MYC and MAX levels from A. (D) Quantification of MYC and MAX levels from B; Omomyc-treated samples (OMO) were represented relative to the control (CTRL).

Given that MYC binds DNA to exert its function, we aimed at confirming that Omomyc mini-protein could displace MYC from its *bona fide* target promoters as part of its inhibitory activity (Beaulieu et al., 2019). We performed chromatin immunoprecipitation (ChIP) followed by qPCR to study the occupancy of various promoters upon treatment with Omomyc. We chose 2 representative cell lines: U266 (MM) because the decrease in MYC levels was constant at both 3 and 5 days of treatment, and Raji (BL), which showed changes in MYC levels only after 5 days (Figure 37). As with the western blot analysis, we treated the cells for 3 and 5 days and studied MYC binding to DNA. We already observed a MYC displacement from all promoters of interest in U266 (Figure 38A) or some in Raji (Figure 38B) in the samples treated for 3 days compared to controls. This effect was confirmed and reinforced after 5 days of Omomyc treatment when we saw a considerable displacement from all the promoters in both cell lines (Figure 38C and D). Curiously, PVT1 and IFRD2 actually showed an increase after 3 days of treatment in Raji cells, but then at 5 days they both appeared consistently decreased, as the rest of gene promoters.

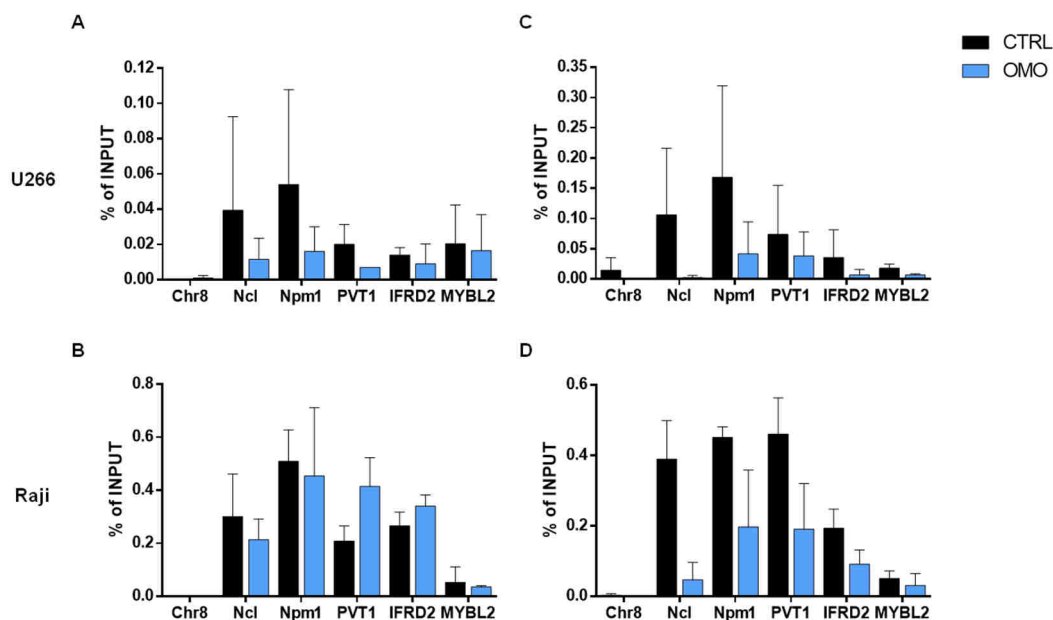


**Figure 38: Omomyc displaced MYC from its target promoters.** MYC chromatin immunoprecipitation (ChIP)–quantitative polymerase chain reaction (qPCR) from U266 (A) and Raji (B) cells treated for 3 days or U266 (C) and Raji (D) cells treated for 5 days with 20  $\mu$ M Omomyc (blue) or untreated (black) is shown for typical MYC target proximal promoter regions: Chromosome 8 “gene desert” region (Chr8), nucleolin (Ncl), nucleophosmin (Npm1), interferon-related developmental regulator 2 (IFRD2), and MYB proto-oncogene–like 2 (MYBL2); mean and SD are shown from 2 independent experiments.

Since MYC got removed from DNA, we wondered if Omomyc mini-protein could be occupying its place in the form of Omomyc homodimers or Omomyc/MAX heterodimers. Hence, our next step was to ChIP using an Omomyc antibody. Since we had never used this protocol before, we had to set up all the experimental conditions for it. To do so, we used our lab standard cell line model, H1299 non-small cell lung cancer (NSCLC) cells, bearing a transgenic Omomyc-RFP construct. Previously, our lab had demonstrated the binding of transgenic Omomyc to DNA in a ChIP-sequencing (-seq) experiment in this same cell line (Jauset et al., in preparation), using a polyclonal antibody generated in collaboration with Immunoglob. Yet, when we checked the binding of Omomyc to DNA from H1299 cells treated with 20  $\mu$ M of the recombinant mini-protein, we could not detect any Omomyc on DNA (Figure 39A). At this point, we wondered whether Omomyc mini-protein was actually behaving differently from its transgenic counterpart and not binding to DNA, or if we were facing technical problems that impeded its detection.

In order to perform some troubleshooting, we focused on the DNA fragmentation step required for the protocol: it is common in ChIP experiments to sonicate DNA in order to fragment it in pieces of 100-300 base pairs (bp). However, sonication can be a slightly aggressive technique for certain protein complexes, because it can break and remove them from their binding sites. With that in mind, we introduced 2 changes into our standard protocol for transgenic Omomyc: 1. we chose a double cross-link with disuccinimidyl glutarate (DSG), to create more stable protein-DNA complexes; 2. we switched to an in house-generated monoclonal Omomyc antibody, which we had proven to work for ChIP before (Figure 39B).

Using these tweaks in our standard protocol, we demonstrated that Omomyc was, indeed, able to bind the promoters from which MYC was displaced in U266 cells (Figure 39C). Furthermore, in line with the increasing displacement of MYC by Omomyc treatment over time, we could detect more Omomyc mini-protein bound to DNA after 5 days, compared to the amount found at 3 days of treatment (Figure 39D).



## Results

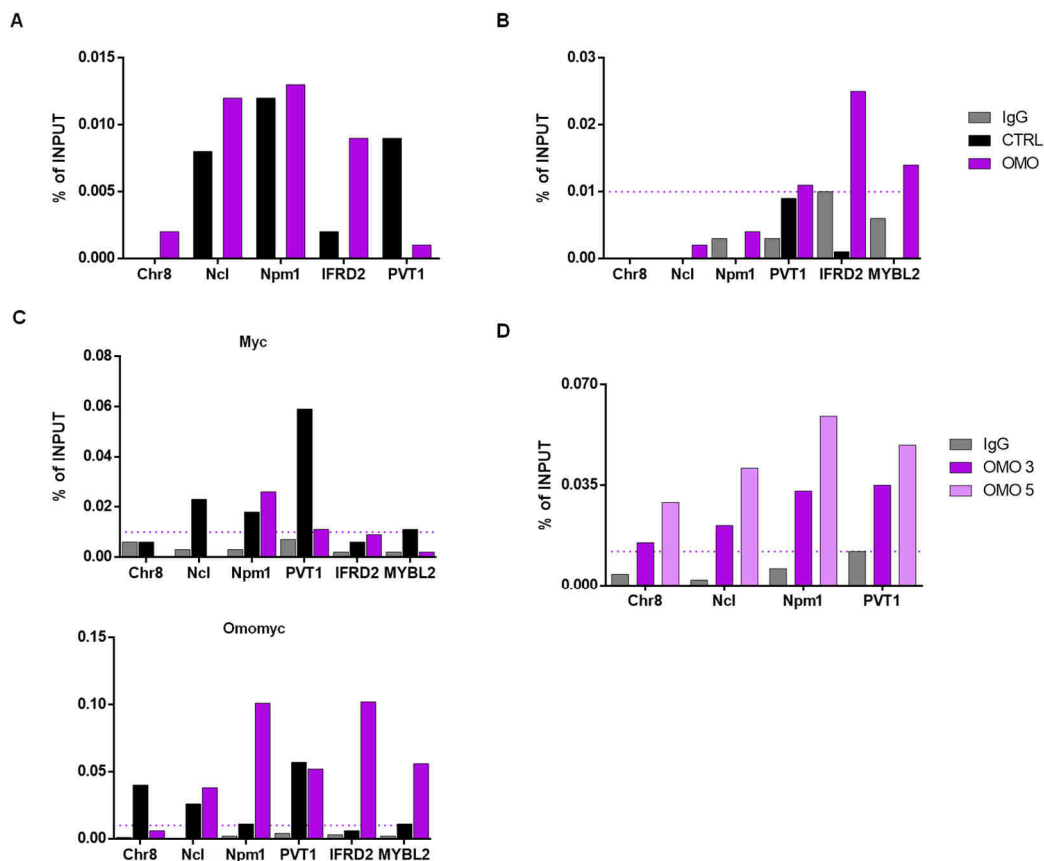


**Figure 39: Omomyc was bound to DNA at the same sites where MYC was displaced.** (A) *Omomyc*<sup>P</sup> ChIP-qPCR from H1299 cells treated for 3 days with 20  $\mu$ M Omomyc (violet) or untreated (black); (B) *Omomyc*<sup>M</sup> or IgGs (grey) ChIP-qPCR from H1299 cells expressing *Omomyc*-RFP; (C) MYC and *Omomyc*<sup>M</sup> ChIP-qPCR from U266 cells treated for 3 days with 20  $\mu$ M Omomyc (violet) or untreated (black) and (D) *Omomyc*<sup>M</sup> ChIP-qPCR from U266 cells treated for 3 (OMO3) or 5 (OMO5) days with 20  $\mu$ M Omomyc are shown for typical MYC target proximal promoter regions [Chromosome 8 “gene desert” region (Chr8), nucleolin (Ncl), nucleophosmin (Npm1), interferon-related developmental regulator 2 (IFRD2), and MYB proto-oncogene-like 2 (MYBL2)]; mean and SD are shown. Each experiment was done once.

Additionally, we were interested in studying whether Omomyc could cause any epigenetic changes, as a potential marker of long-term effect of our inhibitor. For that, we looked into 2 gene activation and 1 repression marks (H3K27ac, H3K4me3 and H3K9me3, respectively). Again, we used U266 and Raji cells, treated them for 3 or 5 days, then looked at the effect of Omomyc treatment on the epigenetic marks of *bona fide* MYC target promoters compared to the control. Raji cells displayed a reduction of both the active enhancer (H3K27ac) and active gene (H3K4me3) marks in almost all the promoters (Figure 40A and B). Said decrease was

cumulative over time since samples from the 5 day-treatment showed more reduction compared to 3 days.

Unexpectedly, instead, U266 cells exhibited an increase in both activation marks, that also seemed to be greater with time (Figure 41A and B). So, in U266, we decided to also look at a repression mark (H3K9me3) involved in transcriptionally silent heterochromatin. To our surprise, we found it generally increased in our Omomyc-treated samples, and to a further extent after 5 days of treatment compared to the 3 days time point (Figure 41C).

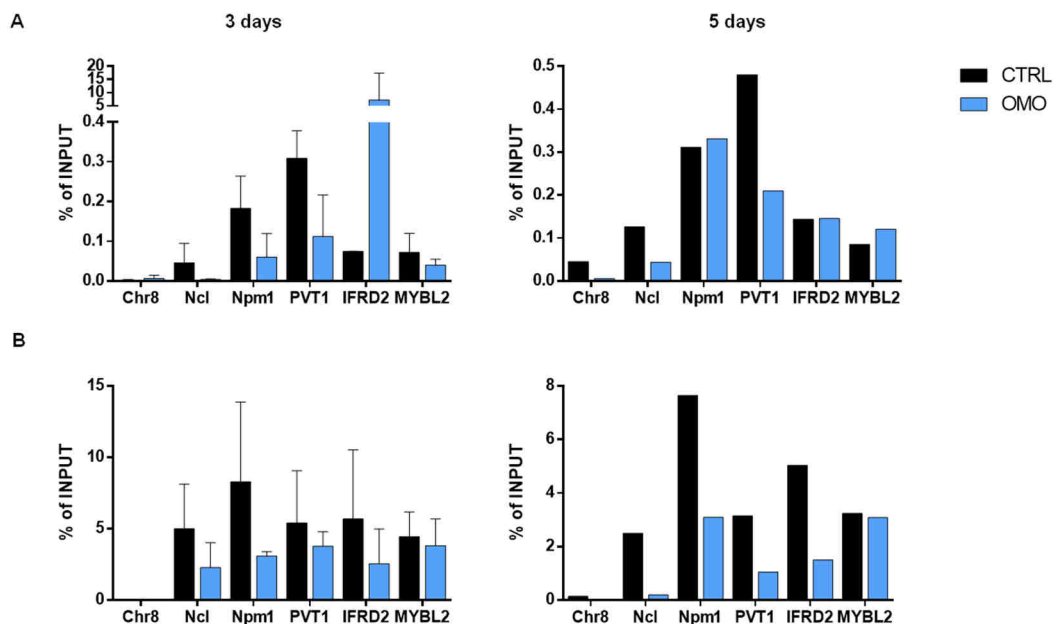


**Figure 40: Omomyc reduced active gene histone marks in Raji cells.** ChIP-qPCR of (A) H3K27ac and (B) H3K4me3 from Raji cells treated for 3 (left panels) or 5 days (right panels) with 20  $\mu$ M Omomyc (blue) or untreated (black) are shown for the typical MYC target proximal promoter regions specified in Figure 38. The 3-day time point experiment was done twice, and the 5-day time point once.

## Results

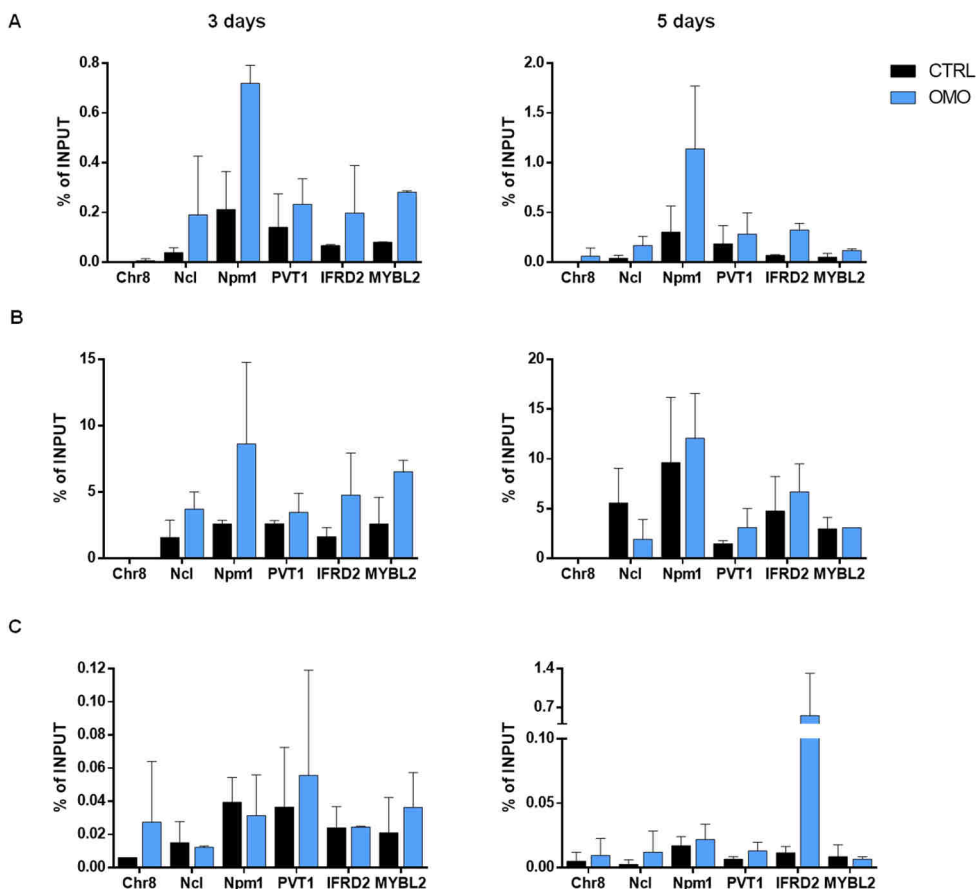


**Figure 41: Omomyc increased active and repressed gene histone marks in U266 cells.** ChIP-qPCR of (A) H3K27ac, (B) H3K4me3 and (C) H3K9me3 from U266 cells treated for 3 (left panels) or 5 days (right panels) with 20  $\mu$ M Omomyc (blue) or untreated (black) are shown for the typical MYC target proximal promoter regions specified in Figure 38. The experiments were performed twice.

### 3.2.2 Therapeutic effect of Omomyc in a zebrafish model

All these results obtained *in vitro* gave us a glance of Omomyc's mechanism of action in MM and BL and encouraged us to evaluate its efficacy *in vivo*.

In the beginning, there were limitations with the amount of mini-protein that could be produced for *in vivo* purposes, mainly because the protein production and purification were done at lab-scale and the upscaling protocol was under development. To overcome this issue, we searched for an *in vivo* model that would allow minimal use of the compound to be tested. In a Cancer Research publication (Sacco et al., 2016), the authors had described the use of zebrafish as a valuable tool to study homing of cells to the haematopoietic niche and as a drug screening platform. This model offered the possibility of admixing experimental (i.e. drug-

treated) and control cells at the same time, thus comparing their ability to reach and colonise the BM in the same animal. So, in order to perform these experiments, we established a collaboration with the laboratory of Dr Victoriano Mulero at Murcia University. Dr Mulero's lab is renowned for its use of the zebrafish model for studying several different diseases.

First, we assessed if Omomyc could impair the migration capacity of U266 (MM) and CA46 (BL) cells. We pretreated the cells in culture, admixed them with an equal number of control cells (without treatment) and inoculated 400 cells in 2 nL through the duct of Cuvier of each zebrafish larva. A different fluorescent dye for treated and untreated cells allowed their distinction. 1 hour postinoculation (hpi), we took images of the BM-like structure present in zebrafish larvae, known as caudal haematopoietic tissue or CHT, and quantified the number of cells that had reached it. Omomyc was able to significantly reduce the number of colonising CA46 (Figure 42A and B) and U266 cells in the CHT (Figure 42C and D).

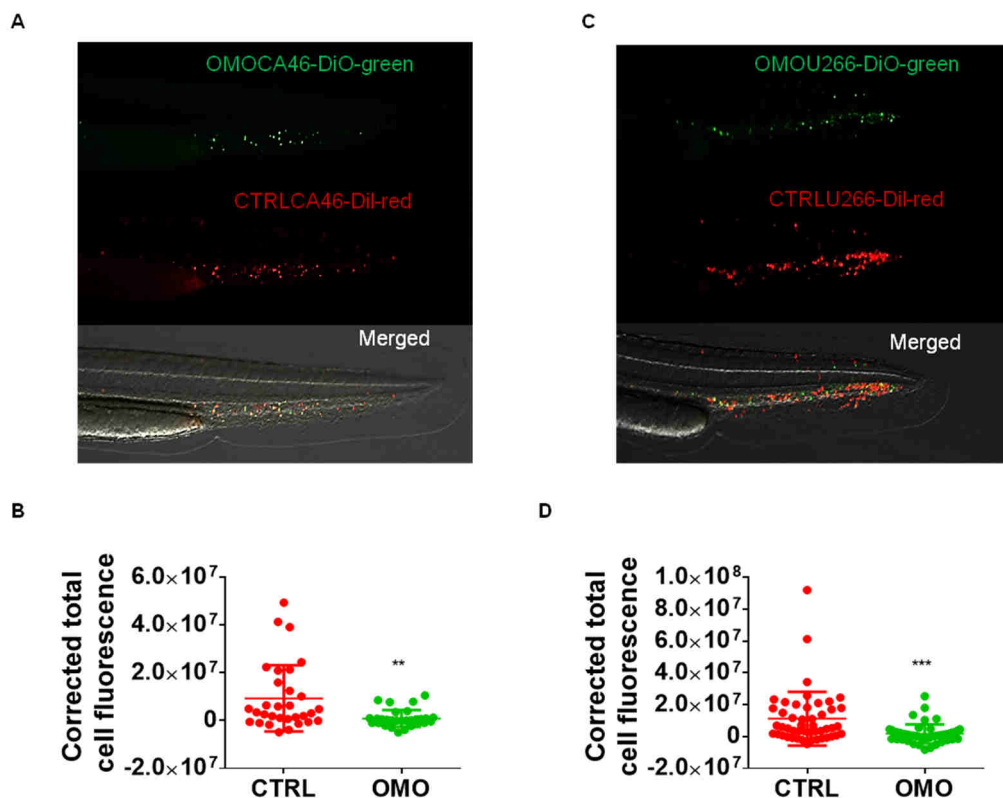


**Figure 42: Pretreatment with Omomyc in culture impaired MM and BL cell migration to the CHT.** CA46 (A and B) and U266 (C and D) cells were pretreated with  $20 \mu\text{M}$  Omomyc for 3 or 5 days, respectively. Cells were then stained with fluorescent membrane dyes, Dil-red for control cells (CTRL), and DiO-green for Omomyc-treated cells (OMO) and mixed at an equal number of the 2 conditions to be inoculated into

## Results

zebrafish larvae. 1 hpi larvae were analysed by confocal microscopy. (A and C) Representative images of the individual channels (Dil-red/DiO-green) and Merged, where the 2 admixed populations were seen. (B and D) Quantification of the number of cells analysed in A and B, respectively, measured as corrected total cell fluorescence using ImageJ. Statistical significance was calculated with a Mann-Whitney test. \*\* indicates a  $p$ -value  $\leq 0.01$ ; \*\*\* indicates a  $p$ -value  $\leq 0.001$ .

To characterise the mechanism by which Omomyc was altering the colonisation of the CHT in zebrafish, we performed *in vitro* experiments. Like we did *in vivo*, we assessed the migration capacity of CA46 and U266 cells after subjecting them to an Omomyc pretreatment for 5 days. Then, we seeded the cells on the upper chamber of a transwell in their regular culture medium. In the lower chamber, we added medium with or without CXCL12, a chemoattractant, and let the cells migrate. After 4 hours, we collected the media from the lower chamber and counted cells by an automated cell-counter, assessing their viability with trypan blue. Omomyc-treated U266 cells displayed reduced migration both in the presence or absence of CXCL12 (Figure 43A), suggesting that Omomyc could act on the general ability of these cells to migrate independently of the chemoattractant signal. In contrast, CA46 cells treated with Omomyc only showed significantly decreased kinesis (migration in the absence of the chemokine), while their chemotaxis (migration towards the chemoattractant) remained unchanged (Figure 43B). To further understand the process, we evaluated potential underlying molecular mechanisms and found that Omomyc reduced the levels of Very Late Antigen-4 (VLA-4), an integrin required for the formation of pseudopodia, in both cell lines (Figure 43C).

To investigate the feasibility of doing more than prevention and performing intervention studies in the zebrafish model, we performed a biodistribution experiment with a fluorescently labelled Omomyc (Omomyc-AF488) treating the larvae by immersion. With this method, Omomyc was added at 20  $\mu$ M concentration into the embryo medium and the zebrafish submerged in it. At the end of the experiment, the fluorescence was assessed by fluorescence microscopy.

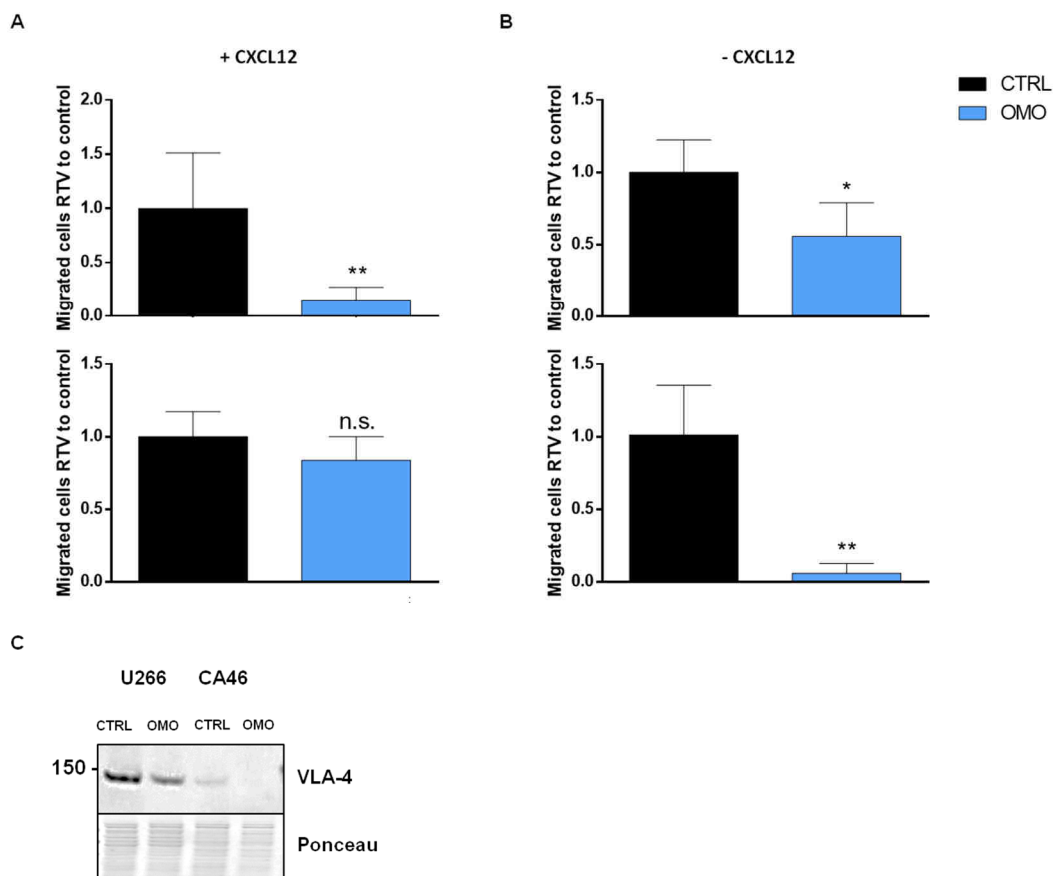


**Figure 43: Omomyc reduced the migration capacity of MM and BL cells in a Boyden's chamber assay.** U266 (A) and CA46 (B) cells were treated for 5 days with 20  $\mu$ M Omomyc. Cells were then plated in the upper chamber of a transwell separated from the lower chamber through a 5  $\mu$ m pore polystyrene membrane. The culture medium from the lower chamber had been supplemented (+) or not (-) with CXCL12 to create a chemotactic gradient. We compared the migration of Omomyc-treated (blue) with control cells (black). (C) Western blot against VLA-4 using lysates from U266 and CA46 cells untreated (CTRL) or treated with Omomyc 20  $\mu$ M (OMO). Ponceau was shown as a protein loading control. Statistical significance was calculated with a Student's *t* test. \* indicates a *p*-value  $\leq 0.05$ ; \*\* indicates a *p*-value  $\leq 0.01$  and *n.s.* stands for non-significant.

First, we added the mini-protein to the embryo medium and incubated for 30 minutes. As seen in Figure 44A, all the fluorescence detected came from the tegument of the larvae, but no molecule had trespassed this barrier. Next, we added 1% DMSO to the solution, in order to increase the permeability of the membranes, and incubated for 1 hour. In this case, not only did we see the fluorescent mini-protein pass through the tegument, but we also saw it in circulation (Figure 44B). However, we also reported severe side effects such as death (9/11

larvae) and haemorrhages coupled to slowed blood flow (11/11 larvae). To reduce the toxicity found at 20  $\mu\text{M}$  of Omomyc, we determined the maximum tolerated dose (MTD) using lower concentrations (1, 5, 10, 15  $\mu\text{M}$ ) and compared it with our positive control for unacceptable side effects (20  $\mu\text{M}$ ). This time we used unlabelled peptide (always in the presence of 1% DMSO) because we considered the possibility that part of the adverse effects could be due to the fluorescent label. As depicted in Table 9, we classified the side effects as slowed blood flow (severe or mild), haemorrhages or death. Our results concluded that 10  $\mu\text{M}$  was the dose of choice to proceed with efficacy studies, due to the noticeable reduction in adverse effects compared to higher doses.

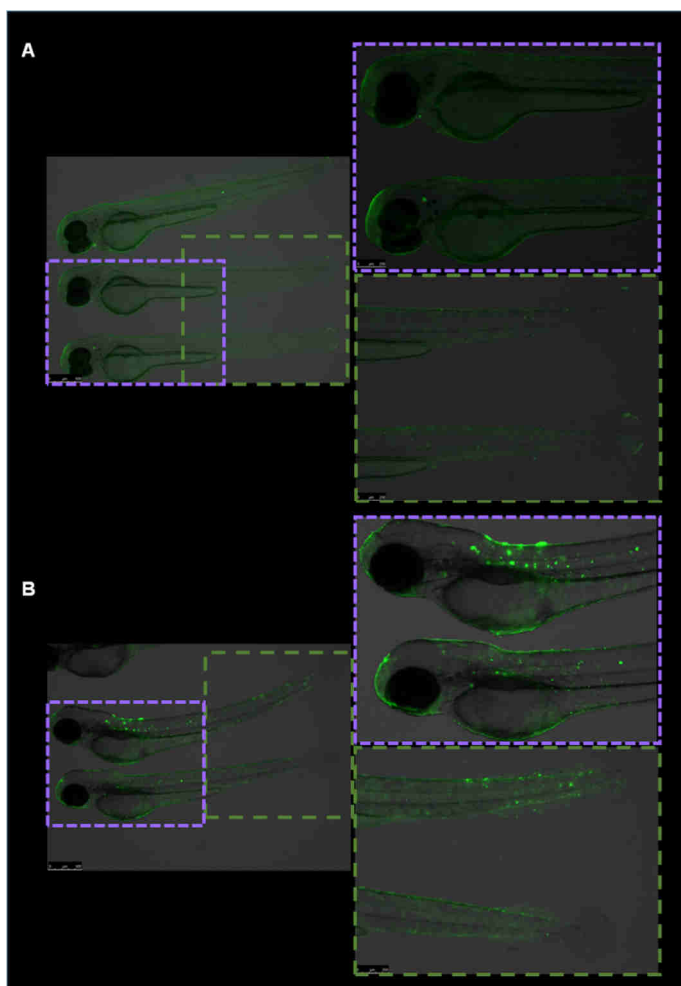


**Figure 44: Omomyc penetrated the tegument of zebrafish larvae.** Zebrafish were immersed in embryo medium containing 20  $\mu\text{M}$  of Omomyc in the absence (A) or presence (B) of 1% DMSO. Animals were incubated at 35°C for 30 minutes (A) or 1 hour (B). After that, larvae were anaesthetised with tricaine, aligned under the confocal microscope and analysed. Representative pictures are shown for each condition.

Peptide concentration	20µM	15µM	10µM	5µM	1µM	Control
Deaths	7/20	6/20	0/20	0/20	0/20	0/20
Haemorrhages	20/20	13/20	1/20	0/20	0/20	0/20
Slowed blood flow (severe)	13/13	13/13	20/20	0/20	0/20	0/20
Slowed blood flow (mild)	0/13	0/13	0/20	20/20	0/20	0/20

**Table 9: Side effects caused upon treatment with Omomyc by immersion.** MTD with 5 different concentrations of Omomyc. Each group was comprised of an *n* of 20 larvae. The side effects reported were: death, haemorrhage or slowed blood flow. The number of larvae affected by each adverse effect are displayed per concentration. Control larvae showed no side effects.

Having established a safe dose, we proceeded to treat larvae previously inoculated with U266 cells. We followed the treatment and evaluation scheme, as depicted in Figure 45A.

In the first experiment, we were able to treat the zebrafish for 72 hours, at which point we recorded the first deaths of larvae, likely due to accumulated toxicity of 3 immersion treatments (10 µM Omomyc with 1% DMSO). Unfortunately, this time, we did not observe any reduction in the number of colonising U266 cells at the CHT (Figure 45B).

In a second experiment, using a similar xenotransplant and treatment regimen (Figure 45C), we tried administering a lower concentration, 5 µM and compared the effects to those seen with 10 µM protein. However, very disappointingly, this time we saw the toxicity at an earlier time point (48 hours as compared to 72 in the previous experiment) after only 1 immersion and no differences between the treatment groups (Figure 45D). Because of that, it should be noted that we ended up with only a tiny *n* of larvae that had a sufficient number of U266 cells that had reached the CHT (more than 10 cells) and, thus, could be included in the analysis. We hypothesised that possible explanations for the earlier and numerous deaths could be accumulated toxicity of continuous treatment, and the engraftment of U266 cells could add up to the toxicity caused by it. To address these issues, we washed the larvae after each treatment and included a group of “healthy” larvae (without U266 cells) that received the 10 µM treatment only. Nonetheless, all larvae from both 10 µM treatment groups died after the second immersion (Figure 45E). Again, we could not see differences in terms of cell number at the CHT between any of the groups (Figure 45F), contradicting the results of our prevention studies.



## Results

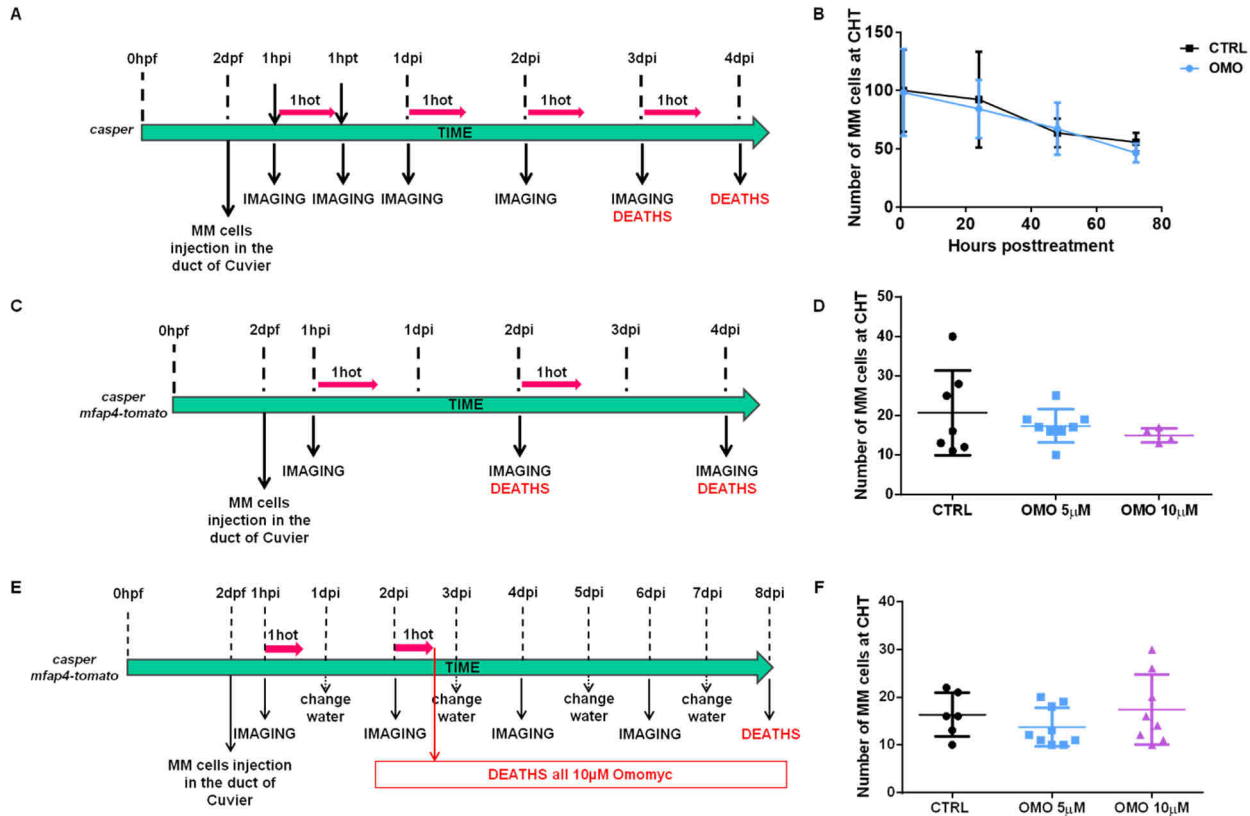


**Figure 45: Omomyc causes the death of zebrafish larvae after repeated treatments.** (A, C and E) Schematic diagram of the schedule followed (xenotransplant, treatment regimen and evaluation by imaging), where each time was specified as hpf: hours post fertilisation; dpf: days post fertilisation; hpi: hours postinjection; hot: hours Omomyc treatment; hpt: hours posttreatment; dpi: days postinjection. (B, D and F) Quantification of the number of cells at the CHT.

In a last attempt to reduce toxicity, we encapsulated Omomyc into liposomal nanoparticles (from now on “Omolips”). The formulation used consisted of DPPC (70%), DOPE (10%) and CHEMS (20%) and it allowed us to obtain an encapsulation efficiency (EE) of ~50%. We had both PEGylated liposomes (coated with 2% PEG) and uncoated nanoparticles (NPs) because our *in vitro* data suggested that the addition of PEG to the formulation could increase the toxicity of the NPs (Figure 46A). With regards to the efficacy, we demonstrated that even though empty liposomes caused partial cell death, Omomyc encapsulation significantly added up to that effect, allowing a reduction of 60% in tumour cell viability, as compared to almost no effect seen when treating with free Omomyc mini-protein at 5  $\mu$ M (Figure 46A). We also looked at the entrance of Omolips by FACS analysis, as we had previously done in 3.2.1, and compared it to the entrance of free labelled Omomyc. To determine the amount of Omomyc from the liposomes reaching the intracellular compartment, we used 10% of Omomyc-AF488 as a tracer, together with 90% of unlabelled Omomyc. Our findings showed no differences in penetrance between free or encapsulated Omomyc (Figure 46B).

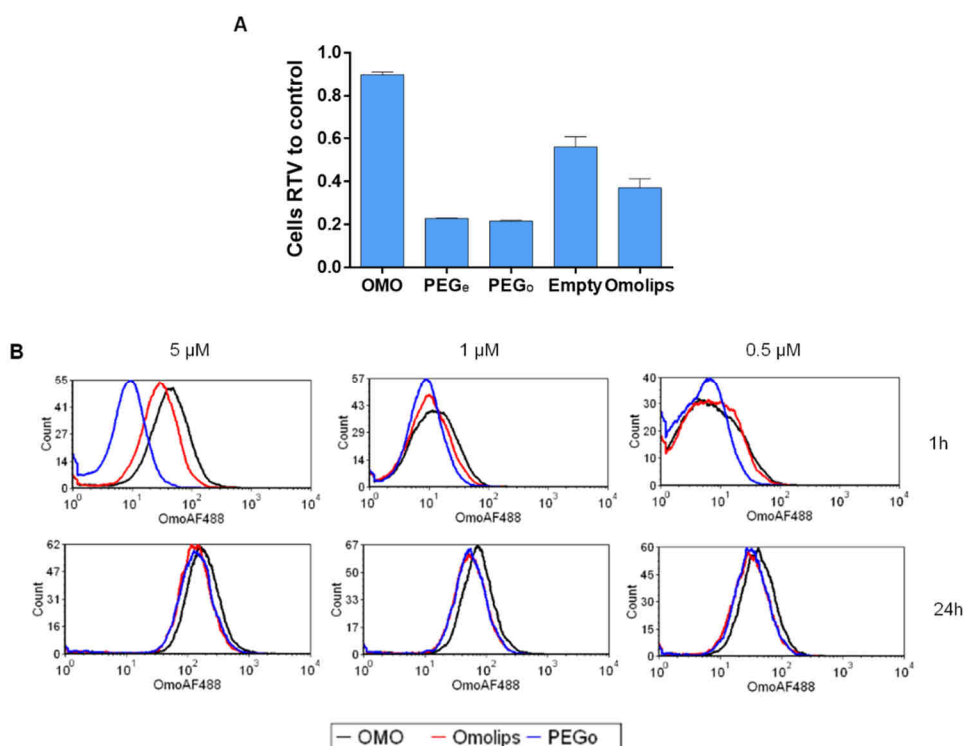


**Figure 46: Omolips did not improve the entrance *in vitro*, and PEGylation increased their toxicity.** (A) Quantification of the number of viable cells after 5 days of treatment with 5  $\mu$ M Omomyc or the equivalent amount of empty liposomes or Omolips using a trypan blue exclusion assay made relative (RTV) to the untreated control (not shown). Treatment groups as follows: free Omomyc mini-protein (OMO), PEG<sub>e</sub> (PEGylated empty liposomes), PEG<sub>o</sub> (PEGylated Omomyc liposomes), Empty

## Results

(empty liposomes) and Omolips (Omomyc liposomes). Mean and SD of triplicates from the experiment performed are shown. (B) U266 cells were preincubated at 4° or 37°C and treated with increasing concentrations (5, 1 or 0.5 µM from left to right) of Omomyc-AF488/Omolips/PEG<sub>0</sub> for 1 hour (upper panels) or 24 hours (lower panels) at the same temperature, trypsinised and analysed by flow cytometry.

To determine if this formulation could be used for efficacy experiments by potentially reducing toxicity at the same time, we performed a biodistribution experiment, similar to what we had done with the free labelled Omomyc (Omomyc-AF488). We used older larvae for this study because they allowed the engraftment of U266 cells for at least 1 day, then extended the duration of the observation to see whether we could broaden our therapeutic window beyond that time point (Figure 47A). We immediately found one limitation with this experiment: to prevent the Omolips from getting disrupted by DMSO (an organic solvent) in the mixture, we did not use our usual 1% DMSO to deliver our drug. Unfortunately, but in a way expected, in these conditions, Omolips, like the free mini-protein, could not penetrate the tegument of zebrafish larvae. In fact, despite seeing some fluorescence inside the animals (which seemed to accumulate in an internal organ), we concluded that the entrance happened only through the mouth (there were peristaltic movements detected), which is already opened at 3dpf (days post fertilisation) (Figure 47B).

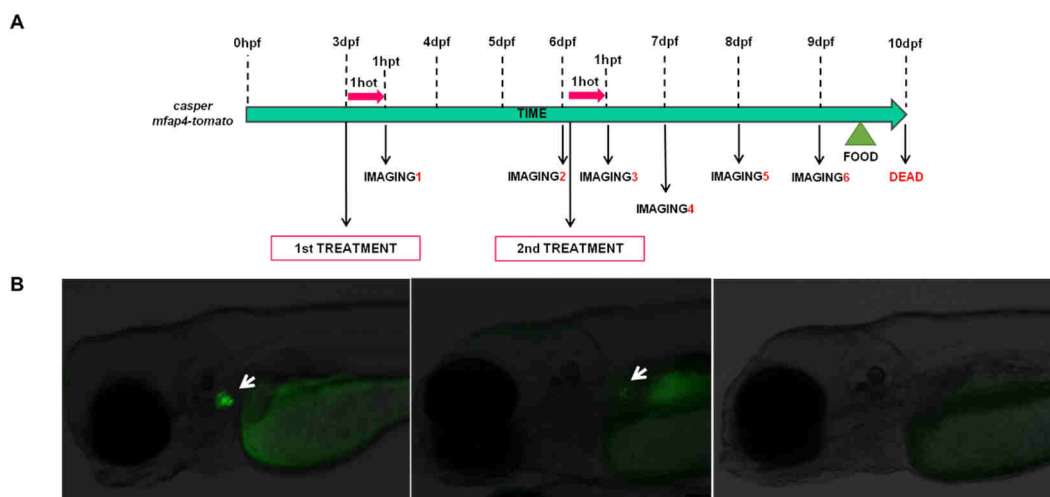


**Figure 47: Omolips could not penetrate the tegument of zebrafish.** (A) Schematic diagram of the schedule followed (treatment regimen and evaluation by imaging), where each time was specified as hpf: hours post fertilisation; dpf: days post fertilisation; hot: hours Omomyc treatment and hpt: hours posttreatment. (B) Representative images of zebrafish larvae treated with Omolips at 5 µM.

Hence, at the end of this biodistribution experiment, we decided to switch to a different animal model that did not require entrance through the tegument.

### 3.2.3 Therapeutic effect of Omomyc in xenograft mouse models of multiple myeloma and Burkitt lymphoma

Encouraged by our previous results that showed that Omomyc impaired the migration of MM and BL cells *in vivo* in the zebrafish model, we decided to proceed and test the therapeutic effect of Omomyc mini-protein in a xenograft mouse model of BL.

First, in a prevention experiment intended to assess the therapeutic impact of Omomyc in affecting lymphoma engraftment, we inoculated 2 million Raji cells *i.v.* through the tail vein of SCID-Bg mice, and the day after, randomised the animals into the treatment groups (control and Omomyc) and treated them with vehicle or Omomyc (32 mg/kg once a week). 10 days postinoculation of Raji cells (hence after 2 treatments with Omomyc), we euthanised the mice to look at the colonisation of spleen and BM of lymphoma cells, as well as the invasion in extramedullary and non-lymphoid organs using CD79 $\alpha$  staining.

Our data showed that there were no significant differences in the number of positive cells detected in the non-lymphoid organs analysed between control and Omomyc-treated groups (Figure 48A), although at this early time point, Raji cells had not migrated much, nor had they particularly engrafted yet in lymphoid organs except for the BM,. At least 1 animal per group showed a positive signal in each organ: brain (Figure 48B), kidney (Figure 48C), lung (Figure 48D) and liver (Figure 48G). However, encouragingly, Omomyc treatment reduced the engraftment of Raji cells in the BM (Figure 48F), consistent with the reduction we had previously shown in the zebrafish model, while we quantified an increase in Raji cell number in the spleen of Omomyc-treated animals as compared to the control (Figure 48E).

Hence, we decided to proceed and perform an intervention study in the MM xenograft model that we had set up in 3.1.2, hoping that longer observation times and different parameters would allow detecting some difference. Taking advantage of the previous knowledge we had gathered, not only in the prevention study with BL cells but also with other cancer models in the lab, we decided to increase the Omomyc dose to 50 mg/kg once a week for 4 weeks (equivalent to 5 doses, as opposed to the 2 doses received in the prevention study).

Notably, mice did not experience any loss of weight associated with the treatment throughout the experiment (Figure 49A-C).

However, we were not able to detect any statistically significant therapeutic impact in the Omomyc-treated group compared to the control. This was particularly disappointing, since, from our observation of the animals, we thought there was a tendency of improvement in the behaviour and mobility of the Omomyc-treated mice. Nevertheless, in the longitudinal analysis following the levels of IgE in sera, despite an initial separation of the lines from the treatment onset (Figure 50A), the

IgE levels were essentially comparable in both groups at endpoint (Figure 50B). In addition, the reduction in cumulative score between groups we had noticed turned out to be statistically non-significant (Figure 50C).

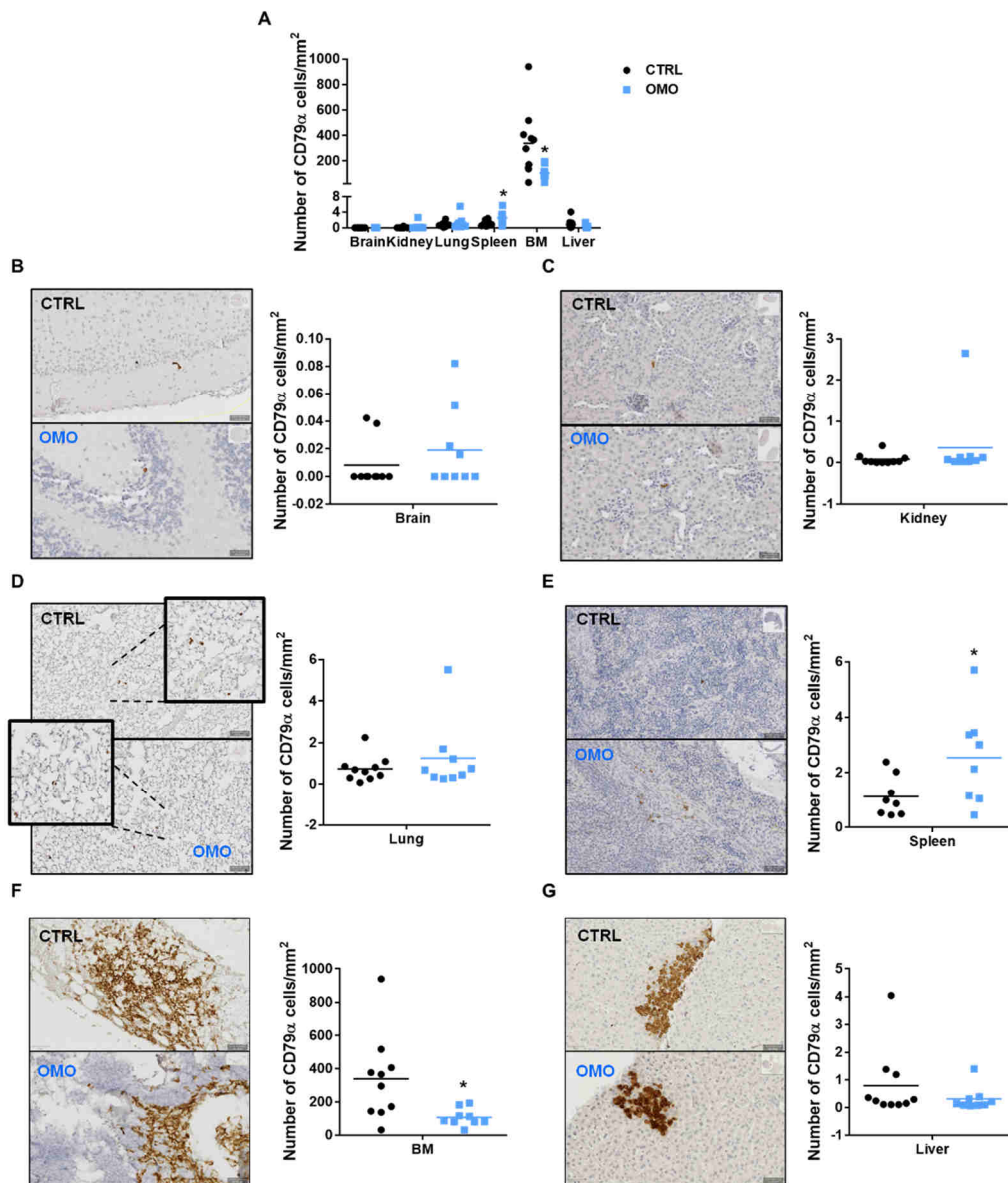


**Figure 48: Intravenous administration of 32 mg/kg of Omomyc did not affect the engraftment and extramedullary invasion of Raji cells, but reduced the homing to the BM.** (A) Summary of the quantifications of CD79 $\alpha$  positive cells in the different organs analysed.  $n=10$  mice per group. Representative microscopy images (right panels) or quantification of the number of CD79 $\alpha$  positive cells (left panels) of (B) brain, (C) kidney, (D) lung, (E) spleen, (F) BM and (G) liver of control (black) and Omomyc-treated (blue) animals. Statistical significance was calculated using a Student's  $t$  test. \* indicates a  $p$ -value  $\leq 0.05$ .

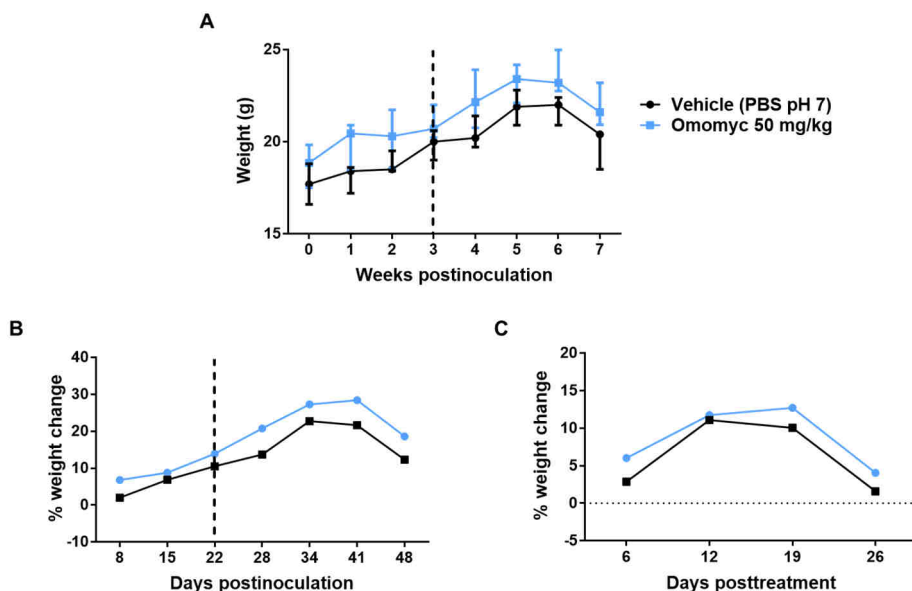


**Figure 49: Intravenous dosing of 50 mg/kg Omomyc did not cause toxicity.** (A) Mice weight median and interquartile range per group. The dashed vertical black line indicates the treatment onset. (B) Median percentage and interquartile range of weight change since the inoculation of U266 cells of each group. (C) Median percentage and interquartile range of weight change since the treatment onset.  $n=8$  mice per group.

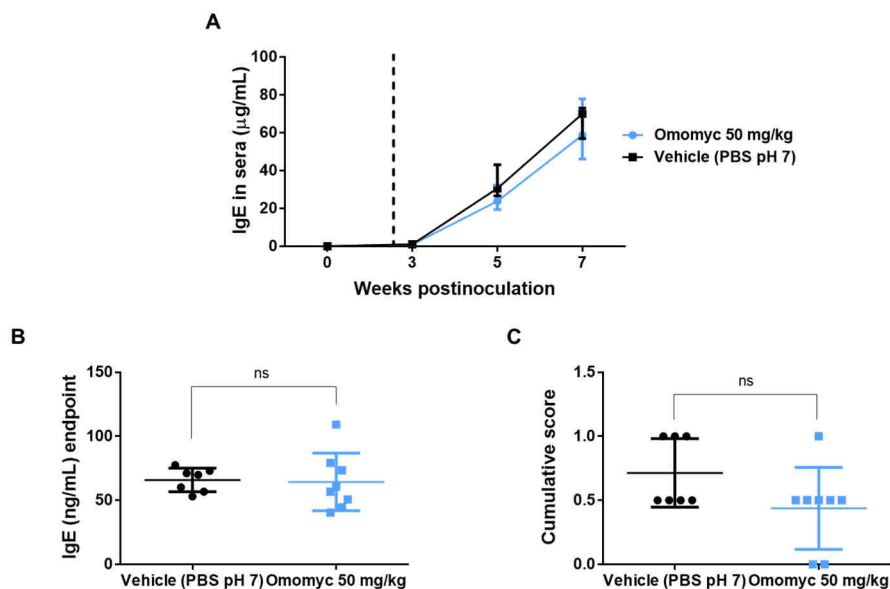


**Figure 50: Omomyc at 50 mg/kg did not reduce the levels of IgE.** (A) Longitudinal analysis of the immunoglobulin E levels in serum. (B) Median percentage and interquartile range of the levels of IgE of control (black) and Omomyc-treated (blue) mice. (C) Mean and SD of the cumulative score, calculated as the sum of all given

scores during the experiment per mouse, of each group. Statistical significance was calculated using a Student's *t* test where *ns* stands for non-significant.

We also analysed the BM by flow cytometry. This time, we added another proliferative marker, phospho-Histone H3 (PHH3), as a marker of cells in the mitotic phase. Sadly, again, we could not see any differences between the 2 groups. As can be seen in Figure 51A and B, if anything, we detected a slight increase in the mean of all the populations studied from the Omomyc-treated group compared to the control.

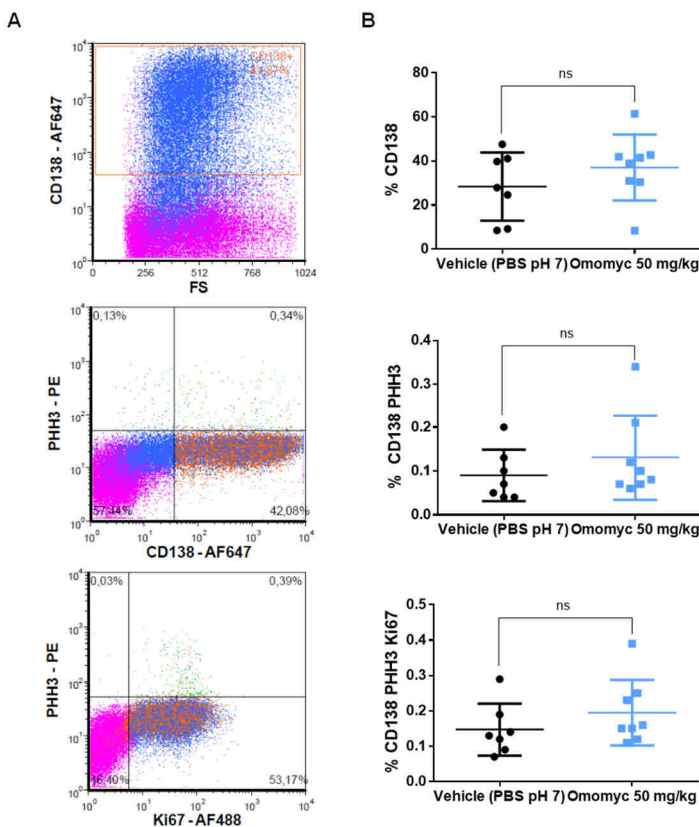


**Figure 51: Omomyc slightly increased the proliferative CD138 positive population.** (A) Representative dot plot images showing the CD138/Ki67/PHH3 populations studied. (B) Quantification of the flow cytometer results of A. Student's *t* test was used to determine the statistical significance, where *ns* stands for non-significant.

Finally, we observed no differences in the secondary bone disease at endpoint either, as measured by mCT and comparing different values (bone volume, tissue MC or bone mineral content) before and after the treatment (Figure 52A and B).

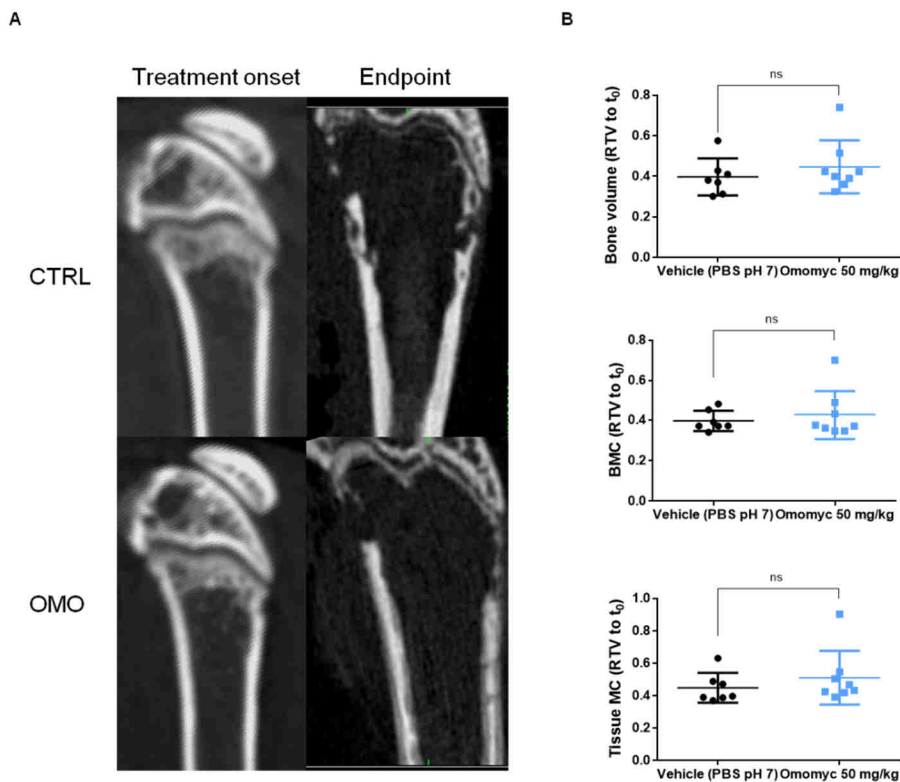


**Figure 52: Omomyc did not have an impact on bone disease.** (A) Representative *ex vivo* mCT images are shown for both treatment groups. (B) Quantification of the bone volume (upper panel), bone mineral content or BMC (medium panel) and tissue mineral content or Tissue MC (lower panel) making the endpoint values relative to those obtained at the treatment onset for each mouse. Student's *t* test was used to determine the statistical significance, where ns stands for non-significant.

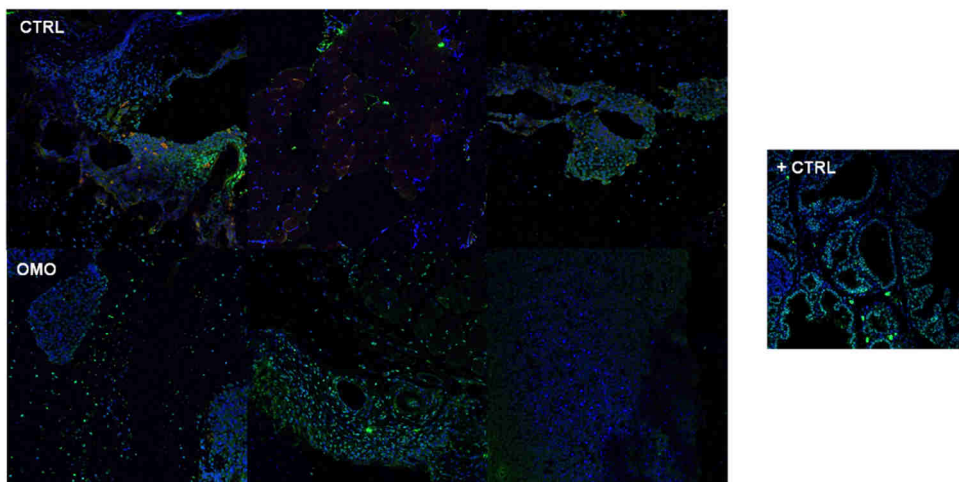
At this point, we wondered whether Omomyc was actually reaching the BM in a sufficient amount to exert its effect or not. To verify it, we performed immunofluorescence (IF) on the tissues of control and treated animals using our mouse monoclonal anti-Omomyc antibody. As depicted in Figure 53A, we obtained non-specific staining from control mice slides too.

Since it is well known that mouse on mouse (MoM) staining can result in higher background, we repeated the IFs adding an F(ab) block step before incubating with the primary antibody. Regrettably, our staining did not improve, and the only positive detection we observed, other than that in the positive control, was non-specific signal accumulated in the cartilage (Figure 53B).



## Results

A



B

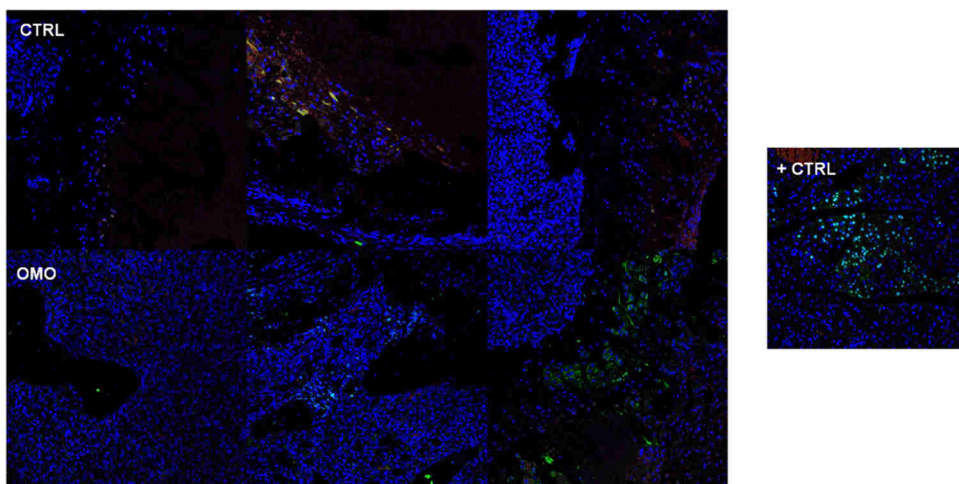


**Figure 53: Omomyc immunofluorescence from tissue samples could not be assessed due to high background.** Representative images from BM cuts of control (upper panels) and Omomyc-treated (lower panels) animals. The tissues were stained with the Omomyc monoclonal antibody with (B) or without (A) an extra blocking step with goat F(ab) anti-mouse (IgG). We added a positive control sample in each experiment. An AF488 conjugated anti-mouse secondary antibody was used to detect Omomyc. Confocal images were acquired using the same exposure settings in each experiment.

Eventually, before definitely excluding that the mini-protein could reach the BM, we took advantage of a biodistribution experiment that was being performed in the laboratory using Omomyc conjugated to another fluorochrome (BDP 650/665), Omomyc-BDP650, in a different mouse model. We administered Omomyc-BDP650 i.v. into FVB/N mice that had been subcutaneously implanted with MDA-

MB-231 cells, to look at the biodistribution of the labelled mini-protein into different organs and the tumour. 30 minutes or 4 hours after the injection, mice were euthanised and the organs of interest removed for their analysis in an IVIS Spectrum *In Vivo* Imaging System. We observed positive signal coming from the femur of treated animals at 2 different time points (Figure 54A and B). Later, we analysed the flushed BM to check for any accumulation of mini-protein in the bone. We found that, indeed, Omomyc-BDP650 was reaching this structure (Figure 54C), and the results suggested that it happened in a time-dependent manner.

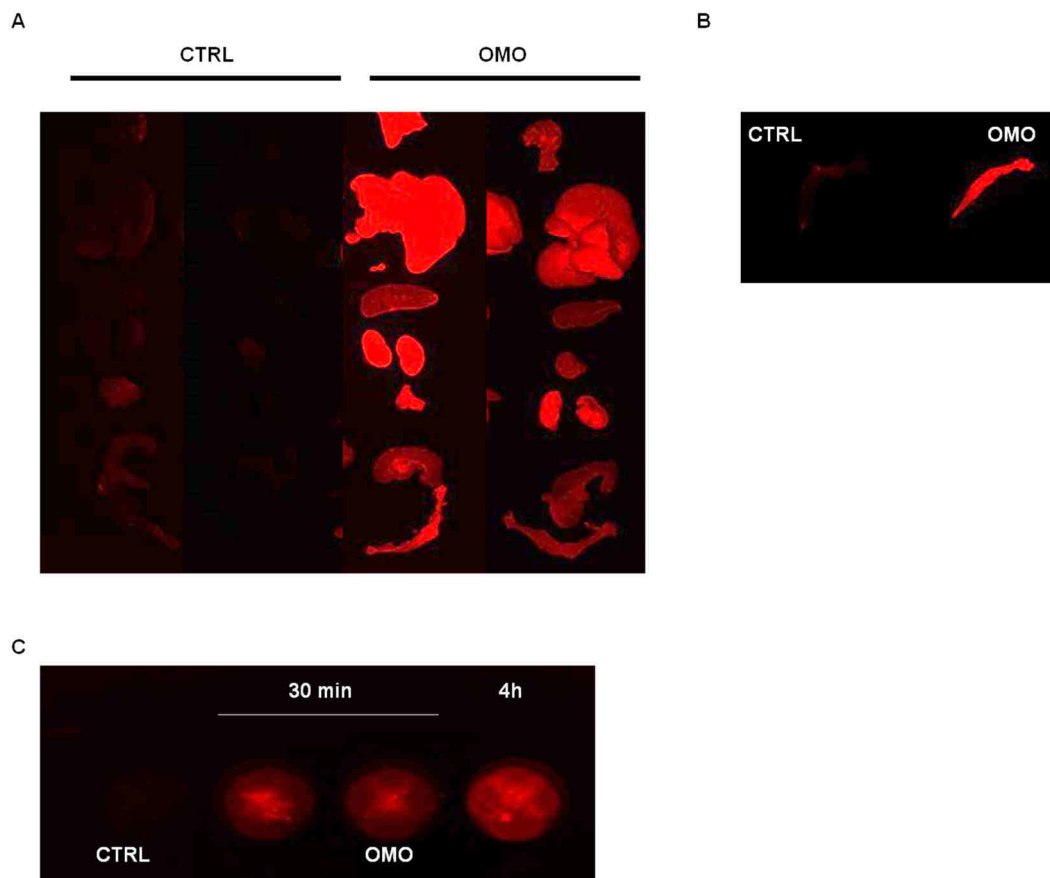


**Figure 54: Omomyc reached the BM in a time-dependent manner.** Representative images from the organs of untreated animals (CTRL) or treated with 50 mg/kg of Omomyc-BDP650 for (A) 30 minutes and (B) 4 hours acquired with the IVIS imaging system. (C) Fluorescence detected in the flushed BM of the animals from A and B using the IVIS.

Hence, our next question was whether Omomyc, once in the BM, was able to enter resident cells or not. To confirm it, we treated a healthy mouse with 100 mg/kg of unlabelled Omomyc (doubling the dose to test whether the lack of penetrance was

## Results

due to a dose-limiting effect), and 14 hours later extracted the BM, lysed it in RIPA buffer and ran it in a western blot.

Despite the high dose of protein administered to the animal, we did not detect any Omomyc in the protein extracts, just a non-specific signal, also present in an untreated control mouse (Figure 55). Nonetheless, we cannot exclude the presence of Omomyc below the limit of detection of the technique.

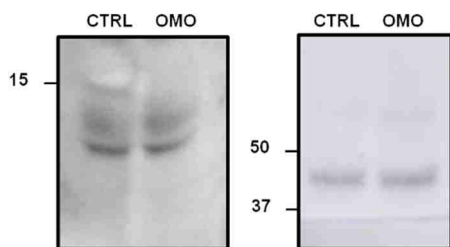


**Figure 55: Omomyc is not found by western blot in lysates from the BM.** Western blot against Omomyc (left) and actin (right) from protein extracts from the BM of an untreated animal (CTRL) and a mouse treated with 100 mg/kg of Omomyc (OMO). We used actin as a loading control.

At this point, since liposomes are known to increase the stability of their cargo in serum (among other advantages they can confer for drug delivery), we decided to test whether our Omolips (Omomyc liposomal formulation) could give better results in the same myeloma xenograft model.

First of all, we had to adapt the Omolips concentration, because 10 mg/mL of lipids and 100  $\mu$ M (or 1 mg/mL) of Omomyc mini-protein would have just allowed the administration of 4 mg/kg of Omomyc and 40 mg/kg of lipids, way too low for *in vivo* use in mice (especially after seeing that 50 mg/kg of free Omomyc did not significantly improve the health of mice affected by MM). Please note that this initial ratio of lipids/Omomyc (10 mg/mL to 1 mg/mL respectively) will be from now on indicated as 1:1.

So, we decided to increase the ratio in order to increase the dose that could be administered. To start, we tried a 3:6 (30 mg/mL of lipids and 6 mg/mL of Omomyc), which would equate to dosing 24 mg/kg Omomyc and 120 mg/kg of lipids. Unfortunately, when we looked at the encapsulation efficiency (EE), we noticed that this ratio had lowered the EE too much, meaning that most of our Omomyc was left outside the liposomes (Figure 56A). So, we went back to a more balanced ratio between lipids and Omomyc, and we tested a 3:3 ratio (30 mg/mL of lipids and 3 mg/mL of Omomyc), hoping it would maintain the EE of the original 1:1 proportions. Indeed that was what we obtained: the EE went back to ~50% (Figure 56A).

Importantly, the Omolips have another particularity: they are negatively charged, a property that actually favours the encapsulation of positively charged Omomyc. Thanks to their negative charge and to the fact that we could not achieve a 100% EE, we assumed that half the positively charged Omomyc molecules were most likely interacting with the outer membrane of the liposomes. In fact, the Omolips

formed aggregates even after the extrusion through 200 nm membranes. Such aggregates could only be seen in the 1:1 and 3:3 ratios, although they were less evident in the latter (Figure 56B).

Also interesting, when we left the Omolips to settle for 48 hours, they formed a biphasic layer: the aggregates at the bottom and a clearer supernatant that could be removed. Hence, we guessed that the outer liposome-interacting Omomyc was acting as a “concentrator” by generating huge NPs (Figure 56C). If that was the case, with these modifications, we expected to have the chance to at least double the dose for *in vivo* testing using the 3:3 ratio.

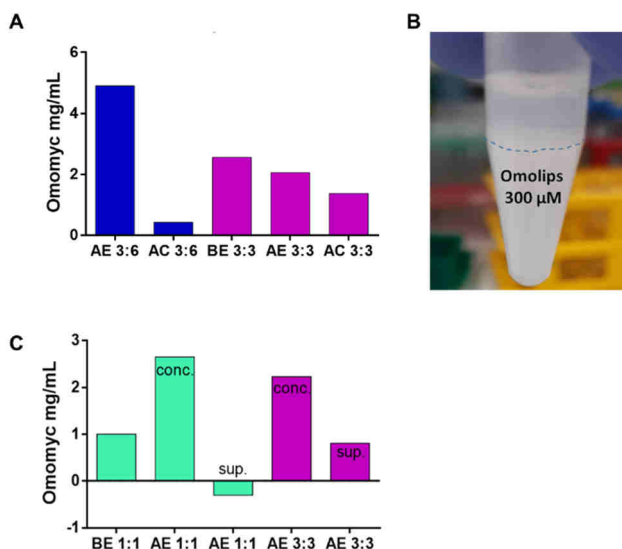


**Figure 56: The encapsulation efficiency of Omolips is highly dependent on the ratio lipids/Omomyc.** (A) Protein quantification by BCA assay of liposomes at different stages of their production; BE: before extrusion, AE: after extrusion, AC: after column. (B) Representative image of the biphasic layer formed by Omolips. (C) Protein quantification by BCA assay of the different fractions of Omolips at 1:1 or 3:3 ratios; BE: before extrusion, AE conc.: after extrusion concentrated, AE sup.: after extrusion supernatant.

## Results

First, to assess the efficacy of the new formulation of Omolips (3:3), we used the myeloma xenograft model with U266 engrafted cells. We compared the therapeutic effect exerted by free Omomyc versus the one from Omolips at an equivalent dose of 12 mg/kg. As a control group, we administered empty liposomes to assess any toxicity that could be associated with the NPs treatment. Fortunately, we found no toxicity in any of the groups, as demonstrated by the increased or maintained weight during the experiment (Figure 57A-C).

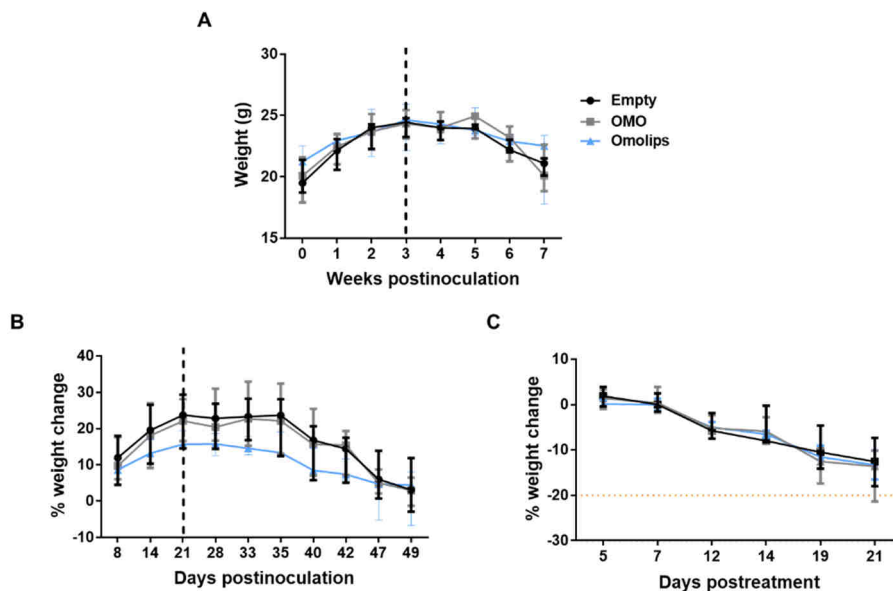


**Figure 57: Intravenous administration of Omolips at 12 mg/kg did not cause toxicity.** (A) Mice weight median and interquartile range per group: empty liposomes (Empty); Omomyc 12 mg/kg (OMO) and Omomyc liposomes 12 mg/kg (Omolips). The dashed vertical black line indicates the treatment onset. (B) Median percentage and interquartile range of weight change since the inoculation of U266 cells of each group. (C) Median percentage and interquartile range of weight change since the treatment onset. The dotted amber line indicates the 20% weight loss.  $n=8$  mice per group.

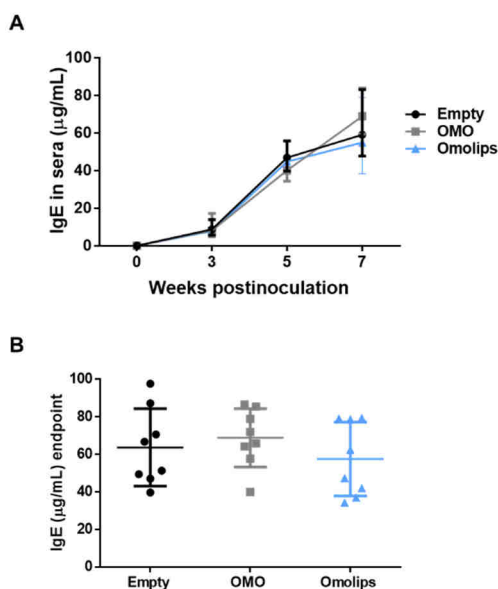
However, we did not find any differences in the levels of IgE in sera either, although we observed a slight improvement in the group of animals treated with Omolips compared to the other 2 (Figure 58A and B).

**Figure 58: Omolips did not improve much the therapeutic effect compared to free Omomyc in terms of IgE levels.**

(A) Longitudinal analysis of the immunoglobulin E levels in serum. (B) Mean and SD of the levels of IgE of control (black), Omomyc-treated (grey) and Omolips-treated (blue) mice at the endpoint.

Following the same trend, we observed no statistically significant differences between the groups in none of the measurements of paralysis (longitudinal score record (Figure 59A), cumulative score (Figure 59B) or maximum score (Figure 59C). However, mice from the Omolips group always had the lowest mean.

When we analysed the BM by flow cytometry (Figure 60A), we observed similar results. Gating live cells, we saw that the Omolips group had the lowest mean in the percentage of CD138 and PHH3 positive cells, but no differences in Ki67 (Figure 60B). In contrast, if instead of gating for live cells we just looked at total positive CD138 cells, we could only see a slight decrease in PHH3 positive cells in both Omomyc-treated groups (either free or encapsulated) and absolutely no differences, or even a slight increase, in the number of double-positive Ki67-PHH3 in these 2 groups when compared to the control (Figure 60C).



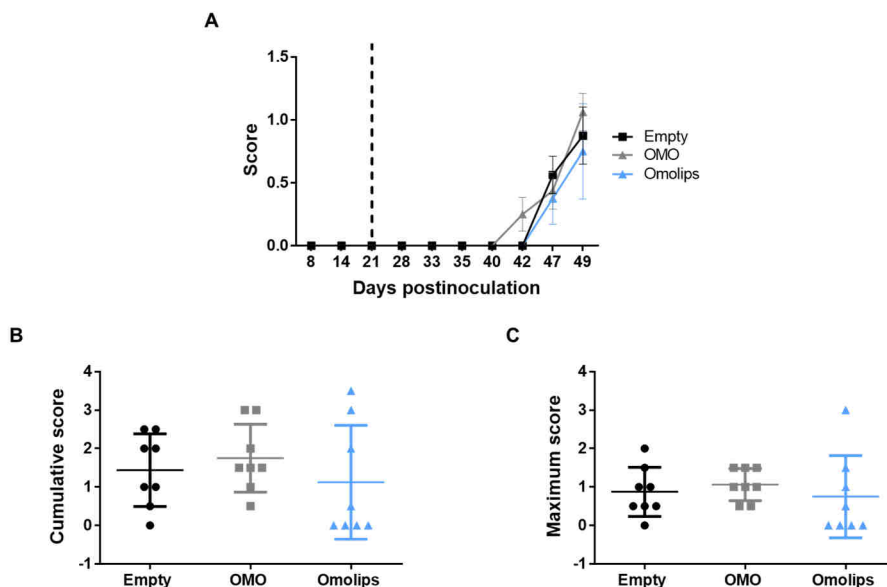


**Figure 59: Omolips did not improve the secondary bone disease.** (A) Longitudinal record of the mean score and SD of each group. Statistical significance was calculated using multiple nonparametric *t*-tests. (B) Cumulative score calculated as the sum of all the values recorded for each mouse throughout the experiment. (C) Maximum score refers to the highest value reached per mouse during the experiment. Mann-Whitney was the statistical analysis used to determine significance.

Finally, we checked whether the liposomal formulation had at least improved Omomyc serum stability and entrance into BM cells. We ran a western blot of sera from mice belonging to the 3 groups. It was encouraging to see that the only serum samples in which Omomyc was detectable were those from the Omolips treated group (Figure 61A). However, we also lysed the flushed BM and stained against Omomyc, yet we were not able to detect it anywhere (Figure 61B). Again, we could not exclude that the intracellular levels of the protein could be under the limit of detection of this technique.

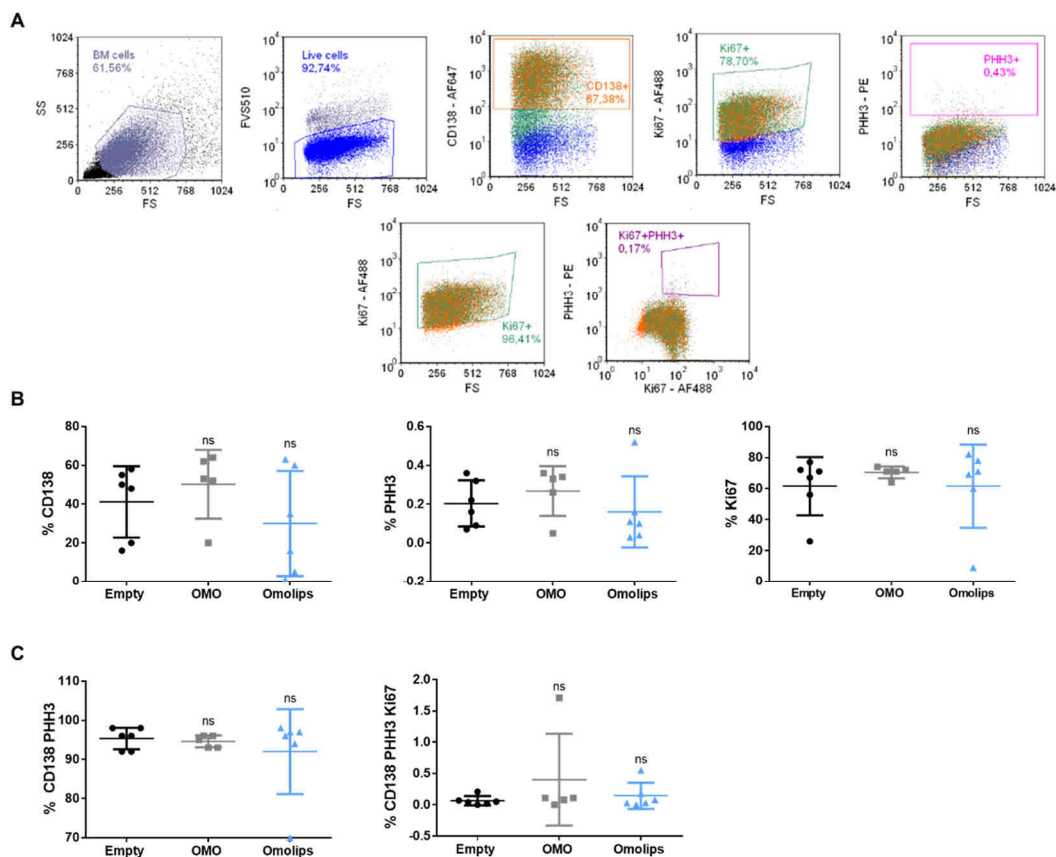


**Figure 60: Omolips did not reduce the proliferative CD138 positive population in the BM.** (A) Representative dot plot images showing the CD138/Ki67/PHH3 populations studied. (B) Quantification of the flow cytometer results of A gating for “live cells”. (C) Quantification of the flow cytometer results of A gating for “CD138 positive cells”. Student’s *t* test was used to determine the statistical significance, where *ns* stands for non-significant.

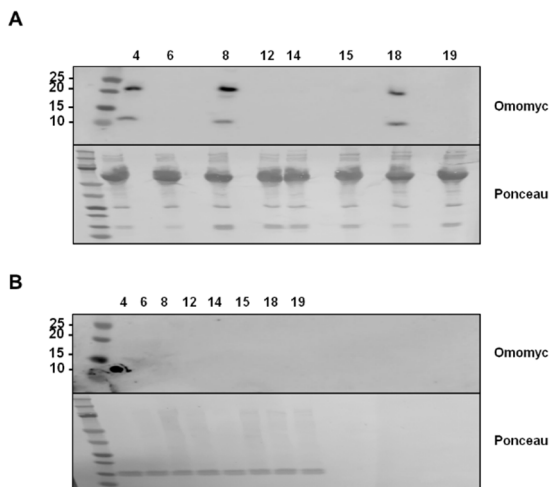


**Figure 61: Omolips significantly increased the stability of Omomyc in sera.** Western blot images against Omomyc from (A) serum samples collected 14 hours posttreatment from mice of all 3 groups (empty liposomes, free Omomyc and Omolips) or (B) BM lysates from the same animals as in A. Ponceau was used as a loading control. The ID numbers of each animal are depicted above the image.



Results

Since the results obtained to this point indicated that the current formulations of Omomyc as monotherapy may not have any significant therapeutic impact either in myeloma or lymphoma, we investigated whether the combination of Omomyc with the standard of care (SoC) could demonstrate a better effect. To do so, we tested *in vitro* the combination of increasing concentrations of both carfilzomib (CFZ), a proteasome inhibitor typically used in the clinic for myeloma patients, and Omomyc mini-protein. Our data showed that the drug combination had an increased therapeutic impact when compared to both monotherapies alone, at specific concentrations ( Figure 62A and B). Both human U266 and mouse 5TGM1 cells responded in a dose-dependent manner to both drugs used, and the effect of the combination was particularly evident at 2.5, and 1.25 nM of CFZ for almost all the concentrations of Omomyc used (2.5-20  $\mu$ M) for U266 cells (Figure 62A). On the other hand, 5TGM1 cells were highly sensitive to both molecules, displaying a synergic effect at concentrations as low as 0.08 nM CFZ and 10  $\mu$ M of Omomyc, but sharing as well a comparable range of concentrations with U266 cells, from 2.5 to 0.3 nM of CFZ and between 2.5-10  $\mu$ M of Omomyc (Figure 62B).

A

7.4	7.7	11.6	27.0	45.8	60.7	63.3	69.6	72.0	59.8	40
7.7	7.8	8.7	18.3	40.7	64.0	75.5	77.9	85.8	86.1	20
7.6	8.1	8.8	18.2	42.3	66.8	78.4	83.7	88.8	98.4	10
8.0	8.1	9.6	21.1	42.4	69.5	79.1	89.2	94.0	108.9	5
7.7	8.3	10.0	22.8	47.9	70.6	86.1	86.9	93.3	99.1	2.5
8.1	9.0	25.6	54.6	76.3	85.5	93.9	90.2	98.9	100.0	0
20	10	5	2.5	1.25	0.63	0.3	0.16	0.08	0	

Carfilzomib(nM)

B

10.0	10.2	10.3	10.3	11.2	11.3	11.2	11.0	11.1	11.3	40
9.2	10.1	10.0	10.5	12.5	13.4	13.8	15.7	14.3	15.5	20
10.0	10.1	10.5	11.3	22.1	34.3	34.9	39.6	26.1	57.8	10
10.1	9.8	11.5	17.0	55.8	68.7	74.3	74.3	71.4	85.8	5
10.1	10.3	12.7	44.3	73.8	79.8	90.7	90.7	89.7	95.3	2.5
11.5	22.5	72.0	93.7	93.8	92.9	98.2	91.2	103.7	100.0	0
20	10	5	2.5	1.25	0.63	0.3	0.16	0.08	0	

Carfilzomib(nM)

**Figure 62: Synergic effect upon combined treatment with Omomyc and CFZ.** (A) U266 and (B) 5TGM1 cells were treated for 5 days with increasing concentrations of Omomyc alone (right column), CFZ alone (lower row) or the combination of both at different concentrations. The cell viability was measured by resazurin dye fluorimetric assay and made relative to that of the untreated control. The mean effect of 2 independent experiments is shown for U266 cells, while for 5TGM1 cells, the experiment was done once.

Given the promising enhanced therapeutic effect demonstrated *in vitro*, we decided to test our combination approach *in vivo* as well. To do so, we used a syngeneic mouse model in which we inoculated 5TGM1 cells, which had shown to be the best responders to Omomyc *in vitro* (see section 3.2.1), but also displayed synergy when Omomyc was combined with a proteasome inhibitor.

We compared the therapeutic effect exerted by Omomyc, administered at 50 mg/kg i.v., or BTZ, at 0.25 mg/kg i.p. alone, versus the combination of both agents and compared to a control vehicle group. Surprisingly, we found an unexpected toxic reaction in both BTZ-treated groups, as demonstrated by the weight plummeting after each treatment, followed by an upturn upon withdrawal (Figure 63A-C). On the contrary, vehicle and Omomyc-treated mice gradually gained weight throughout the initial stages of the experiment (Figure 63A-C). Unfortunately, 4 out of 7 mice from the BTZ-only-treated group needed euthanasia after treatment, causing an important reduction in the final number of individuals, consequently reducing the statistical power. On the other hand, mice from the combination group (OMO/BTZ) did not require euthanasia, indicating that Omomyc was somehow reducing the toxicity of BTZ. However, due to the loss of weight the animals were experiencing, we opted for giving “drug holidays” (on days 14 and 28) to all the BTZ-treated groups that ended up receiving only half of the planned doses.

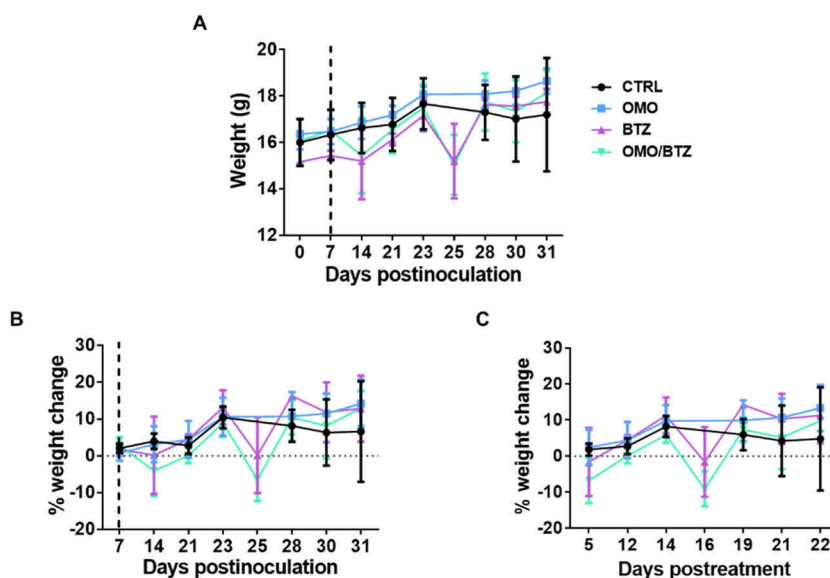


**Figure 63: BTZ caused weight loss and toxicity, while Omomyc did not.** (A) Mice weight median and interquartile range per group: control vehicle (CTRL); Omomyc 50 mg/kg (OMO); bortezomib 0.25 mg/kg (BTZ) and the combination Omomyc 50 mg/kg + bortezomib 0.25 mg/kg (OMO/BTZ). The dashed vertical black line indicates the treatment onset. (B) Median percentage and interquartile range of weight change since treatment onset. (C) Median percentage and interquartile range of weight change since treatment onset.

## Results

the inoculation of 5TGM1 cells of each group. (C) Median percentage and interquartile range of weight change since the treatment onset.  $n=7$  for CTRL and BTZ groups and  $n=8$  for OMO and OMO/BTZ groups.

Despite this, the analysis of IgG2b levels in sera -as a read-out of tumour burden - showed a statistically significant reduction in the Omomyc and BTZ-treated group compared to the control, while Omomyc and BTZ monotherapies did not (Figure 64A-C). Looking at the fold change of the IgG2b levels, we also observed a significant reduction in the progression of MM in the combination group (Figure 64D-F). However, the score, our surrogate indicative of secondary bone disease, did not reveal any differences between groups (Figure 65).

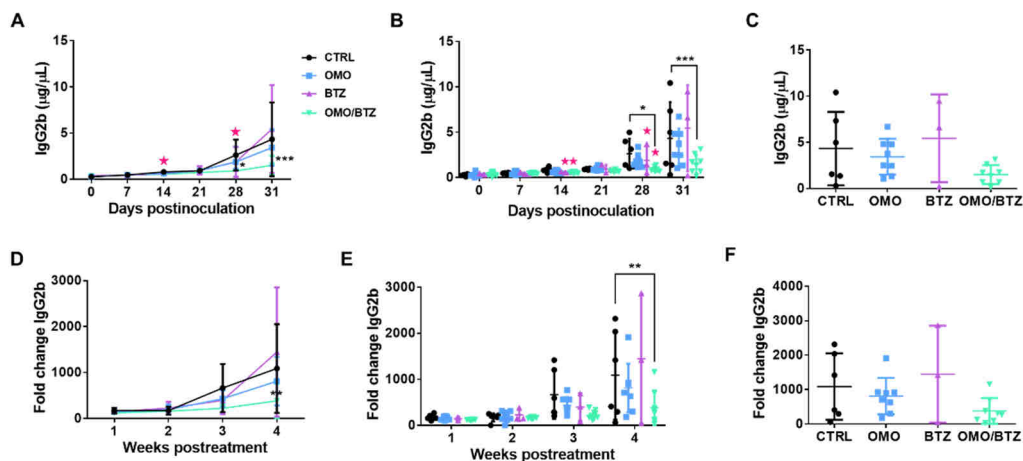


**Figure 64: The combination of OMO/BTZ significantly reduced MM progression.** Longitudinal analysis of the immunoglobulin G2b (IgG2b) levels in serum of CTRL (black), OMO (blue), BTZ (violet) and OMO/BTZ (turquoise). Pink stars indicate “drug holidays” for the BTZ-treated groups plotted as (A) XY connected lines and (B) grouped. (C) Mean and SD of the levels of IgG2b at the endpoint. Longitudinal analysis of the fold change of IgG2b plotted as (D) XY connected lines and (E) grouped. (F) Mean and SD of the fold change of IgG2b at the endpoint. Statistical significance was calculated using a 2way ANOVA. \* indicates a  $p$ -value  $\leq 0.05$ ; \*\* indicates a  $p$ -value  $\leq 0.01$ ; \*\*\* indicates a  $p$ -value  $\leq 0.001$ .

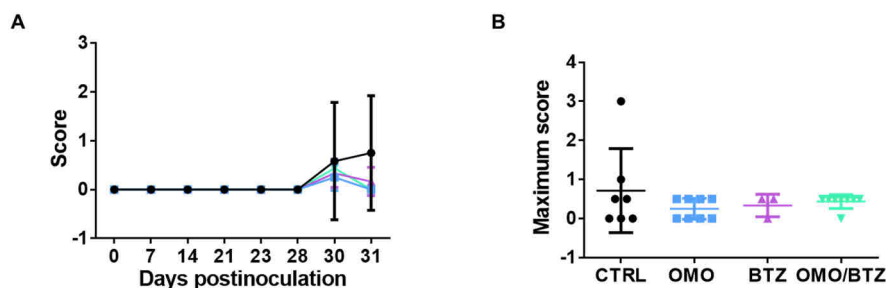


**Figure 65: None of the treatment groups significantly impacted on the secondary bone disease (score).** (A) Longitudinal record of the mean score and SD of each (B) Maximum score refers to the highest value reached per mouse during the experiment. Mann-Whitney was the statistical analysis used to determine significance.

These experiments opened up the possibility of combinatorial treatments to improve the therapeutic impact of Omomyc. Such a possibility is currently being explored in the lab.

### 3.2.4 Variant 26 (V26): a derivative of the Omomyc mini-protein sequence

Another possible strategy to increase the effectiveness of our treatment could be the development of variant molecules derived from the Omomyc mini-protein based on additional structural and biological data and literature about functional sequences.

For this objective, we rationally designed variant 26 (V26), a prototype aimed at improving the nuclear localisation and the release from endosomes compared to the original Omomyc. For that, V26 includes an extra nuclear localisation signal (NLS) of c-MYC and additional histidine residues to favour endosomal escape (see the introduction for more details).

In order to verify whether V26 is a *bona fide* MYC inhibitor as its parent molecule, we characterised the dimerisation of V26 with the bHLHLZ domains of MYC (MYC<sup>o</sup>) and MAX (MAX<sup>o</sup>) and the DNA binding of the complexes in solution using circular dichroism (CD). The CD spectrum of V26 in the absence of DNA in CD buffer was comparable to that of Omomyc and MAX<sup>o</sup> (Figure 66B), showing deep minima of around 208 and 222 nm, typical of high helical content and in contrast to the negligible minima observed for MYC<sup>o</sup> at these wavelengths, which is consistent with the spectra expected for an intrinsically disordered protein domain (Figure 66F). Interestingly, V26 did not gain ellipticity in the presence of a canonical E-box duplex as Omomyc does. However, there was an increase in the ratio 222/208 nm from 1.02 for V26 alone to 1.25 for the mixture of V26 with DNA (subtracting the contribution of DNA) suggestive of an increase in helicity and potentially associate tertiary structure content (Cooper and Woody, 1990), which could indicate an interaction between V26 and the probe (Figure 66A). Moreover,

## Results

the thermal denaturation of V26 in the presence of the oligonucleotide evidenced the formation of a thermally stable complex between V26 and DNA, coherent with a specific molecular recognition between the protein and the probe (Figure 66D-E). Also interesting and in contrast with the Omomyc results, we did not observe any gain in helical-specific signal intensity of the experimental mixture V26/MAX<sup>o</sup> (Figure 66B), and only a very mild increase in V26/MYC<sup>o</sup> (Figure 66F) compared to their respective theoretical arithmetic sums. Even more intriguing, in the presence of the E-box duplex, not only did we not observe a gain in ellipticity, but we noticed that the signal from the experimental mixtures was reduced compared to the arithmetic sum of each component's curves (Figure 66B and G).

To further confirm (or exclude) the homo- and heterodimerisation of V26, and determine the binding capacity of the different protein populations to a canonical E-box duplex, we then performed thermal denaturation of equimolar mixtures of V26/MAX<sup>o</sup> or V26/MYC<sup>o</sup> in the presence or absence of the DNA probe. As depicted in Figure 66D, V26 formed homodimers that were slightly more thermostable than those formed by MAX<sup>o</sup>. Besides, the thermal denaturation of V26 in the presence of MAX<sup>o</sup> confirmed their ability to form heterodimers. Indeed, the helicity displayed by the mixture sample containing both V26 and MAX<sup>o</sup> was superior to the arithmetic sum of both individual proteins (Figure 66D) and evidenced the population of a species with higher thermostability compared to that of either V26 or MAX<sup>o</sup> samples alone.

The shift in the melting temperature (at which 50% of the helical signal is lost) towards a higher temperature confirmed that both MAX<sup>o</sup> and V26 homodimers formed a stable complex with the oligonucleotide. In addition, the heterodimeric complex V26/MAX<sup>o</sup> with the probe was further stabilised, confirming its binding to DNA as well (Figure 66E). Contrary to these results (but as expected according to the literature), MYC<sup>o</sup> formed a lower population of homodimers at lower temperatures, much less thermostable compared to those from V26 or MAX<sup>o</sup> and proved unable to bind DNA (Figure 66H). The denaturing curve for the V26/MYC<sup>o</sup> heterodimer was inconclusive by itself to confirm or deny the formation of this dimeric population, due to the similarity displayed by the experimental mixture with the arithmetic sum of both individual curves (Figure 66H). Coherently, the binding of the V26/MYC<sup>o</sup> dimers to DNA was also inconclusive (Figure 66I), and further experiments would be required to determine whether the complexes V26/MYC<sup>o</sup> and V26/MYC<sup>o</sup>/DNA form or not.

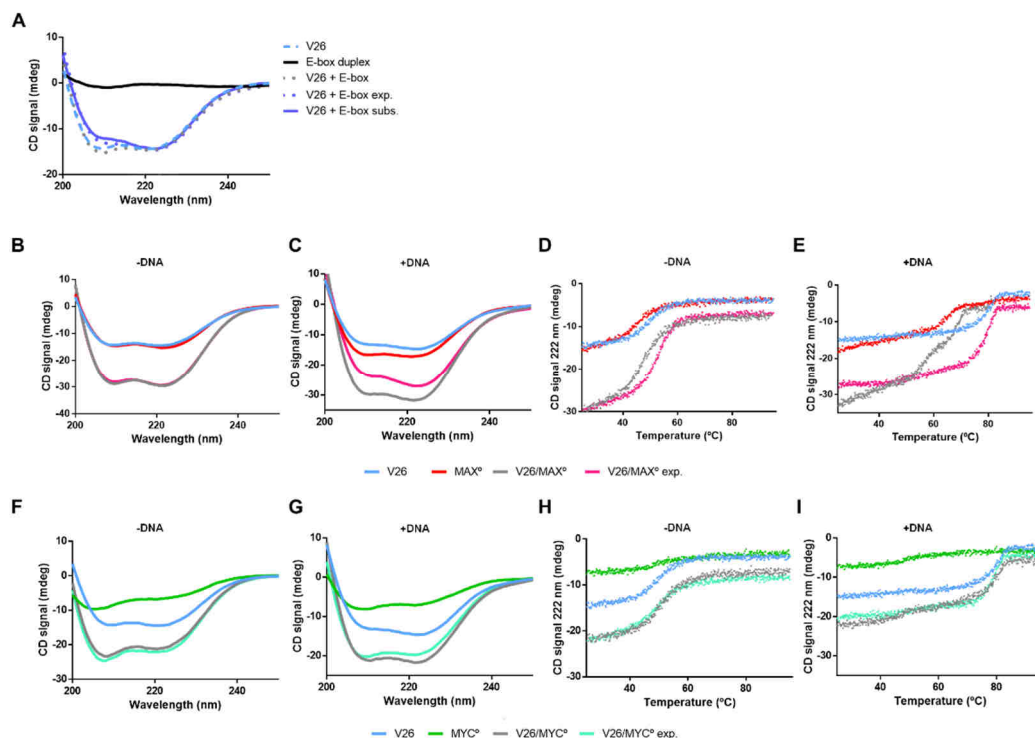


**Figure 66: V26 forms highly thermodynamically stable DNA binding homodimers and heterodimers with MAX<sup>o</sup>** (A) Far-ultraviolet (UV) CD spectra of V26 in CD buffer (blue, 8  $\mu$ M monomer units) E-box duplex probe (black), the arithmetic sum of both blue and black spectra (grey), the spectrum of V26 and equimolar amounts of a DNA E-box probe (in dimer units) (dotted purple) and the arithmetic subtraction of the black spectrum from the dotted purple one to remove the contribution of DNA (purple) recorded at 25°C. Far-ultraviolet (UV) CD spectra of V26 (blue, 8  $\mu$ M monomer units), MAX<sup>o</sup> (red, 8  $\mu$ M monomer units), the arithmetic sum of both blue and red spectra (grey) and the spectrum of an equimolar mix of V26 and MAX<sup>o</sup> at a total concentration of 16  $\mu$ M in monomer units (fuchsia) in the absence (B) or presence of equimolar amounts of a DNA E-box probe (in dimer units) (C) recorded at 25°C. (D) Thermal denaturation of the solutions described in (B). (E) Thermal denaturation of the solutions described in (C). Far-ultraviolet (UV) CD spectra of V26 (blue, 8  $\mu$ M monomer units), MYC<sup>o</sup> (green, 8  $\mu$ M monomer units), the arithmetic sum of both blue and green spectra (grey) and the spectrum of an equimolar mix of V26 and MYC<sup>o</sup> at a total concentration of 16  $\mu$ M in monomer units (turquoise) in the absence (F) or presence of equimolar amounts of a DNA E-box probe (in dimer units) (G) recorded at 25°C. (H) Thermal denaturation of the solutions described in (F). (I) Thermal denaturation of the solutions described in (G).

## Results

To determine the subcellular localisation of V26, we treated H1299 NSCLC cells with 5  $\mu\text{M}$  V26 conjugated to the AF488 fluorochrome for 4 hours and analysed them by confocal microscopy. As per design, this variant displayed superior nuclear localisation in live treated cells, compared to the original Omomyc mini-protein (Figure 67A). Moreover, treatment with 20  $\mu\text{M}$  of V26 caused much more death in myeloma and lymphoma cells than the original Omomyc, resulting in a dramatic reduction in cell number (Figure 67B) and drastic changes in cell cycle profile (Figure 67C). Somewhat worryingly, though, was the fact that V26 had a similar  $\text{IC}_{50}$  in fibroblasts as well (Figure 67D). So, to further characterise its effects in non-cancerous cells, we treated human fibroblasts (EMTs) and peripheral blood mononuclear cells (PBMCs) with 10 and 20  $\mu\text{M}$  of V26 for 3 days and looked at their growth. Intriguingly, we observed a comparable reduction in cell number between V26 and Omomyc-treated cells at both concentrations, although V26 significantly increased the percentage of dead cells. In fact, despite this difference in cell death, the final count of viable cells was the same for both conditions (Figure 67E-H). We also found a striking phenotypic change in morphology in cells treated with V26, but not with Omomyc (Figure 67I and J). It should also be noted that in all these experiments, we also noticed that V26 had inferior solubility to Omomyc in the culture medium. Thus, if found promising for further studies, V26 would require further formulation efforts to enable its use *in vivo*. In any case, V26 might have offered some clues regarding useful features that might be pursued to improve Omomyc.

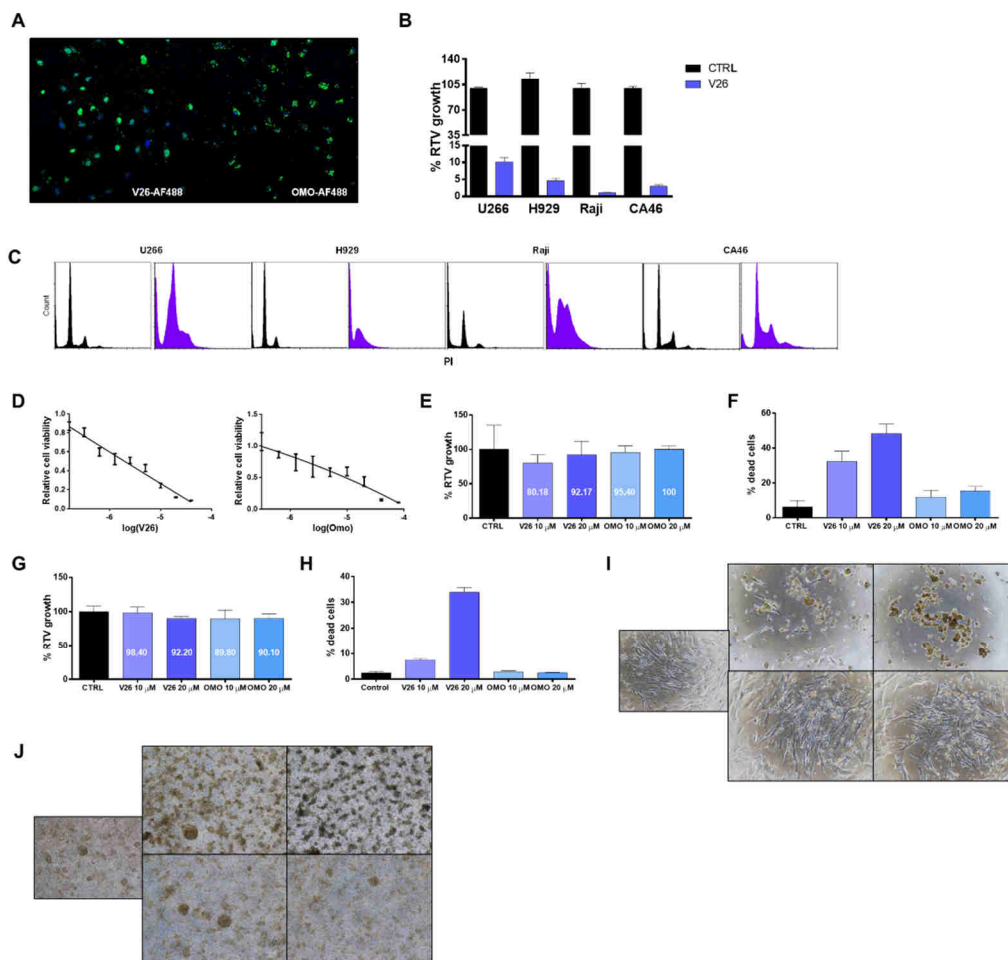


**Figure 67: V26 localises in the nucleus and selectively kills myeloma and lymphoma cells.** (A) H1299 cells were treated with 5  $\mu\text{M}$  V26-AF488 (left) or OMO-AF488 (right) for 4 hours, stained with Hoechst 3342, washed, mounted, and analysed by confocal microscopy. (B) U266, NCI-H929, Raji, and CA46 cells were treated with 20  $\mu\text{M}$  V26 for 5 days and proliferation assessed by trypan blue exclusion assay. Mean and SD of the relative (RTV) cell number of V26-treated (violet) normalised to the untreated control (black) are shown. (C) Cell cycle profiles from flow cytometric analysis of PI incorporation after 5 days of treatment with 20  $\mu\text{M}$  V26 compared to untreated control (CTRL). (D) Dose-response to increasing concentrations of V26 (left) or Omomyc (right) measured by resazurin dye fluorimetric assay in human fibroblasts. Both  $\text{IC}_{50}$  values were ambiguous. Human fibroblasts (EMTs) (E-F) or PBMCs (G-H) were treated with 20  $\mu\text{M}$  (dark coloured) or 10  $\mu\text{M}$  (light coloured) V26 (violet) or Omomyc (blue) for 3 days and proliferation assessed by trypan blue exclusion assay. Mean and SD of the relative (RTV) cell number of treated cells normalised to the untreated control (black) (E and G) or the percentage of dead cells (F and H) are shown. Representative images of the morphological changes in EMTs (I) or PBMCs (J) upon treatment with 20  $\mu\text{M}$  (right panels) or 10  $\mu\text{M}$  (medium panels) of V26 (upper panels) or Omomyc (lower panels) compared to the untreated control (left panel).





## DISCUSSION

MYC is a master TF found deregulated in more than 50% of human cancers and frequently associated with poor prognosis and treatment resistance (Chen et al., 2018). However, more than 40 years of research in the field and efforts to design a clinically viable MYC inhibitor have not yielded such a molecule just yet. Direct targeting of MYC has entailed an enormous challenge, mainly due to its “undruggable” disordered protein structure (Carabet et al., 2018). MYC is a highly changeable protein that adopts several conformations and lacks an active binding pocket, making it difficult to develop small molecules for its targeting. Also challenging for drug development purpose is the issue of reaching the nucleus to stop MYC from regulating all the cellular processes in which it is involved (Carabet et al., 2018).

Despite that, Dr Soucek designed a dominant negative mutant of the bHLHLZ domain of MYC, Omomyc, bearing 4 point mutations that changed its dimerisation specificity, allowing it to homodimerise and heterodimerise with both MYC and MAX (Soucek et al., 1998). This transgene marked a milestone in the development of MYC inhibitors, demonstrating that, not only it was possible to directly target MYC, achieving for the first time the clearance of lung tumours in a mouse model, but also do it with mild, tolerable and completely reversible side effects (Soucek et al., 2008, Soucek et al., 2013).

Here we discussed 2 strategies directed against MYC for the treatment of 2 haematological malignancies such as Burkitt lymphoma (BL) and multiple myeloma (MM), in which, as mentioned above, MYC dysregulation affects a significant percentage of patients: 100% for BL (Albihn et al., 2010) and 67% for MM (Jovanovic et al., 2018).

### 4.1 Small molecule peptidomimetics

#### 4.1.1 *In vitro*

First, we used a therapeutic approach based on small molecules directed against MYC. We tested 3 peptidomimetic compounds selected among a more extensive library of drugs for their specific MYC targeting and induction of MYC degradation. These drugs typically disrupt the MYC-MAX heterodimer through the interference with protein-protein interactions (Carabet et al., 2018). Our results show that all compounds reduce the number of viable cells *in vitro* (IC<sub>50</sub> value) within the micromolar range, similarly to other peptidomimetics disruptors of the MYC-MAX heterodimer shown in recent studies (Chauhan et al., 2014, Stellas et al., 2014, Hart et al., 2014, Choi et al., 2017, Castell et al., 2018).

Because compounds X and Z displayed slightly better efficacy than Y *in vitro*, we decided to prioritise them for *in vivo* experiments.

#### 4.1.1 *In vivo*

We initially saw some encouraging results:

Treatment with X resulted in a non-significant but downward trend in the clinical score and significant reduction of the CD138/Ki67 and increase in the CD138/AVPI populations, suggestive of increased apoptosis and decreased proliferation. These results are partially consistent with the work from Stellas et al. and Hart et al. (Stellas et al., 2014, Hart et al., 2014), who demonstrated not only an increase in cell death and a decrease in their proliferation but also a reduction in tumour growth in a PDAC and breast cancer model after treatment with Mycro3 or KJ-Pyr-9 respectively, both small molecule inhibitors of the MYC-MAX dimer (Stellas et al., 2014, Hart et al., 2014).

In contrast, at least in the first experiment, the treatment with Z improved the secondary bone disease (indirectly assessed by the score), possibly because of the intensive treatment every 12 hours that mice received the first 4 days, after which the dosing schedule had to be reduced to 3 times per week due to severe toxicity. During that period, we possibly achieved a sufficient and sustained concentration of Z in the blood of the animals, able to exert some inhibition on circulating U266 cells, preventing them from creating the appropriate niche responsible for the osteolytic lesions to happen.

Encouraged by these partial effects, we decided to test both compounds in terms of their effect on mouse survival. Unfortunately, neither X nor Z showed any improvement in mice survival, IgE levels or even score.

It is important to note that, according to their half-life, both peptidomimetics should have been administered every 12 hours intraperitoneally to sustain their bloodstream levels; however, the toxic reactions they caused did not allow us to follow the original drug dosing schedule. Actually, even after adopting more spaced treatments, the toxicity did not entirely disappear. However, lowering their dose further would largely reduce their chance to demonstrate any efficacy at all. Indeed, as it has been previously reported, small molecules against MYC often lack efficacy *in vivo* due to poor biodistribution and bioavailability, as well as rapid metabolism and, consequently, only little amounts of them eventually reach the tumour (Whitfield et al., 2017).

As mentioned before in this thesis, numerous other studies have been published regarding different kinds of small molecules, also able to inhibit MYC either via blockade of MYC transcription, translation or stabilisation, or directly impeding MYC transcription through the formation/stabilisation of G-quadruplexes in the promoter region of the gene (Chen et al., 2018). However, they all share some

limitations, and on many occasions, they have caused unwanted toxic reactions due to lack of specificity, indicating that they still require further development efforts to reduce off-target effects.

Hence, in order to reduce the toxicity of the X and Z peptidomimetics without reducing further their dose regimen, we tested an improved version of both, termed X<sub>1</sub> and Z<sub>1</sub>. These were designed to reduce the local toxicity that we had observed with the original compounds using a new formulation that allowed intravenous administration. We tested them at 2 doses, 5 and 10 mg/kg. This time, we did not observe any local toxicity associated with the administration, nor did we report any long term side effects. However, we also did not see any efficacy with either of the 2 compounds, except for a slight downward trend in IgE levels and proliferative CD138 cells in the BM with the 10 mg/kg Z<sub>1</sub> treatment. Taking into account that the new formulations had displayed a somewhat better effect *in vitro* compared to the original ones, but had failed to do so *in vivo*, we suspected that the stability of the molecules might have been compromised throughout the *in vivo* experiments and confirmed that it was the case: we saw that storage in solution at 4°C must have gradually degraded the molecules, rendering the final concentration only 20% of the initial one. This observation was rather unexpected since peptidomimetics are usually designed to circumvent proteolytic degradation ([Vagner et al., 2008](#)).

Thus, we repeated the experiment a second time, taking care of avoiding degradation by aliquotting the compounds and storing them at -20°C. Strikingly, after the first inoculation of the 10 mg/kg dose of Z<sub>1</sub> all mice died, a clear sign of toxicity associated with the dose, since animals treated with 5 mg/kg were fine. Hence, we thought that the maximum tolerated dose (MTD) in mice for this molecule ranged between 5 and 10 mg/kg. As the treatment continued, however, we reported necrotic tissue in the tail of 5 mg/kg Z<sub>1</sub> treated animals that worsened as the experiment advanced. From these results, we can infer that Z<sub>1</sub> and X<sub>1</sub> were degraded from the very beginning of the previous *in vivo* study because we could not detect any toxicity in the tail of the animals, and of course, we had not previously observed any mouse death.

At that point, given the high toxicity of the compounds, we decided to discontinue the studies.

To our surprise, our collaborators informed us later that they ran more experiments using a different mouse strain and observed no toxicity. Indeed, others have demonstrated that even if NSG mice are the ideal strain for high-engraftment efficacy of human cancer cells, their complex genetic background and severe immunodeficiency makes them particularly susceptible to 5-FU based therapies and potentially to other drugs ([Maletzki et al., 2020](#)).

Altogether, these results confirm that the peptidomimetics described in this thesis can be promising anti-cancer therapies. However, their short half-life and high toxicity require extensive drug development efforts to solve these issues, increasing their chances to pass early phases of clinical development. It is also essential to study in-depth the reasons behind any adverse effect found, mainly those including sudden death, to determine whether inherent characteristics of mice or even patients, would be decisive for their treatment. Such features could, in the end, be used as inclusion/exclusion criteria for future clinical trials assessing these new drugs.

## **4.2 Omomyc derived peptides**

### **4.2.1 Omomyc mini-protein *in vitro***

In a second study, we used another strategy for direct MYC inhibition, meant to disrupt the protein-protein interactions of the MYC-MAX dimer.

The Omomyc mini-protein is a biological anti-cancer agent with a long history behind. In its transgenically expressed form, Omomyc served as proof of concept that MYC inhibition is a viable cancer therapy and addressed the principal concern of the adverse effects caused by ubiquitous expression of a MYC inhibitor in healthy proliferating tissues. These side effects were only mild, well-tolerated and completely reversible ([Soucek et al., 2008](#), [Soucek et al., 2013](#)).

Later on, Omomyc was finally used as a drug candidate, thanks to its intrinsic cell-penetrating properties. This result defied once again the preconceived notion that due to its size (91 amino acids), Omomyc could not internalise efficiently ([Montagne et al., 2012](#)). We demonstrated that Omomyc mini-protein is indeed able to penetrate cancer cells via different endocytic pathways ([Beaulieu et al., 2019](#)) and this observation is reproduced in this thesis in B lymphocytes from MM and BL cell lines. Interestingly, in CA46 BL cells, we defined a new mechanism of Omomyc's entrance in an energy-independent manner. As [Walrant et al.](#) describe in their work, some cationic CPPs cross the plasma membrane even at 4°C, when all active transport and endocytic pathways are inhibited, using a translocation mechanism or exploiting defects in the cell membrane, and they do so primarily at low micromolar concentrations, ranging between <2-3 μM ([Walrant et al., 2017](#)), as it is in our case.

In this thesis, we also demonstrate, as we had previously done in NSCLC cell lines ([Beaulieu et al., 2019](#)), that Omomyc has a therapeutic impact *in vitro* in MM and BL cells. More in detail, it causes an arrest in proliferation in different phases of the cell cycle, in what seems to be a cell-dependent process, with no common mechanism of action shared between different cell lines. The only common effect among them is a general increase in the subG1 population, although cell death

cannot be presented as the leading cause of the cell number reduction, but more likely a contributor.

In addition, we show a general decrease in both MYC and MAX protein levels upon treatment with Omomyc. Such a reduction happens in a time-dependent manner, with a more pronounced reduction after 5 days of treatment. Demma et al. recently showed similar results in HCT116 (CRC cell line), in which incubation with Omomyc for as short as 2 hours already caused a big reduction in MYC levels owing to MYC destabilisation and degradation through the proteasome (Demma et al., 2019). They also present the complete disappearance of MYC after 24 hours of treatment with Omomyc, which differs from our observations in both NSCLC (Beaulieu et al., 2019) and MM, where MYC levels remain unchanged even after 3 days of treatment. Together, these results suggest that the decrease in MYC protein levels could also be a cell-dependent response to MYC inhibition by Omomyc.

Interestingly, during all our *in vitro* experiments, we could still find intracellular Omomyc in all the cancer cell lines 5 days after a one-time treatment. In fact, the levels detected at 5 days were quite similar to those observed at 3 days, suggestive of its high stability.

Our lab demonstrated that one of the mechanisms by which Omomyc exerts its MYC inhibition is through the effective displacement of MYC from known target promoters (Beaulieu et al., 2019). Here we confirm that in MM and BL cell lines, MYC is sequestered away from DNA in a time-dependent manner, with a greater effect observed at 5 days compared to 3 days of treatment. In this same context, not only do we show the displacement of MYC from DNA, but we also note the occupancy of Omomyc on those same regions. Consistently, Demma et al. unveil in their study how Omomyc binds DNA as a heterodimer with MAX or as a homodimer on the same regions as MYC-MAX dimers in HCT116 CRC cells (Demma et al., 2019). However, the balance between homodimers (Omomyc/Omomyc) and heterodimers (Omomyc/MAX) is likely dependent on the relative amounts of the different monomers in each cellular context. Hence, in our MM and BL samples, they could be different.

To complete the mechanistic aspect of the study, we finally checked the impact of MYC inhibition on epigenetics, looking at changes in molecular marks that could be a consequence of Omomyc's effect, leading to chromatin remodelling, which could be translated into a longer-term and sustained transcriptional changes. In Beaulieu et al., we had described for the first time some reduction in the acetylation of lysine 27 residues on histone H3, a well-known mark of active enhancers, upon Omomyc mini-protein treatment of NSCLC cells (Beaulieu et al., 2019). Now, we confirmed this result in Raji lymphoma cells and looked at another mark of active genes, trimethylation of lysine 4 residues on histone H3. Also, this mark appeared

to decrease upon treatment. In both cases, the reduction occurs in a time-dependent manner, with a more apparent drop observed after 5 days of treatment compared to 3.

Surprisingly, in U266 myeloma cells, we observe quite the opposite: a general increase in both epigenetic marks indicative of open chromatin upon Omomyc treatment. To gain more insight into this apparent incoherence, we also check for the status of a heterochromatin signature, trimethylation of lysine 9 residues on histone H3, which is as well increased in Omomyc-treated samples from U266 cells.

It should be noted that even though H3K4me3 is an epigenetic mark widely related to gene activation and open chromatin ([Sharifi-Zarchi et al., 2017](#)), Howe et al. describe that an increase of this mark in certain DNA regions does not necessarily translate into the additional transcription of those genes ([Howe et al., 2017](#)). Researchers state that H3K4me3 can be associated with both transcriptional activation or repression, because it corresponds to the recruitment of several co-factors, both activator and repressors, depending on neighbouring modifications ([Howe et al., 2017](#)). Other studies, for example, show that H3K4me3 interacts with Rpd3L to promote transcriptional repression in yeast through histone deacetylation, in a novel mechanism termed transcriptional repression memory ([Lee et al., 2018](#)). Another scenario in which increased levels of H3K4me3 are associated with transcriptional repression is that where co-repressors, like the Groucho/transducin-like Enhancer of split (TLE) family, are recruited at transcriptional start sites (TSSs) in chromatin permissive to transcription to attenuate gene expression ([Kaul et al., 2014](#)).

### **4.2.2 Omomyc mini-protein *in vivo*: zebrafish model**

After demonstrating Omomyc's *in vitro* effect, we tested its efficacy *in vivo*. As an emerging animal model for cancer therapy modelling, we initially used zebrafish, because of its advantages in terms of both cost-effectiveness and time-efficiency, while also being as informative as the more commonly used murine models in some contexts ([Shull et al., 2017](#)). First, we showed that pre-treatment with Omomyc in culture for 3 or 5 days significantly prevents the homing of lymphoma and myeloma cells to a BM-like structure present in zebrafish larvae, the CHT. We confirmed that migration was also impeded using *in vitro* assays. We identified the reduction in VLA-4 levels as one of the foremost players involved in such impairment, consistent with previously published data by Sacco et al., where VLA-4 silencing through shRNA phenocopies Omomyc's effect ([Sacco et al., 2016](#)).

Next, we aimed at demonstrating the therapeutic impact of Omomyc in an intervention study. To do so, we first confirmed that we could administer Omomyc to zebrafish larvae by dissolving it in their embryo medium, facilitating the permeabilisation of larvae's tegument with DMSO. However, apart from observing

no anti-cancer effect in the short therapeutic window of 72 hours allowed by this experimental model, we had several other issues, including high toxicity, resulting in larvae death at relatively low micromolar concentrations. In an attempt to prevent toxicity, we administered a liposomal Omomyc formulation. Unfortunately, the liposomes could not be used in the presence of DMSO and proved unable to cross the tegument.

Other research groups have also used the zebrafish model to test their chemotherapeutic drugs with xenograft transplanted tumour cells. Hsieh et al. co-inoculated breast cancer cells, and their CPP, an inhibitor of the  $\beta$ -catenin and LEF-1 interaction, into the yolk sack of the fish larvae, and reported attenuated tumorigenesis (Hsieh et al., 2016). On the other hand, Yang et al., for example, demonstrate a 5-fold reduction in the dose of doxorubicin (delivered in decorated with a coiled coil peptide NPs) required to observe growth inhibition of HeLa cells transgenically modified to express the complementary coiled coil peptide pair in their plasma membrane, with the consequent reduction in potential adverse effects. However, in contrast to our method, they delivered the decorated liposomes via microinjection in the duct of Cuvier 5 hpi of the xenografted cancer cells (Yang et al., 2016).

### 4.2.3 Omomyc mini-protein *in vivo*: mouse models

#### BL studies:

Given our difficulties in systemic delivery of Omomyc in zebrafish, we decided to proceed with testing it in murine xenograft models. As we had shown that Omomyc could impair the homing of lymphoma cells in the zebrafish model, we performed a prevention experiment with Raji cells, to see whether we could prevent their colonisation to mouse tissues. Indeed, Omomyc-treated animals display a reduction in the colonisation of the BM, whose functional analogue organ in teleosts is represented by the CHT (Wolf et al., 2017). The concomitant increase in positive CD79 $\alpha$  cells observed in the spleen could be explained by the fact that the splenic red pulp usually removes aged, dead or opsonised cells from circulation, suggesting that Omomyc could induce their elimination (Lewis et al., 2019). Taking into account that the treatment with Omomyc *in vitro* increased cell death in both MM and BL cell lines, it is plausible that the same could be happening *in vivo*. Further histologic characterisation of the tissues could help confirm or refute this hypothesis.

Sadly, however, we cannot demonstrate the prevention of colonisation of Raji cells into any other organ analysed after 2 treatment cycles. Chances are, though, that longer treatments could achieve better results.

In addition, we did not verify whether the impairment of the engraftment would happen more efficiently upon pre-conditioning before inoculation.



MM studies:

While we obtained the same disappointing overall lack of efficacy in the myeloma model (after 4 treatment cycles with a slightly higher dose compared to the BL xenograft model), we did observe some promising trends in the clinical score and IgE levels upon Omomyc treatment, pointing towards a potential therapeutic impact that could be enhanced by, for example, more frequent doses or improved delivery. Importantly, we cannot detect evident staining of Omomyc in the tissue of interest, the BM, 24 hours after the treatment, indeed suggestive of inadequate biodistribution of the protein to this target tissue compartment. Interestingly though, in separate experiments, we observed the presence of fluorescently labelled Omomyc in the BM of treated mice, 4 hours post inoculation. However, BM lysates from a high-dose treated mouse (100 mg/kg of unlabelled protein) do not reveal the band corresponding to Omomyc in an immunoblot. All these findings together suggest a suboptimal concentration of the mini-protein reaching the target cells, a concentration that is below the limit of detection of our techniques.

On the other hand, in a recent publication, Demma et al. inferred that rapid metabolism in tissues could be responsible for quick Omomyc elimination ([Demma et al., 2019](#)). To clarify this issue, it would be interesting to analyse the tissues by mass spectrometry to accurately define the amount of drug getting to myeloma and lymphoma cells ([An et al., 2014](#)). However, the possibility still exists that the low local concentration results in insufficient molecules of active Omomyc able to exert MYC inhibition ([Demma et al., 2019](#)). As it happens, researchers have shown that wide biodistribution of CPPs can lead to a less efficient performance of the drugs ([Habault and Poyet, 2019](#)).

With this in mind, we tried to use a well-investigated strategy to assist drug delivery and improve its biodistribution: liposomal nanoparticles ([Bulbake et al., 2017](#)). As described before, one of the advantages of encapsulating drugs into these nanocarriers is the reduction of the required dose of therapy, due to enhanced delivery to the tissue, with the possibility of reducing unwanted toxic reactions as well ([Sercombe et al., 2015](#)).

In these experiments, we used a formulation containing CHEMS, a negatively charged lipid that proved to achieve the highest encapsulation efficiency compared to the others tested (unpublished data). Indeed, we believe, at least partly because of the slightly negative net charge of our liposomes, that the positively charged Omomyc mini-protein gets trapped in the aqueous phase of the NPs. Also, due to the electrostatic interaction between Omomyc and the lipids in the outer membrane of the liposomes, we propose the formation of large liposomal complexes. These cause a biphasic separation of “concentrated” NPs at the bottom of the tube and an aqueous, liposome free, upper layer. Surprisingly, this bilayer can only be seen with a 1:1 ratio of liposomes:Omomyc, but not when we double the concentration

of Omomyc only (3:6). This observation suggests that saturation with too many molecules of Omomyc could result in neutralisation of all negative charges from the lipids in the outer membrane of the liposomes, which would be interacting with positively charged Omomyc. Hence, the net charge of the liposomes could be switched to positive and potentially result in repulsion from neighbour “Omomyc-coated” NPs, but most definitely it could abrogate the possibility of occupied lipids to interact with other Omomyc molecules in the solution, which instead could as well act as bridges between neighbouring nanocarriers.

Importantly, we found 2 major limitations when producing our liposomal formulation: 1. extrusion through 200 nm membranes of liposomes generated from a 30 mg/mL of a lipid mixture was already mechanically very tough; 2. our 50% EE only allowed us to achieve the administration of around 6 mg/kg of encapsulated Omomyc.

Given the complexity of extrusion of the solutions already with a 3:6 ratio, we did not explore increasing the ratio to 6:6, which would have potentially increased the dose administered to 12 mg/kg. However, we demonstrated that our liposomal formulation could significantly increase the stability of the Omomyc mini-protein in plasma, where instead 12 mg/kg of the free drug get already cleared 16 hours after the treatment. Despite this improved stability in serum, though, we still cannot observe intracellular Omomyc in BM lysates.

Finally, like the Omomyc free drug, also the Omolips failed to be an effective treatment as monotherapy in our myeloma model.

All these results suggest the need for further efforts to obtain better delivery of our therapy to BM cells. For instance, decorated targeting nanocarriers could overcome the obstacle of penetrating resident cells in the BM. Indeed, researchers have shown that targeted NPs carrying a MYC inhibitor can prolong the survival of treated mice in a disseminated model of myeloma ([Soodgupta et al., 2015](#)). In a different publication, de la Puente et al. report increased overall survival of myeloma-bearing mice treated with anti-CD38 targeted NPs loaded with BTZ ([de la Puente et al., 2018](#)).

Nevertheless, we would like to stress some encouraging results obtained with Omomyc in combination therapy: we saw synergy both *in vitro* and more importantly, *in vivo*, when combining Omomyc and one of the standard chemotherapeutic agents for MM, a proteasome inhibitor. Combinatorial approaches are typically used to overcome treatment resistance, potentiate the effect of individual drugs and, thus, co-administration of different agents may provide a more durable response ([Allen-Petersen and Sears, 2019](#)).

### 4.3.1 Variant 26

Last but not least, in this thesis, we examined the potential applicability of a derivative of the Omomyc sequence, variant 26 (V26). Such a variant shares some of Omomyc properties, in that it can homodimerise and heterodimerise with MAX, and these dimers can form complexes with DNA. However, the lower solubility of V26 compared to Omomyc presents a significant drawback and poses the requirement of further experimental and developmental efforts to make it a potential suitable clinical candidate. One of the complications we faced due to V26 aggregation was difficulty in determining its affinity by CD spectra for MAX or MYC and for the canonical E-box sequences. In fact, during the overnight incubation, V26 in the presence of DNA appeared as a cloudy solution that, after heating for the thermal denaturation, ended up with macroscopically visible white aggregates. Hence, even though V26 homodimers and V26/MAX heterodimers form (as are evidenced by the thermal denaturation curves), one possible explanation for the lack of increased ellipticity could be the reduction of soluble protein in the mixture. As a matter of fact, CD spectra analysis is highly sensitive to solutes concentration, which in this case are likely diminished because of the precipitation of the variant, resulting in a reduced signal. The same can also be inferred from the thermal denaturation curves, in which both experimental mixtures of V26/MAX and V26/MYC heterodimers with DNA register a lesser CD signal compared to their arithmetic sum.

Although V26 was proven to have a better nuclear localisation compared to Omomyc, it clearly requires formulation improvements to refine the solubility issues identified so far, especially for its *in vivo* use.

Nevertheless, V26 constitutes a prototype that helps us to guide the design of performant anti-MYC agents that, based on the original sequence of Omomyc, could achieve improved biodistribution, nuclear localisation, enhanced cell-death and endosomal escape among others. Other Omomyc variants encompassing a more limited subset of changes have also been designed and successfully expressed and purified in our lab, but remain to be characterised.

Brown et al. propose the use of significantly truncated fragments of Omomyc instead of the full-length molecule. Such smaller fragments still need to prove their potency, permeability as much as their pharmacokinetic properties *in vivo* (Brown et al., 2019).

One essential thing to bear in mind when inhibiting TFs is that they exert their function through protein-protein or protein-DNA interactions that involve a relatively extensive and diffuse surface area, hard to disrupt with popular small-molecule strategies (Inamoto and Shin, 2019). Hence, harsh minimisation of the size of a mini-protein like Omomyc could likely end up in invalidation of its higher specificity and therapeutic potential.

Altogether, our results set the basis for future improved formulations/molecules for the treatment of myeloma, lymphoma, and potentially other haematological malignancies, and outline the necessity for further research efforts to generate non-toxic, effectively-delivered or targeted MYC inhibitors, either peptidomimetics or disruptors of the MYC-MAX dimer.

In addition, exploration of combinatorial approaches involving Omomyc with SoC chemotherapeutics promises to be another powerful investigation line worth pursuing.



## CONCLUSIONS

1. X and Z peptidomimetics display efficacy *in vitro*, but their poor stability and bioavailability, high local toxicity and lack of effectiveness *in vivo* rule them out as a novel therapy for myeloma treatment.
2. Z<sub>1</sub> peptidomimetics' improved formulation is also effective *in vitro* but does not overcome the severe toxic reactions to the compound, proving unsuitable for *in vivo* use.
3. The Omomyc mini-protein penetrates myeloma and lymphoma cell lines to block their proliferation, displacing MYC-MAX dimers on DNA and causing a general reduction in MYC and MAX protein levels.
4. The Omomyc mini-protein impairs the homing of pre-conditioned myeloma and lymphoma cells to a bone-marrow-like structure present in zebrafish larvae, the caudal haematopoietic tissue.
5. Similarly, immediate intravenous treatment (prevention) with Omomyc reduces the homing of lymphoma cells to the bone marrow in a xenograft mouse model.
6. Intravenous administration of Omomyc mini-protein in a myeloma xenograft mouse model does not prevent disease progression.
7. The Omomyc mini-protein distributes to the bone marrow in a time-dependent manner but does not reach the intracellular compartment of resident bone marrow cells.
8. Encapsulation in liposomes improves the plasma stability of Omomyc mini-protein but does not enhance the entrance into bone marrow resident cells.
9. Combination of Omomyc mini-protein with proteasome inhibitors, the standard of care in the clinics, shows synergy *in vitro* and *in vivo*.
10. Variant 26 (like Omomyc) can homodimerise and heterodimerise with MAX, and these dimers can bind canonical E-boxes.
11. Variant 26 exhibits better nuclear localisation than Omomyc and induces increased cell death, but displays worse solubility, needing further improvements for *in vivo* use.



## REFERENCES

- Albihn, A., Johnsen, J. I. & Henriksson, M. A. 2010. MYC in oncogenesis and as a target for cancer therapies. *Adv Cancer Res*, 107, 163-224.
- Alfayez, M., Kantarjian, H., Kadia, T., Ravandi-Kashani, F. & Daver, N. 2020. CPX-351 (vyxeos) in AML. *Leuk Lymphoma*, 61, 288-297.
- Allen-Petersen, B. L. & Sears, R. C. 2019. Mission Possible: Advances in MYC Therapeutic Targeting in Cancer. *BioDrugs*, 33, 539-553.
- An, B., Zhang, M. & Qu, J. 2014. Toward sensitive and accurate analysis of antibody biotherapeutics by liquid chromatography coupled with mass spectrometry. *Drug Metab Dispos*, 42, 1858-66.
- Annibali, D., Whitfield, J. R., Favuzzi, E., Jauset, T., Serrano, E., Cuartas, I., Redondo-Campos, S., Folch, G., Gonzalez-Junca, A., Sodir, N. M., Masso-Valles, D., Beaulieu, M. E., Swigart, L. B., Mc Gee, M. M., Somma, M. P., Nasi, S., Seoane, J., Evan, G. I. & Soucek, L. 2014. Myc inhibition is effective against glioma and reveals a role for Myc in proficient mitosis. *Nat Commun*, 5, 4632.
- Arora, V., Knapp, D. C., Smith, B. L., Statfield, M. L., Stein, D. A., Reddy, M. T., Weller, D. D. & Iversen, P. L. 2000. c-Myc antisense limits rat liver regeneration and indicates role for c-Myc in regulating cytochrome P-450 3A activity. *J Pharmacol Exp Ther*, 292, 921-8.
- Arvanitis, C. & Felsher, D. W. 2005. Conditionally MYC: insights from novel transgenic models. *Cancer Lett*, 226, 95-9.
- Asosingh, K., Radl, J., Van Riet, I., Van Camp, B. & Vanderkerken, K. 2000. The 5TMM series: a useful in vivo mouse model of human multiple myeloma. *Hematol J*, 1, 351-6.
- Badalian-Very, G. 2014. Personalized medicine in hematology - A landmark from bench to bed. *Comput Struct Biotechnol J*, 10, 70-7.
- Baker, D. & Amor, S. 2012. Publication guidelines for refereeing and reporting on animal use in experimental autoimmune encephalomyelitis. *J Neuroimmunol*, 242, 78-83.
- Balik, K., Modrakowska, P., Maj, M., Kaźmierski, Ł. & Bajek, A. 2019. *Limitations of molecularly targeted therapy*.
- Barrett, J., Birrer, M. J., Kato, G. J., Dosaka-Akita, H. & Dang, C. V. 1992. Activation domains of L-Myc and c-Myc determine their transforming potencies in rat embryo cells. *Mol Cell Biol*, 12, 3130-7.
- Beaulieu, M. E., Jauset, T., Masso-Valles, D., Martinez-Martin, S., Rahl, P., Maltais, L., Zacarias-Fluck, M. F., Casacuberta-Serra, S., Serrano Del Pozo, E., Fiore, C., Foradada, L., Cano, V. C., Sanchez-Hervas, M., Guenther, M., Romero Sanz, E., Oteo, M., Tremblay, C., Martin, G., Letourneau, D., Montagne, M., Morcillo Alonso, M. A., Whitfield, J. R., Lavigne, P. & Soucek, L. 2019. Intrinsic cell-penetrating activity propels Omomyc from proof of concept to viable anti-MYC therapy. *Sci Transl Med*, 11.



## References

- Berg, T., Cohen, S. B., Desharnais, J., Sonderegger, C., Maslyar, D. J., Goldberg, J., Boger, D. L. & Vogt, P. K. 2002. Small-molecule antagonists of Myc/Max dimerization inhibit Myc-induced transformation of chicken embryo fibroblasts. *Proc Natl Acad Sci U S A*, 99, 3830-5.
- Bhullar, K. S., Lagaron, N. O., MCGowan, E. M., Parmar, I., Jha, A., Hubbard, B. P. & Rupasinghe, H. P. V. 2018. Kinase-targeted cancer therapies: progress, challenges and future directions. *Mol Cancer*, 17, 48.
- Bidwell, G. L., 3rd, Perkins, E., Hughes, J., Khan, M., James, J. R. & Raucher, D. 2013. Thermally targeted delivery of a c-Myc inhibitory polypeptide inhibits tumor progression and extends survival in a rat glioma model. *PLoS One*, 8, e55104.
- Blum, K. A., Lozanski, G. & Byrd, J. C. 2004. Adult Burkitt leukemia and lymphoma. *Blood*, 104, 3009-20.
- Brooks, T. A. & Hurley, L. H. 2010. Targeting MYC Expression through G-Quadruplexes. *Genes Cancer*, 1, 641-649.
- Brown, R. V., Danford, F. L., Gokhale, V., Hurley, L. H. & Brooks, T. A. 2011. Demonstration that drug-targeted down-regulation of MYC in non-Hodgkins lymphoma is directly mediated through the promoter G-quadruplex. *J Biol Chem*, 286, 41018-27.
- Brown, Z. Z., Mapelli, C., Farasat, I., Shoultz, A. V., Johnson, S. A., Orvieto, F., Santoprete, A., Bianchi, E., Mccracken, A. B., Chen, K., Zhu, X., Demma, M. J., Lacey, B. M., Canada, K. A., Garbaccio, R. M., O'neil, J. & Walji, A. 2019. Multiple Synthetic Routes to the Mini-Protein Omomyc and Coiled-Coil Domain Truncations. *J Org Chem*.
- Bulbake, U., Doppalapudi, S., Kommineni, N. & Khan, W. 2017. Liposomal Formulations in Clinical Use: An Updated Review. *Pharmaceutics*, 9.
- Cai, Q., Medeiros, L. J., Xu, X. & Young, K. H. 2015. MYC-driven aggressive B-cell lymphomas: biology, entity, differential diagnosis and clinical management. *Oncotarget*, 6, 38591-616.
- Caldeira De Araújo Lopes, S., Dos Santos Giuberti, C., Guieiro Ribeiro Rocha, T., Dos Santos Ferreira, D., Amaral Leite, E. & Cristina Oliveira, M. 2013. *Liposomes as Carriers of Anticancer Drugs, Cancer Treatment*, IntechOpen.
- Cancer Research UK 2016. <https://www.cancerresearchuk.org/health-professional/cancer-statistics/statistics-by-cancer-type/myeloma#heading-Four>.
- Carabet, L. A., Rennie, P. S. & Cherkasov, A. 2018. Therapeutic Inhibition of Myc in Cancer. Structural Bases and Computer-Aided Drug Discovery Approaches. *Int J Mol Sci*, 20.
- Castell, A., Yan, Q., Fawcner, K., Hydbring, P., Zhang, F., Verschut, V., Franco, M., Zakaria, S. M., Bazzar, W., Goodwin, J., Zinzalla, G. & Larsson, L. G. 2018. A selective high affinity MYC-binding compound inhibits MYC:MAX interaction and MYC-dependent tumor cell proliferation. *Sci Rep*, 8, 10064.
- Chae, Y. K., Pan, A. P., Davis, A. A., Patel, S. P., Carneiro, B. A., Kurzrock, R. & Giles, F. J. 2017. Path toward Precision Oncology: Review of Targeted

- Therapy Studies and Tools to Aid in Defining "Actionability" of a Molecular Lesion and Patient Management Support. *Mol Cancer Ther*, 16, 2645-2655.
- Chauhan, J., Wang, H., Yap, J. L., Sabato, P. E., Hu, A., Prochownik, E. V. & Fletcher, S. 2014. Discovery of methyl 4'-methyl-5-(7-nitrobenzo[c][1,2,5]oxadiazol-4-yl)-[1,1'-biphenyl]-3-carboxylate, an improved small-molecule inhibitor of c-Myc-max dimerization. *ChemMedChem*, 9, 2274-2285.
- Chen, H., Liu, H. & Qing, G. 2018. Targeting oncogenic Myc as a strategy for cancer treatment. *Signal Transduct Target Ther*, 3, 5.
- Chesler, L., Schlieve, C., Goldenberg, D. D., Kenney, A., Kim, G., Mcmillan, A., Matthay, K. K., Rowitch, D. & Weiss, W. A. 2006. Inhibition of phosphatidylinositol 3-kinase destabilizes Mycn protein and blocks malignant progression in neuroblastoma. *Cancer Res*, 66, 8139-46.
- Chipumuro, E., Marco, E., Christensen, C. L., Kwiatkowski, N., Zhang, T., Hatheway, C. M., Abraham, B. J., Sharma, B., Yeung, C., Altabef, A., Perez-Atayde, A., Wong, K. K., Yuan, G. C., Gray, N. S., Young, R. A. & George, R. E. 2014. CDK7 inhibition suppresses super-enhancer-linked oncogenic transcription in MYCN-driven cancer. *Cell*, 159, 1126-1139.
- Choi, S. H., Mahankali, M., Lee, S. J., Hull, M., Petrassi, H. M., Chatterjee, A. K., Schultz, P. G., Jones, K. A. & Shen, W. 2017. Targeted Disruption of Myc-Max Oncoprotein Complex by a Small Molecule. *ACS Chem Biol*, 12, 2715-2719.
- Choi, Y. J., Kim, D. H., Yoon, D. H., Suh, C., Choi, C. M., Lee, J. C., Hong, J. Y. & Rho, J. K. 2019. Efficacy of the novel CDK7 inhibitor QS1189 in mantle cell lymphoma. *Sci Rep*, 9, 7193.
- Cochran, A. G., Conery, A. R. & Sims, R. J., 3rd 2019. Bromodomains: a new target class for drug development. *Nat Rev Drug Discov*, 18, 609-628.
- Conacci-Sorrell, M., McFerrin, L. & Eisenman, R. N. 2014. An overview of MYC and its interactome. *Cold Spring Harb Perspect Med*, 4, a014357.
- Conriot, J., Silva, J. M., Fernandes, J. G., Silva, L. C., Gaspar, R., Brocchini, S., Florindo, H. F. & Barata, T. S. 2014. Cancer immunotherapy: nanodelivery approaches for immune cell targeting and tracking. *Front Chem*, 2, 105.
- Cooper, T. M. & Woody, R. W. 1990. The effect of conformation on the CD of interacting helices: a theoretical study of tropomyosin. *Biopolymers*, 30, 657-76.
- Dang, C. V. 2012. MYC on the path to cancer. *Cell*, 149, 22-35.
- Dang, C. V., Reddy, E. P., Shokat, K. M. & Soucek, L. 2017. Drugging the 'undruggable' cancer targets. *Nat Rev Cancer*, 17, 502-508.
- Danko, D., Blay, J. Y. & Garrison, L. P. 2019. Challenges in the value assessment, pricing and funding of targeted combination therapies in oncology. *Health Policy*, 123, 1230-1236.
- Davis, A. C., Wims, M., Spotts, G. D., Hann, S. R. & Bradley, A. 1993. A null c-myc mutation causes lethality before 10.5 days of gestation in

## References

- homozygotes and reduced fertility in heterozygous female mice. *Genes Dev*, 7, 671-82.
- De La Puente, P. & Azab, A. K. 2017. Nanoparticle delivery systems, general approaches, and their implementation in multiple myeloma. *Eur J Haematol*, 98, 529-541.
- De La Puente, P., Luderer, M. J., Federico, C., Jin, A., Gilson, R. C., Egbulefu, C., Alhallak, K., Shah, S., Muz, B., Sun, J., King, J., Kohnen, D., Salama, N. N., Achilefu, S., Vij, R. & Azab, A. K. 2018. Enhancing proteasome-inhibitory activity and specificity of bortezomib by CD38 targeted nanoparticles in multiple myeloma. *J Control Release*, 270, 158-176.
- Delmore, J. E., Issa, G. C., Lemieux, M. E., Rahl, P. B., Shi, J., Jacobs, H. M., Kastritis, E., Gilpatrick, T., Paranal, R. M., Qi, J., Chesi, M., Schinzel, A. C., Mckeown, M. R., Heffernan, T. P., Vakoc, C. R., Bergsagel, P. L., Ghobrial, I. M., Richardson, P. G., Young, R. A., Hahn, W. C., Anderson, K. C., Kung, A. L., Bradner, J. E. & Mitsiades, C. S. 2011. BET bromodomain inhibition as a therapeutic strategy to target c-Myc. *Cell*, 146, 904-17.
- Demma, M. J., Mapelli, C., Sun, A., Bodea, S., Ruprecht, B., Javaid, S., Wiswell, D., Muise, E., Chen, S., Zelina, J., Orvieto, F., Santoprete, A., Altezza, S., Tucci, F., Escandon, E., Hall, B., Ray, K., Walji, A. & O'neil, J. 2019. Omomyc Reveals New Mechanisms To Inhibit the MYC Oncogene. *Mol Cell Biol*, 39.
- Dhillon, P. & Evan, G. 2019. In conversation with Gerard Evan. *FEBS J*, 286, 4824-4831.
- Dominguez-Sola, D. & Gautier, J. 2014. MYC and the control of DNA replication. *Cold Spring Harb Perspect Med*, 4.
- Dozzo, M., Carobolante, F., Donisi, P. M., Scattolin, A., Maino, E., Sancetta, R., Viero, P. & Bassan, R. 2017. Burkitt lymphoma in adolescents and young adults: management challenges. *Adolesc Health Med Ther*, 8, 11-29.
- Fabbro, D., Cowan-Jacob, S. W. & Moebitz, H. 2015. Ten things you should know about protein kinases: IUPHAR Review 14. *Br J Pharmacol*, 172, 2675-700.
- Fathi, S. & Oyelere, A. K. 2016. Liposomal drug delivery systems for targeted cancer therapy: is active targeting the best choice? *Future Med Chem*, 8, 2091-2112.
- Felsher, D. W. & Bishop, J. M. 1999. Reversible tumorigenesis by MYC in hematopoietic lineages. *Mol Cell*, 4, 199-207.
- Ferry, J. A. 2006. Burkitt's lymphoma: clinicopathologic features and differential diagnosis. *Oncologist*, 11, 375-83.
- Fletcher, S. & Prochownik, E. V. 2015. Small-molecule inhibitors of the Myc oncoprotein. *Biochim Biophys Acta*, 1849, 525-43.
- Fukazawa, T., Maeda, Y., Matsuoka, J., Yamatsuji, T., Shigemitsu, K., Morita, I., Faiola, F., Durbin, M. L., Soucek, L. & Naomoto, Y. 2010. Inhibition of Myc effectively targets KRAS mutation-positive lung cancer expressing high levels of Myc. *Anticancer Res*, 30, 4193-200.

- Gabay, M., Li, Y. & Felsher, D. W. 2014. MYC activation is a hallmark of cancer initiation and maintenance. *Cold Spring Harb Perspect Med*, 4.
- Galardi, S., Savino, M., Scagnoli, F., Pellegatta, S., Pisati, F., Zambelli, F., Illi, B., Annibali, D., Beji, S., Orecchini, E., Alberelli, M. A., Apicella, C., Fontanella, R. A., Michienzi, A., Finocchiaro, G., Farace, M. G., Pavesi, G., Ciafre, S. A. & Nasi, S. 2016. Resetting cancer stem cell regulatory nodes upon MYC inhibition. *EMBO Rep*, 17, 1872-1889.
- Garcia-Gomez, A., Sanchez-Guijo, F., Del Canizo, M. C., San Miguel, J. F. & Garayoa, M. 2014. Multiple myeloma mesenchymal stromal cells: Contribution to myeloma bone disease and therapeutics. *World J Stem Cells*, 6, 322-43.
- Giorello, L., Clerico, L., Pescarolo, M. P., Vikhanskaya, F., Salmona, M., Colella, G., Bruno, S., Mancuso, T., Bagnasco, L., Russo, P. & Parodi, S. 1998. Inhibition of cancer cell growth and c-Myc transcriptional activity by a c-Myc helix 1-type peptide fused to an internalization sequence. *Cancer Res*, 58, 3654-9.
- Giuriato, S., Rabin, K., Fan, A. C., Shachaf, C. M. & Felsher, D. W. 2004. Conditional animal models: a strategy to define when oncogenes will be effective targets to treat cancer. *Semin Cancer Biol*, 14, 3-11.
- Globocan. 2018a. *Cancer Today* [Online]. Available: [http://gco.iarc.fr/today/online-analysis-table?v=2018&mode=cancer&mode\\_population=continents&population=900&populations=994&key=asr&sex=0&cancer=39&type=0&statistic=5&prevalence=0&population\\_group=0&ages\\_group%5B%5D=0&ages\\_group%5B%5D=17&nb\\_items=5&group\\_cancer=1&include\\_nmsc=1&include\\_nmsc\\_other=1#collapse-group-1-3-3](http://gco.iarc.fr/today/online-analysis-table?v=2018&mode=cancer&mode_population=continents&population=900&populations=994&key=asr&sex=0&cancer=39&type=0&statistic=5&prevalence=0&population_group=0&ages_group%5B%5D=0&ages_group%5B%5D=17&nb_items=5&group_cancer=1&include_nmsc=1&include_nmsc_other=1#collapse-group-1-3-3) [Accessed].
- Globocan. 2018b. *Cancer Tomorrow* [Online]. Available: [http://gco.iarc.fr/tomorrow/graphic-isotype?type=0&population=900&mode=population&sex=0&cancer=39&age\\_group=value&apc\\_male=0&apc\\_female=0](http://gco.iarc.fr/tomorrow/graphic-isotype?type=0&population=900&mode=population&sex=0&cancer=39&age_group=value&apc_male=0&apc_female=0) [Accessed].
- Habault, J. & Poyet, J. L. 2019. Recent Advances in Cell Penetrating Peptide-Based Anticancer Therapies. *Molecules*, 24.
- Hammerl, L., Colombet, M., Rochford, R., Ogwang, D. M. & Parkin, D. M. 2019. The burden of Burkitt lymphoma in Africa. *Infect Agent Cancer*, 14, 17.
- Hanahan, D. & Weinberg, R. A. 2011. Hallmarks of cancer: the next generation. *Cell*, 144, 646-74.
- Hann, S. R. 2014. MYC cofactors: molecular switches controlling diverse biological outcomes. *Cold Spring Harb Perspect Med*, 4, a014399.
- Hantschel, O., Rix, U. & Superti-Furga, G. 2008. Target spectrum of the BCR-ABL inhibitors imatinib, nilotinib and dasatinib. *Leuk Lymphoma*, 49, 615-9.
- Hart, J. R., Garner, A. L., Yu, J., Ito, Y., Sun, M., Ueno, L., Rhee, J. K., Baksh, M. M., Stefan, E., Hartl, M., Bister, K., Vogt, P. K. & Janda, K. D. 2014. Inhibitor of MYC identified in a Krohnke pyridine library. *Proc Natl Acad Sci U S A*, 111, 12556-61.

## References

- Higgs, J. T., Lee, J. H., Wang, H., Ramani, V. C., Chanda, D., Hardy, C. Y., Sanderson, R. D. & Ponnazhagan, S. 2017. Mesenchymal stem cells expressing osteoprotegerin variants inhibit osteolysis in a murine model of multiple myeloma. *Blood Adv*, 1, 2375-2385.
- Howe, F. S., Fischl, H., Murray, S. C. & Mellor, J. 2017. Is H3K4me3 instructive for transcription activation? *Bioessays*, 39, 1-12.
- Hsieh, T. H., Hsu, C. Y., Tsai, C. F., Chiu, C. C., Liang, S. S., Wang, T. N., Kuo, P. L., Long, C. Y. & Tsai, E. M. 2016. A novel cell-penetrating peptide suppresses breast tumorigenesis by inhibiting beta-catenin/LEF-1 signaling. *Sci Rep*, 6, 19156.
- Hu, S., Marineau, J. J., Rajagopal, N., Hamman, K. B., Choi, Y. J., Schmidt, D. R., Ke, N., Johannessen, L., Bradley, M. J., Orlando, D. A., Alnemy, S. R., Ren, Y., Ciblat, S., Winter, D. K., Kabro, A., Sprott, K. T., Hodgson, J. G., Fritz, C. C., Carulli, J. P., Di Tomaso, E. & Olson, E. R. 2019. Discovery and Characterization of SY-1365, a Selective, Covalent Inhibitor of CDK7. *Cancer Res*, 79, 3479-3491.
- Huang, H. L., Weng, H. Y., Wang, L. Q., Yu, C. H., Huang, Q. J., Zhao, P. P., Wen, J. Z., Zhou, H. & Qu, L. H. 2012. Triggering Fbw7-mediated proteasomal degradation of c-Myc by oridonin induces cell growth inhibition and apoptosis. *Mol Cancer Ther*, 11, 1155-65.
- Inamoto, I. & Shin, J. A. 2019. Peptide therapeutics that directly target transcription factors. *Peptide Science*, 111, e24048.
- Jacobson, C. & Lacasce, A. 2014. How I treat Burkitt lymphoma in adults. *Blood*, 124, 2913-20.
- Jain, M., Arvanitis, C., Chu, K., Dewey, W., Leonhardt, E., Trinh, M., Sundberg, C. D., Bishop, J. M. & Felsher, D. W. 2002. Sustained loss of a neoplastic phenotype by brief inactivation of MYC. *Science*, 297, 102-4.
- Jain, S., Wang, X., Chang, C. C., Ibarra-Drendall, C., Wang, H., Zhang, Q., Brady, S. W., Li, P., Zhao, H., Dobbs, J., Kyrish, M., Tkaczyk, T. S., Ambrose, A., Sistrunk, C., Arun, B. K., Richards-Kortum, R., Jia, W., Seewaldt, V. L. & Yu, D. 2015. Src Inhibition Blocks c-Myc Translation and Glucose Metabolism to Prevent the Development of Breast Cancer. *Cancer Res*, 75, 4863-75.
- Jauset González, T. 2018. *Inhibiting Myc in cancer using Omomyc: from defining the fundamental mechanism of action to its pharmacological application*. PhD in Biochemistry, Molecular Biology and Biomedicine, Universitat Autònoma de Barcelona.
- Jeong, K. C., Kim, K. T., Seo, H. H., Shin, S. P., Ahn, K. O., Ji, M. J., Park, W. S., Kim, I. H., Lee, S. J. & Seo, H. K. 2014. Intravesical instillation of c-MYC inhibitor KSI-3716 suppresses orthotopic bladder tumor growth. *J Urol*, 191, 510-8.
- Jovanovic, K. K., Roche-Lestienne, C., Ghobrial, I. M., Facon, T., Quesnel, B. & Manier, S. 2018. Targeting MYC in multiple myeloma. *Leukemia*, 32, 1295-1306.

Kaplan-Medical. Available:

[http://jasperwp.kaptest.com/content/media/82/41082.134.OL855Patho\\_22-UA0150.png](http://jasperwp.kaptest.com/content/media/82/41082.134.OL855Patho_22-UA0150.png) [Accessed].

- Kaul, A., Schuster, E. & Jennings, B. H. 2014. The Groucho co-repressor is primarily recruited to local target sites in active chromatin to attenuate transcription. *PLoS Genet*, 10, e1004595.
- Kazandjian, D. 2016. Multiple myeloma epidemiology and survival: A unique malignancy. *Semin Oncol*, 43, 676-681.
- Keefe, D. M. K. & Bateman, E. H. 2019. Potential Successes and Challenges of Targeted Cancer Therapies. *J Natl Cancer Inst Monogr*, 2019.
- Kelso, T. W., Baumgart, K., Eickhoff, J., Albert, T., Antrecht, C., Lemcke, S., Klebl, B. & Meisterernst, M. 2014. Cyclin-dependent kinase 7 controls mRNA synthesis by affecting stability of preinitiation complexes, leading to altered gene expression, cell cycle progression, and survival of tumor cells. *Mol Cell Biol*, 34, 3675-88.
- Kiessling, A., Wiesinger, R., Sperl, B. & Berg, T. 2007. Selective inhibition of c-Myc/Max dimerization by a pyrazolo[1,5-a]pyrimidine. *ChemMedChem*, 2, 627-30.
- Kim, A., Yun, M. O., Oh, Y. K., Ahn, W. S. & Kim, C. K. 1999. Pharmacodynamics of insulin in polyethylene glycol-coated liposomes. *Int J Pharm*, 180, 75-81.
- Koh, C. M., Sabo, A. & Guccione, E. 2016. Targeting MYC in cancer therapy: RNA processing offers new opportunities. *Bioessays*, 38, 266-75.
- Kovalchuk, A. L., Mushinski, E. B. & Janz, S. 2000. Clonal diversification of primary BALB/c plasmacytomas harboring T(12;15) chromosomal translocations. *Leukemia*, 14, 909-21.
- Kumar, S. K., Rajkumar, V., Kyle, R. A., Van Duin, M., Sonneveld, P., Mateos, M. V., Gay, F. & Anderson, K. C. 2017. Multiple myeloma. *Nat Rev Dis Primers*, 3, 17046.
- Kurtin, S. E. 2013. Relapsed or relapsed/refractory multiple myeloma. *Journal of the Advanced Practitioner in Oncology*, 4, 5-14.
- Kwiatkowski, N., Zhang, T., Rahl, P. B., Abraham, B. J., Reddy, J., Ficarro, S. B., Dastur, A., Amzallag, A., Ramaswamy, S., Tesar, B., Jenkins, C. E., Hannett, N. M., Mcmillin, D., Sanda, T., Sim, T., Kim, N. D., Look, T., Mitsiades, C. S., Weng, A. P., Brown, J. R., Benes, C. H., Marto, J. A., Young, R. A. & Gray, N. S. 2014. Targeting transcription regulation in cancer with a covalent CDK7 inhibitor. *Nature*, 511, 616-20.
- Kyle, R. A., Remstein, E. D., Therneau, T. M., Dispenzieri, A., Kurtin, P. J., Hodnefield, J. M., Larson, D. R., Plevak, M. F., Jelinek, D. F., Fonseca, R., Melton, L. J., 3rd & Rajkumar, S. V. 2007. Clinical course and prognosis of smoldering (asymptomatic) multiple myeloma. *N Engl J Med*, 356, 2582-90.
- Kyle, R. A., Therneau, T. M., Rajkumar, S. V., Offord, J. R., Larson, D. R., Plevak, M. F. & Melton, L. J., 3rd 2002. A long-term study of prognosis in monoclonal gammopathy of undetermined significance. *N Engl J Med*, 346, 564-9.

## References

- Landgren, O., Kyle, R. A., Pfeiffer, R. M., Katzmann, J. A., Caporaso, N. E., Hayes, R. B., Dispenzieri, A., Kumar, S., Clark, R. J., Baris, D., Hoover, R. & Rajkumar, S. V. 2009. Monoclonal gammopathy of undetermined significance (MGUS) consistently precedes multiple myeloma: a prospective study. *Blood*, 113, 5412-7.
- Lee, B. B., Choi, A., Kim, J. H., Jun, Y., Woo, H., Ha, S. D., Yoon, C. Y., Hwang, J. T., Steinmetz, L., Buratowski, S., Lee, S., Kim, H. Y. & Kim, T. 2018. Rpd3L HDAC links H3K4me3 to transcriptional repression memory. *Nucleic Acids Res*, 46, 8261-8274.
- Lee, J. C., Hayman, E., Pegram, H. J., Santos, E., Heller, G., Sadelain, M. & Brentjens, R. 2011. In vivo inhibition of human CD19-targeted effector T cells by natural T regulatory cells in a xenotransplant murine model of B cell malignancy. *Cancer Res*, 71, 2871-81.
- Lewis, S. M., Williams, A. & Eisenbarth, S. C. 2019. Structure and function of the immune system in the spleen. *Sci Immunol*, 4.
- Li, H., Song, J. H., Park, J. S. & Han, K. 2003. Polyethylene glycol-coated liposomes for oral delivery of recombinant human epidermal growth factor. *Int J Pharm*, 258, 11-9.
- Li, L., Sun, W., Zhang, Z. & Huang, Y. 2016. Time-staggered delivery of docetaxel and H1-S6A,F8A peptide for sequential dual-strike chemotherapy through tumor priming and nuclear targeting. *J Control Release*, 232, 62-74.
- Maifrede, S., Martin, K., Podszycwalow-Bartnicka, P., Sullivan-Reed, K., Langer, S. K., Nejati, R., Dasgupta, Y., Hulse, M., Gritsyuk, D., Nieborowska-Skorska, M., Lupey-Green, L. N., Zhao, H., Piwocka, K., Wasik, M. A., Tempera, I. & Skorski, T. 2017. IGH/MYC Translocation Associates with BRCA2 Deficiency and Synthetic Lethality to PARP1 Inhibitors. *Mol Cancer Res*, 15, 967-972.
- Maletzki, C., Bock, S., Fruh, P., Macius, K., Witt, A., Prall, F. & Linnebacher, M. 2020. NSG mice as hosts for oncological precision medicine. *Lab Invest*, 100, 27-37.
- Manier, S., Salem, K. Z., Park, J., Landau, D. A., Getz, G. & Ghobrial, I. M. 2017. Genomic complexity of multiple myeloma and its clinical implications. *Nat Rev Clin Oncol*, 14, 100-113.
- Marinkovic, D., Marinkovic, T., Mahr, B., Hess, J. & Wirth, T. 2004. Reversible lymphomagenesis in conditionally c-MYC expressing mice. *Int J Cancer*, 110, 336-42.
- Matos, A. I., Carreira, B., Peres, C., Moura, L. I. F., Connot, J., Fourniols, T., Scomparin, A., Martinez-Barriocanal, A., Arango, D., Conde, J. P., Preat, V., Satchi-Fainaro, R. & Florindo, H. F. 2019. Nanotechnology is an important strategy for combinational innovative chemo-immunotherapies against colorectal cancer. *J Control Release*, 307, 108-138.
- Miyakawa, Y., Ohnishi, Y., Tomisawa, M., Monnai, M., Kohmura, K., Ueyama, Y., Ito, M., Ikeda, Y., Kizaki, M. & Nakamura, M. 2004. Establishment of a new model of human multiple myeloma using NOD/SCID/gammac(null) (NOG) mice. *Biochem Biophys Res Commun*, 313, 258-62.

- Mo, H. & Henriksson, M. 2006. Identification of small molecules that induce apoptosis in a Myc-dependent manner and inhibit Myc-driven transformation. *Proc Natl Acad Sci U S A*, 103, 6344-9.
- Molyneux, E. M., Rochford, R., Griffin, B., Newton, R., Jackson, G., Menon, G., Harrison, C. J., Israels, T. & Bailey, S. 2012. Burkitt's lymphoma. *Lancet*, 379, 1234-44.
- Montagne, M., Beaudoin, N., Fortin, D., Lavoie, C. L., Klinck, R. & Lavigne, P. 2012. The Max b-HLH-LZ can transduce into cells and inhibit c-Myc transcriptional activities. *PLoS One*, 7, e32172.
- Moreno, V., Braña, I., Sanchez, J. M. M. S., Villar, M. V., Hernandez-Guerrero, T., Doger, B., Saavedra, O., Ferrero, O., Sarmiento, R., Arias, M., Alvaro, J. D., Dimartino, J. F., Zuraek, M., Pérez, T. S., Filvaroff, E., Aronchik, I., Lamba, M., Hanna, B. & Nikolova, Z. G. 2019. Phase I study of CC-90010 in patients with advanced solid tumors and relapsed/refractory non-Hodgkin lymphoma (R/R NHL). *Journal of Clinical Oncology*, 37, 3015-3015.
- Nasi, S., Ciarapica, R., Jucker, R., Rosati, J. & Soucek, L. 2001. Making decisions through Myc. *FEBS Lett*, 490, 153-62.
- Nesbit, C. E., Grove, L. E., Yin, X. & Prochownik, E. V. 1998. Differential apoptotic behaviors of c-myc, N-myc, and L-myc oncoproteins. *Cell Growth Differ*, 9, 731-41.
- Nih, N. C. I. *Targeted Cancer Therapies* [Online]. Available: <https://www.cancer.gov/about-cancer/treatment/types/targeted-therapies/targeted-therapies-fact-sheet#what-targeted-therapies-have-been-approved-for-specific-types-of-cancer> [Accessed].
- Olusanya, T. O. B., Haj Ahmad, R. R., Ibegbu, D. M., Smith, J. R. & Elkordy, A. A. 2018. Liposomal Drug Delivery Systems and Anticancer Drugs. *Molecules*, 23.
- Oyajobi, B. O., Munoz, S., Kakonen, R., Williams, P. J., Gupta, A., Wideman, C. L., Story, B., Grubbs, B., Armstrong, A., Dougall, W. C., Garrett, I. R. & Mundy, G. R. 2007. Detection of myeloma in skeleton of mice by whole-body optical fluorescence imaging. *Mol Cancer Ther*, 6, 1701-8.
- Pei, Y., Liu, K. W., Wang, J., Garancher, A., Tao, R., Esparza, L. A., Maier, D. L., Udaka, Y. T., Murad, N., Morrissy, S., Seker-Cin, H., Brabetz, S., Qi, L., Kogiso, M., Schubert, S., Olson, J. M., Cho, Y. J., Li, X. N., Crawford, J. R., Levy, M. L., Kool, M., Pfister, S. M., Taylor, M. D. & Wechsler-Reya, R. J. 2016. HDAC and PI3K Antagonists Cooperate to Inhibit Growth of MYC-Driven Medulloblastoma. *Cancer Cell*, 29, 311-323.
- Pelengaris, S., Khan, M. & Evan, G. I. 2002. Suppression of Myc-induced apoptosis in beta cells exposes multiple oncogenic properties of Myc and triggers carcinogenic progression. *Cell*, 109, 321-34.
- Pelengaris, S., Littlewood, T., Khan, M., Elia, G. & Evan, G. 1999. Reversible activation of c-Myc in skin: induction of a complex neoplastic phenotype by a single oncogenic lesion. *Mol Cell*, 3, 565-77.
- Ravi, P., Kumar, S. K., Cerhan, J. R., Maurer, M. J., Dingli, D., Ansell, S. M. & Rajkumar, S. V. 2018. Defining cure in multiple myeloma: a comparative



## References

- study of outcomes of young individuals with myeloma and curable hematologic malignancies. *Blood Cancer J*, 8, 26.
- Rempel, R. E., Jiang, X., Fullerton, P., Tan, T. Z., Ye, J., Lau, J. A., Mori, S., Chi, J. T., Nevins, J. R. & Friedman, D. R. 2014. Utilization of the Emu-Myc mouse to model heterogeneity of therapeutic response. *Mol Cancer Ther*, 13, 3219-29.
- Roohi, A. & Hojjat-Farsangi, M. 2017. Recent advances in targeting mTOR signaling pathway using small molecule inhibitors. *J Drug Target*, 25, 189-201.
- Rossi, J. F. 2015. Targeted Therapies in Adult B-Cell Malignancies. *Biomed Res Int*, 2015, 217593.
- Sabnis, A. J. & Bivona, T. G. 2019. Principles of Resistance to Targeted Cancer Therapy: Lessons from Basic and Translational Cancer Biology. *Trends Mol Med*, 25, 185-197.
- Sabo, A. & Amati, B. 2014. Genome recognition by MYC. *Cold Spring Harb Perspect Med*, 4.
- Sacco, A., Roccaro, A. M., Ma, D., Shi, J., Mishima, Y., Moschetta, M., Chiarini, M., Munshi, N., Handin, R. I. & Ghobrial, I. M. 2016. Cancer Cell Dissemination and Homing to the Bone Marrow in a Zebrafish Model. *Cancer Res*, 76, 463-71.
- Savino, M., Annibali, D., Carucci, N., Favuzzi, E., Cole, M. D., Evan, G. I., Soucek, L. & Nasi, S. 2011. The action mechanism of the Myc inhibitor termed Omomyc may give clues on how to target Myc for cancer therapy. *PLoS One*, 6, e22284.
- Schaub, F. X., Dhankani, V., Berger, A. C., Trivedi, M., Richardson, A. B., Shaw, R., Zhao, W., Zhang, X., Ventura, A., Liu, Y., Ayer, D. E., Hurlin, P. J., Cherniack, A. D., Eisenman, R. N., Bernard, B., Grandori, C. & Cancer Genome Atlas, N. 2018. Pan-cancer Alterations of the MYC Oncogene and Its Proximal Network across the Cancer Genome Atlas. *Cell Syst*, 6, 282-300 e2.
- Schindelin, J., Arganda-Carreras, I., Frise, E., Kaynig, V., Longair, M., Pietzsch, T., Preibisch, S., Rueden, C., Saalfeld, S., Schmid, B., Tinevez, J. Y., White, D. J., Hartenstein, V., Eliceiri, K., Tomancak, P. & Cardona, A. 2012. Fiji: an open-source platform for biological-image analysis. *Nat Methods*, 9, 676-82.
- Schmid, I., Uittenbogaart, C. H. & Giorgi, J. V. 1991. A gentle fixation and permeabilization method for combined cell surface and intracellular staining with improved precision in DNA quantification. *Cytometry*, 12, 279-85.
- Schmitz, R., Ceribelli, M., Pittaluga, S., Wright, G. & Staudt, L. M. 2014. Oncogenic mechanisms in Burkitt lymphoma. *Cold Spring Harb Perspect Med*, 4.
- Schwartzberg, L., Kim, E. S., Liu, D. & Schrag, D. 2017. Precision Oncology: Who, How, What, When, and When Not? *American Society of Clinical Oncology Educational Book*, 160-169.

- Sercombe, L., Veerati, T., Moheimani, F., Wu, S. Y., Sood, A. K. & Hua, S. 2015. Advances and Challenges of Liposome Assisted Drug Delivery. *Front Pharmacol*, 6, 286.
- Sharifi-Zarchi, A., Gerovska, D., Adachi, K., Totonchi, M., Pezeshk, H., Taft, R. J., Scholer, H. R., Chitsaz, H., Sadeghi, M., Baharvand, H. & Arauzo-Bravo, M. J. 2017. DNA methylation regulates discrimination of enhancers from promoters through a H3K4me1-H3K4me3 seesaw mechanism. *BMC Genomics*, 18, 964.
- Shin, S. H., Bode, A. M. & Dong, Z. 2017. Precision medicine: the foundation of future cancer therapeutics. *NPJ Precis Oncol*, 1, 12.
- Shull, A. Y., Hu, C. A. & Teng, Y. 2017. Zebrafish as a model to evaluate peptide-related cancer therapies. *Amino Acids*, 49, 1907-1913.
- Siu, K. T., Ramachandran, J., Yee, A. J., Eda, H., Santo, L., Panaroni, C., Mertz, J. A., Sims Iii, R. J., Cooper, M. R. & Raje, N. 2017. Preclinical activity of CPI-0610, a novel small-molecule bromodomain and extra-terminal protein inhibitor in the therapy of multiple myeloma. *Leukemia*, 31, 1760-1769.
- Sodir, N. M., Swigart, L. B., Karnezis, A. N., Hanahan, D., Evan, G. I. & Soucek, L. 2011. Endogenous Myc maintains the tumor microenvironment. *Genes Dev*, 25, 907-16.
- Soodgupta, D., Pan, D., Cui, G., Senpan, A., Yang, X., Lu, L., Weilbaecher, K. N., Prochownik, E. V., Lanza, G. M. & Tomasson, M. H. 2015. Small Molecule MYC Inhibitor Conjugated to Integrin-Targeted Nanoparticles Extends Survival in a Mouse Model of Disseminated Multiple Myeloma. *Mol Cancer Ther*, 14, 1286-94.
- Sorolla, A., Wang, E., Golden, E., Duffy, C., Henriques, S. T., Redfern, A. D. & Blancafort, P. 2020. Precision medicine by designer interference peptides: applications in oncology and molecular therapeutics. *Oncogene*, 39, 1167-1184.
- Soucek, L. & Evan, G. I. 2010. The ups and downs of Myc biology. *Curr Opin Genet Dev*, 20, 91-5.
- Soucek, L., Helmer-Citterich, M., Sacco, A., Jucker, R., Cesareni, G. & Nasi, S. 1998. Design and properties of a Myc derivative that efficiently homodimerizes. *Oncogene*, 17, 2463-72.
- Soucek, L., Jucker, R., Panacchia, L., Ricordy, R., Tato, F. & Nasi, S. 2002. Omomyc, a potential Myc dominant negative, enhances Myc-induced apoptosis. *Cancer Res*, 62, 3507-10.
- Soucek, L., Whitfield, J., Martins, C. P., Finch, A. J., Murphy, D. J., Sodir, N. M., Karnezis, A. N., Swigart, L. B., Nasi, S. & Evan, G. I. 2008. Modelling Myc inhibition as a cancer therapy. *Nature*, 455, 679-83.
- Soucek, L., Whitfield, J. R., Sodir, N. M., Masso-Valles, D., Serrano, E., Karnezis, A. N., Swigart, L. B. & Evan, G. I. 2013. Inhibition of Myc family proteins eradicates KRas-driven lung cancer in mice. *Genes Dev*, 27, 504-13.
- Stefan, E. & Bister, K. 2017. MYC and RAF: Key Effectors in Cellular Signaling and Major Drivers in Human Cancer. *Curr Top Microbiol Immunol*, 407, 117-151.

## References

- Stellas, D., Szabolcs, M., Koul, S., Li, Z., Polyzos, A., Anagnostopoulos, C., Cournia, Z., Tamvakopoulos, C., Klinakis, A. & Efstratiadis, A. 2014. Therapeutic effects of an anti-Myc drug on mouse pancreatic cancer. *J Natl Cancer Inst*, 106.
- Stine, Z. E., Walton, Z. E., Altman, B. J., Hsieh, A. L. & Dang, C. V. 2015. MYC, Metabolism, and Cancer. *Cancer Discov*, 5, 1024-39.
- Sun, K., Atoyan, R., Borek, M. A., Dellarocca, S., Samson, M. E., Ma, A. W., Xu, G. X., Patterson, T., Tuck, D. P., Viner, J. L., Fattaey, A. & Wang, J. 2017. Dual HDAC and PI3K Inhibitor CUDC-907 Downregulates MYC and Suppresses Growth of MYC-dependent Cancers. *Mol Cancer Ther*, 16, 285-299.
- Sun, X. X., He, X., Yin, L., Komada, M., Sears, R. C. & Dai, M. S. 2015. The nucleolar ubiquitin-specific protease USP36 deubiquitinates and stabilizes c-Myc. *Proc Natl Acad Sci U S A*, 112, 3734-9.
- Tannock, I., Hill, R., Bristow, R. & Harrington, L. 2013. *Basic Science of Oncology, Fifth Edition*, McGraw-Hill Professional.
- Terpos, E., Ntanasis-Stathopoulos, I., Gavriatopoulou, M. & Dimopoulos, M. A. 2018. Pathogenesis of bone disease in multiple myeloma: from bench to bedside. *Blood Cancer J*, 8, 7.
- Tolcher, A. W. & Mayer, L. D. 2018. Improving combination cancer therapy: the CombiPlex((R)) development platform. *Future Oncol*, 14, 1317-1332.
- Tolcher, A. W., Papadopoulos, K. P., Patnaik, A., Rasco, D. W., Martinez, D., Wood, D. L., Fielman, B., Sharma, M., Janisch, L. A., Brown, B. D., Bhargava, P. & Ratain, M. J. 2015. Safety and activity of DCR-MYC, a first-in-class Dicer-substrate small interfering RNA (DsiRNA) targeting MYC, in a phase I study in patients with advanced solid tumors. *Journal of Clinical Oncology*, 33, 11006-11006.
- Vagner, J., Qu, H. & Hruby, V. J. 2008. Peptidomimetics, a synthetic tool of drug discovery. *Curr Opin Chem Biol*, 12, 292-6.
- Van Slooten, M. L., Storm, G., Zoepfel, A., Kupcu, Z., Boerman, O., Crommelin, D. J., Wagner, E. & Kircheis, R. 2000. Liposomes containing interferon-gamma as adjuvant in tumor cell vaccines. *Pharm Res*, 17, 42-8.
- Wallington-Beddoe, C. T., Sobieraj-Teague, M., Kuss, B. J. & Pitson, S. M. 2018. Resistance to proteasome inhibitors and other targeted therapies in myeloma. *Br J Haematol*, 182, 11-28.
- Walrant, A., Cardon, S., Burlina, F. & Sagan, S. 2017. Membrane Crossing and Membranotropic Activity of Cell-Penetrating Peptides: Dangerous Liaisons? *Acc Chem Res*, 50, 2968-2975.
- Wang, H., Mannava, S., Grachtchouk, V., Zhuang, D., Soengas, M. S., Gudkov, A. V., Prochownik, E. V. & Nikiforov, M. A. 2008. c-Myc depletion inhibits proliferation of human tumor cells at various stages of the cell cycle. *Oncogene*, 27, 1905-15.
- Webb, M. S., Tortora, N., Cremese, M., Kozłowska, H., Blaquiere, M., Devine, D. V. & Kornbrust, D. J. 2001. Toxicity and toxicokinetics of a phosphorothioate oligonucleotide against the c-myc oncogene in cynomolgus monkeys. *Antisense Nucleic Acid Drug Dev*, 11, 155-63.

- Weinhold, N., Ashby, C., Rasche, L., Chavan, S. S., Stein, C., Stephens, O. W., Tytarenko, R., Bauer, M. A., Meissner, T., Deshpande, S., Patel, P. H., Buzder, T., Molnar, G., Peterson, E. A., Van Rhee, F., Zangari, M., Thanendrarajan, S., Schinke, C., Tian, E., Epstein, J., Barlogie, B., Davies, F. E., Heuck, C. J., Walker, B. A. & Morgan, G. J. 2016. Clonal selection and double-hit events involving tumor suppressor genes underlie relapse in myeloma. *Blood*, 128, 1735-44.
- White, R. M., Sessa, A., Burke, C., Bowman, T., Leblanc, J., Ceol, C., Bourque, C., Dovey, M., Goessling, W., Burns, C. E. & Zon, L. I. 2008. Transparent adult zebrafish as a tool for in vivo transplantation analysis. *Cell Stem Cell*, 2, 183-9.
- Whitfield, J. R., Beaulieu, M. E. & Soucek, L. 2017. Strategies to Inhibit Myc and Their Clinical Applicability. *Front Cell Dev Biol*, 5, 10.
- Wiegering, A., Uthe, F. W., Jamieson, T., Ruoss, Y., Huttenrauch, M., Kuspert, M., Pfann, C., Nixon, C., Herold, S., Walz, S., Taranets, L., Germer, C. T., Rosenwald, A., Sansom, O. J. & Eilers, M. 2015. Targeting Translation Initiation Bypasses Signaling Crosstalk Mechanisms That Maintain High MYC Levels in Colorectal Cancer. *Cancer Discov*, 5, 768-781.
- Wolf, A., Aggio, J., Campbell, C., Wright, F., Marquez, G., Traver, D. & Stachura, D. L. 2017. Zebrafish Caudal Haematopoietic Embryonic Stromal Tissue (CHEST) Cells Support Haematopoiesis. *Sci Rep*, 7, 44644.
- Yang, D. & Hurley, L. H. 2006. Structure of the biologically relevant G-quadruplex in the c-MYC promoter. *Nucleosides Nucleotides Nucleic Acids*, 25, 951-68.
- Yang, J., Shimada, Y., Olsthoorn, R. C., Snaar-Jagalska, B. E., Spaink, H. P. & Kros, A. 2016. Application of Coiled Coil Peptides in Liposomal Anticancer Drug Delivery Using a Zebrafish Xenograft Model. *ACS Nano*, 10, 7428-35.
- Yin, X., Giap, C., Lazo, J. S. & Prochownik, E. V. 2003. Low molecular weight inhibitors of Myc-Max interaction and function. *Oncogene*, 22, 6151-9.

